Comparative Study of the Effect of Tread Rubber Compound on Tire Performance on Ice

Mohit Nitin Shenvi

Thesis submitted to the Faculty of the Virginia Polytechnic Institute and State University in partial fulfillment of the requirements for the degree of

Master of Science
in
Mechanical Engineering

Corina Sandu, Chair
Saied Taheri
Ronald H. Kennedy

5th August, 2020
Blacksburg, Virginia, USA

Keywords: Tire-ice friction, tread rubber compound, winter tires, genetic algorithm

Comparative Study of the Effect of Tread Rubber Compound on Tire Performance on Ice

Mohit Nitin Shenvi

Abstract

The tire-terrain interaction is complex and tremendously important; it impacts the performance and safety of the vehicle and its occupants. Icy roads further enhance these complexities and adversely affect the handling of the vehicle. The analysis of the tire-ice contact focusing on individual aspects of tire construction and operation is imperative for tire industry's future. This study investigates the effects of the tread rubber compound on the drawbar pull performance of tires in contact with an ice layer near its melting point.

A set of sixteen tires of eight different rubber compounds were considered. The tires were identical in design and tread patterns but have different tread rubber compounds. To study the effect of the tread rubber compound, all operational parameters were kept constant during the testing conducted on the Terramechanics Rig at the Terramechanics, Multibody, and Vehicle Systems laboratory. The tests led to conclusive evidence of the effect of the tread rubber compound on the drawbar performance (found to be most prominent in the linear region of the drawbar-slip curve) and on the resistive forces of free-rolling tires.

Modeling of the tire-ice contact for estimation of temperature rise and water film height was performed using ATIIM 2.0. The performance of this in-house model was compared against three classical tire-ice friction models. A parametrization of the Magic Formula tire model was performed using experimental data and a Genetic Algorithm. The dependence of individual factors of the Magic Formula on the ambient temperature, tire age, and tread rubber compounds was investigated.

Comparative Study of the Effect of Tread Rubber Compound on Tire Performance on Ice

Mohit Nitin Shenvi

General Audience Abstract

The interaction between the tire and icy road conditions in the context of the safety of the occupants of the vehicle is a demanding test of the skills of the driver. The expected maneuvers of a vehicle in response to the actions of the driver become heavily unpredictable depending on a variety of factors like the thickness of the ice, its temperature, ambient temperature, the conditions of the vehicle and the tire, etc. To overcome the issues that could arise, the development of winter tires got a boost, especially with siping and rubber compounding technology. This research focuses on the effects on the tire performance on ice due to the variation in the tread rubber compounds.

The experimental accomplishment of the same was performed using the Terramechanics rig at the Terramechanics, Multibody, and Vehicle Systems (TMVS) laboratory. It was found that the effect of the rubber compound is most pronounced in the region where most vehicles operate under normal circumstances.

An attempt was made to simulate the temperature rise in the contact patch and the water film that exists due to the localized melting of ice caused by frictional heating. Three classical friction models were used to compare the predictions against ATIIM 2.0, an in-house developed model. Using an optimization technique namely the Genetic Algorithm, efforts were made to understand the effects of the tread rubber compound, the ambient temperature, and the aging of the tire on the parameters of the Magic Formula model, an empirical model describing the performance of the tire.

Acknowledgements

First and foremost, I would like to express my sincere gratitude for the constant guidance and support that my advisor Prof. Corina Sandu has offered during the course of my master's studies. She has been a source of inspiration and I thank her for the efforts she has put in as an advisor for the continual growth of my knowledge and skills in this field. It has been an honor and a blessing in disguise to have her as my advisor.

I thank Prof. Saied Taheri for agreeing to be on my committee and for the important lessons learnt in his course of Vehicle Control. I would also like to thank Dr. Ronald Kennedy for the valuable interactions I have had with him.

Special thanks to Sumitomo Rubber Industries Ltd. for partially funding this work. Thanks are also due to Dr. Toshio Tada for the support he has provided during the course of this research project.

I take this opportunity to thank all my colleagues in the TMVS Laboratory, especially two of my seniors in the lab, Dr. Rui He for teaching me the various equipment and systems in the laboratory, and Hoda Mousavi for her help during the preparatory, maintenance issues and testing phase of the project. They have been very helpful throughout my tenure as a graduate master's student. I thank Adwait Verulkar for the investment of his time and efforts during the experimental testing phase of this project as well as the various discussions I have had with him since the time he has joined the lab. I would also like to thank Dr. Chen Liang for the interactions I had with him during his time in the lab, and Xiangtong Chen and Darshan Rajasekaran for their help during the pressure distribution measurement phase of the tires. Two alumni of our lab, Dr. Anudeep Bhoopalam, and Dr. Emilio Jimenez have been of great help with their suggestions/directions at critical points during the course of ice testing and this project in general, and I am grateful to them, too.

There are a lot of people in my family and my friend circle here as well as in India, who deserve a mention as they have been helpful at various points of time in academic as well as personal ventures and have sailed with me through troubled and smooth waters. I would like to thank my undergraduate Professors for imparting the foundational knowledge in this field by in-class or out-of-class interactions, during the course of my undergraduate studies.

Most importantly, my parents have always been a source of inspiration and support at all points of my life. By words or by actions, I won't ever be able to show how thankful I am to them. My elder sister, Madhura, too has been supporting in every venture and these three are the people I will always look up to whenever life tests me in any arena.

Lastly, I would like to thank the creator for I believe he helps and guides us in times when nothing seems right.

Table of Contents

List of Figures

List of Tables

Chapter 1 Introduction

The focus of this chapter is to acquaint the reader with the research conducted as a part of this thesis. This chapter presents the motivation, the objectives, and the approach followed during the period of this study. A general outline of this thesis is presented at the end of the chapter.

1.1. Motivation of research

A pneumatic tire acts as the primary point of force and motion generation in the majority of vehicles. Delving even further, the type of terrain that a pneumatic tire traverses on could be primarily classified under the category of either rigid terrain, like asphalt, ice, etc. or deformable terrain, like snow, sand, soil, etc. The presence of snow and/or ice greatly affects the friction available at the interface between the tire and the terrain.

Amongst the rigid terrains, ice is a tricky terrain and requires great skill on the part of the driver in crucial circumstances. A lot of factors related to the ice affect the friction available at the contact patch of the tire. All these factors cannot be estimated accurately during the design process. Thus, a generalized effort is made to increase the available friction coefficient, decrease the rolling resistance of the tires, increase the passage of water obtained from melted ice away from the contact patch, etc. Consideration of all of these has given a boost to the promotion and adoption of winter tires.

Around 70% of USA's roadways (US. Department of Transportation and Administration, 2020) are located in regions where the average annual snowfall is greater than 5 inches and these areas also have around 70% of the population. The reduced friction due to the presence of snow and ice affects the handling of the vehicle and is a concern particularly due to the large number of accidents occurring due to the same. During the period between 2007 and 2016, icy pavements have led to an annual average of about 156,164 crashes with 521 average fatalities (US. Department of Transportation, 2020) per year.

Another motivation for the importance of analysis of tire performance on ice is to reduce the dependence on the skill of the driver. If the effects of different environmental and operational factors on the performance of the tire on ice can be predicted in the design stage, it will help the

design of the controllers and overall the vehicle performance, especially as the industry is looking into tire design for the field of autonomous vehicles.

1.2. Objectives of the research

As we know, the tire is the primary point of motion generation. The effect of the terrain on the performance of the tire is very important as it will, in turn, affect the safety of the vehicle and its occupants. Many efforts have been made to understand this phenomenon when the terrain is ice, as will be detailed in Chapter 2 of this document. This work focusses on the effects of variation in tread rubber compound on the performance of tire on ice.

The primary objective of this work is to experimentally investigate the performance of tires on ice when the tread rubber compound is changed. All other parameters which can affect the tire performance like inflation pressure, normal load, the temperature of the ice surface, etc. were kept constant throughout the experimental investigation so that the tread rubber compound can be the only variable.

Another objective of this study is to investigate the effect on the water film height and on the rise in temperature at the tire-ice interface, as predicted by ATIIM 2.0, an in-house model developed by Mousavi (Mousavi and Sandu, 2020a), and correlate these results with the performance of tire on ice, in order to provide a deeper understanding about how the material properties of the tread rubber compound affect the performance of the tire.

The last objective of this work is to compare the predictions of ATIIM 2.0 with other models previously developed by researchers in order to analyze the friction between the tire and ice. An attempt was made to find the Magic Formula parameters (Pacejka and Bakker, 1992) for all the tires tested using a genetic algorithm, in order to investigate the effect of change in the rubber compound on the individual terms of the Magic Formula.

1.3 Approach followed

The accomplishment of the objectives was based either on the experimental investigation or simulation. The primary objective is completely based on the experimental investigation that

was conducted at the Terramechanics, Multibody and Vehicle Systems (TMVS) Laboratory at Virginia Tech. The tests were conducted in the indoor Terramechanics rig. Several steps were involved in the preparation for testing that included preparation of the tires as well as preparation of the ice surface. Sixteeen tires were tested in nearly identical conditions, for eight different tread rubber compounds (two tires per rubber compound). The completion of the testing provided tangible evidence of the effect that variation in material properties of tread rubber compounds can have on the performance of the tire on ice.

For the accomplishment of the second objective, the pressure distribution of all the tires was collected for various configurations using the Tekscan 3150 pressure measurement system. The collected data was pre-processed to remove the noise and interpolation of data was performed in case of missing cell information due to damage to the system. The collected pressure distributions were then simulated using the ATIIM 2.0 to estimate the rise in temperature and the height of water film at the contact patch.

To achieve the last objective, three models developed earlier to analyze the tire-ice friction coefficient were used to estimate the friction force at the contact patch and height of water film generated. These models namely are:

- Hayhoe and Shapley model (Hayhoe and Shapley, 1989)
- Peng et. al. 1st model (Peng et al., 1999)
- Peng et. al. 2nd model (Peng et al., 2000)

These estimates were then compared with the predictions of ATIIM 2.0 and the results of the experimental investigation to benchmark the accuracy of the same.

1.4 Major contributions

This study provides a conclusive evidence of the extent to which the variation in tread rubber compound can affect the performance of the tire. Through experimental results it was found that the tires of rubber compound C did not perform well throughout as well as also had the highest amount of resistive forces per unit normalized load in the free rolling condition. It was also found that the tire of rubber compound H performed the best and the average maximum value of the drawbar pull was more than twice in the case of rubber compound H when compared to rubber

compound C. In majority of the cases the highest experimental rise in temperature measured at the contact patch was for the tires of rubber compound H. A reduction in the ambient temperature (the ambient temperature in the laboratory being positive) was found to reduce the drawbar pull coefficient experienced by the tires of the same rubber compound. The extent to which this effect manifests varies with the rubber compounds as for the same reduction in ambient temperature the percentage decrease in the maximum value of drawbar pull coefficient displayed by the tires of rubber compounds F and H is different. Another notable finding of the experimental results is that the effect of the variation in tread rubber compound on the tire performance on ice is most notable in the case of the lower slip region, in which most of the vehicles operate. As the slip ratio increases and approaches 30%, the value of the drawbar pull experienced by the tires of different rubber compounds is nearly the same.

An attempt to parametrize the Magic Formula parameters led to insights about the effects of aging and the change in ambient temperature on the value of the Magic Formula parameters. The aging of the tire was found to increase the absolute value of the stiffness factor as well as a higher value of the angle at the origin. It was also found that the variation in ambient temperature not only affected the peak value factor but also the stiffness factor of the tire. The shape factor is not highly affected by this effect. In the simulation phase it was found that the classical models do predict the transition point, thus effectively predicting the presence or absence of melting but the slip ratio at which melting initiates was found to be around 20% in the case of Hayhoe and Shapley model which is higher than the two Peng et al. models as well as ATIIM2.0. All the other models predicted the initiation of melting as the slip ratio crossed 10% in majority of the cases. Also, as the classical models neglect the variation of pressure in the lateral direction of the contact patch, the same values of predictions will be found in the case of various tires if the rubber compound and all operational parameters are same, but this is not the case as the water film height predicted by ATIIM2.0 for tires 1 and 3 of the same rubber compound are found to be varying even if the order of magnitude is same for both the tires. Also, in the temperature rise simulations by ATIIM, it was found that the point of highest rise in temperature may vary in the lateral direction of the tire and this effect cannot be captured by the classical models as they neglect the variation of pressure in the lateral direction of the contact patch. The advantage found was that even after consideration of the small set of properties used as input to the classical models, the highest total friction coefficient predicted by all the three classical models was for the rubber compound H,

which also is the rubber compound that experiences the maximum drawbar pull coefficient based on experimental results.

1.5 Outline of the Thesis

The thesis is divided into several chapters. Chapter 2 presents a detailed review of relevant literature, performed for this research. The major topics covered relate to the mechanisms of rubber-ice friction, tire-ice friction, winter tires, effects of the ambient and ice temperatures on the tire performance, and some modeling approaches relevant to this work.

Chapter 3 details the setup and preparation for the experimental investigation of tire performance in this study. It also comprises of the procedures followed for collection of the pressure distribution, the design of experiments followed during the investigation and the methodology of testing followed.

Chapter 4 presents the results of the experimental investigation and discussions on the same. It includes the effects of variation in the tread rubber compound, variation in the ambient temperature during testing, and the effect of aging on the performance of tire on ice. The chapter also presents data related to the rise in temperature in the tread found experimentally by the use of thermocouples.

Chapter 5 presents results from the simulation of water film height and temperature rise by using ATIIM 2.0. This chapter also includes comparison of predictions performed by ATIIM 2.0 with previous models.

Chapter 6 summarizes the overall conclusions from this work and suggestions for future work.

Chapter 2 Review of relevant literature

This chapter presents a detailed review of the literature studied during the course of this work. The major focus is on the studies related to the tire-ice contact phenomenon but relevant literature related to the rubber-ice friction is also featured. The chapter has been further subdivided into sections as below:

- Introduction to the tire-ice contact phenomenon
- Introduction to winter tires
- Effects of rubber/tread compound on friction on ice
- Effects of ambient temperature on the performance of the tire
- Various approaches for modeling tire-ice friction

The major goal of this chapter is to introduce the reader to various aspects related to tire-ice friction analysis. It will also serve as a reference point to focus on the aspects of the tread rubber that affect the friction on ice the most. Another intention of this chapter is for the reader to have a consolidated document detailing the prior modeling efforts in this field and the benefits and drawbacks of them.

2.1 Introduction to the tire-ice contact phenomenon

In general, the friction between the tire and terrain is a complex mechanism. The classical laws of friction are not fully able to explain the friction at the tire-terrain interface due to the high pressure (Moore, 1975). This is evident in the Stribeck curve in which the increase in sliding speed reduces the friction to a minimum value and an increase thereafter as shown in Figure 2-1 (Waluś and Olszewski, 2011).

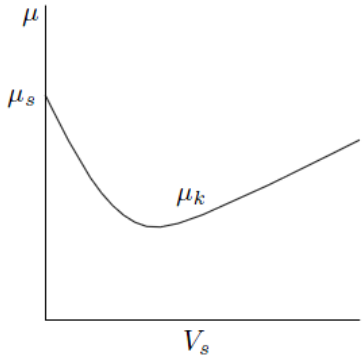

Figure 2-1: Stribeck curve of friction dependence on sliding velocity (Van der Steen, 2007)

In general, the friction generated between the tire and the surface is attributed to two factors namely adhesion and sliding/hysteresis. Generally, adhesion is the more prominent component amongst the two, especially on dry roads, but it is reduced substantially when the terrain is ice or is contaminated with water (Michael Blundell, Damian Harty, 2004). An experimental investigation on the influence of surface roughness of rubber on the sliding friction was performed by Xu et al (Xu et al., 2013). In this investigation, there were two different types of rubber specimens having the same properties except for surface roughness. They were tested at varying speeds of sliding under dry and lubricated conditions. It was postulated that in the case of dry friction, the area of contact of the textured specimen is lower than its less textured counterpart leading to lower friction between the surfaces. On the other hand, in the case of lubricated surface, it was observed that the friction of textured surface was higher in the low-speed region whereas in the high-speed zone (>0.1 m/s), the friction of textured surface reduced which was attributed to an enhanced formation of the liquid film and occurrence of micro-cavitations because of the surface roughness of the rubber.

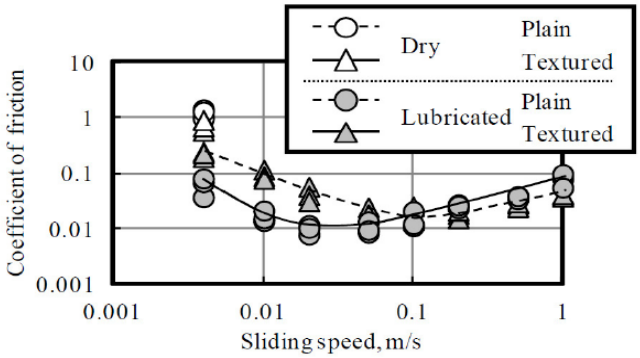

Figure 2-2: Effect of surface roughness and type of surface on the coefficient of friction (Xu et al., 2013)

If the terrain is ice, the number of factors contributing to the complexity of the friction mechanism rises even further. Some of these factors like the ambient temperature, the temperature of the tire, etc. maybe transient i.e. changing over time. The coefficient of friction on an icy surface is also affected by the temperature of the ice. Previously it was assumed that the friction on the ice being low is due to localized melting of ice due to the pressure but that notion is replaced by the thought that frictional heating of the ice surface is a more dominant factor causing the melting of ice and water layer formation. This is attributed to the presence of a quasi-liquid layer of melted ice which has a low shear strength at temperatures nearly equal to the melting point (Nakajima, 2019). If the velocity of the rubber/tread block is high and/or the normal load is increased, the heat generated due to frictional contact between the tire and ice increases which in turn increases the height of the water layer contributing to a reduction in friction. Thus, the temperature of the ice, the normal load on the tire, and the velocity of the tire are some parameters that dictate the interaction in the contact patch leading to the presence of a thin film of water being formed and being present between the tire and ice.

The friction of a tire on ice is subdivided into several categories as follows (Nakajima, 2019):

- Adhesion
- Sliding
- Viscous shear
- Plowing
- Squeeze-out of water

Of the above, squeeze-out of water is one category that has not been studied at large.

Another factor worthy of interest is the effect of material acting as aggregates after it settles on the ice surface. This can be due to a wide variety of reasons but the presence of these aggregates between the tire and ice affects the friction, depending on the nature of the material and its interactional properties with ice. This effect was studied in detail experimentally by Bhoopalam (Bhoopalam, 2015) and displays the change in performance of tire as shown in Figure 2-11.

A generalized range of the coefficient of traction, Φ, was presented in the study on the braking and traction characteristics by Sokolovskij (Sokolovskij, 2007). The values presented in their work are displayed in Table 2-1 according to the different types of ice surface possible.

Table 2-1: Coefficient of traction of ice. Adapted from (Sokolovskij, 2007)

Type of Ice Surface	Generalized description of surface	Traction Coefficient, Φ
Smooth Ice	Layer of ice sufficiently thick but without any traces created due to chains, studs, etc.	0.054-0.19
Ice (with chains mounted on tires)	Sufficiently thick layer of ice with traces due to movement of wheels having steel chains	0.12-0.18
Black Ice	Thick ice layer having the appearance of a black wet road surface, not easily distinguishable for the driver	0.12-0.26

As will be detailed in section 2.4 further, the ambient temperature also plays an important role in the friction at the tire-ice interface. A drop in the ambient temperature is generally assumed to increase the grip of the tire on the ice leading to an increase in the drawbar pull coefficient observed.

2.2 Introduction to winter tires

Generally, as discussed earlier, in snowy or icy conditions, the friction available at the tire/ice interface reduces greatly. For this reason, two types of tires are generally preferred, namely all-season tires and winter tires.

All-season tires, as the name suggests are designed to improve the traction performance for all seasons. They are often designed to reduce the rolling resistance due to the hysteresis effect which can improve the mileage of the vehicle. They primarily have higher stability on asphalt as their maximum life is traversed on asphalt and hence it is one of the prior considerations (Kaltire, 2020). Another goal during the design process is the maximization of tread life. Generally, the tread rubber compound used in an all-season tire is harder to reduce wear due to abrasion. But when the weather is cold during snowy/icy conditions, it is expected that the stiffening of rubber

of the tire will occur which will lead to a reduction in the grip available for the tire on the surface. Another advantage is that the tread design leads to a reduction in the noise generated.

In the case of winter tires, there are two variants namely studded and studless winter tires. As the name suggests, studded tires have small pins embedded throughout its tread which are used to bite into the ice/snow to reduce slipping and improve grip. But to accommodate these pins, the tread depth is increased a bit. But the presence of such studded winter tires during the non-winter season can lead to damage in the asphalt pavement. This is also the reason why their usage is regulated by the authorities. Besides, it also leads to an increase in noise.

The other variant of the winter tires is the studless version. It particularly got a boost considering the drawbacks of the studded winter tires. To overcome them, the salient features of the winter tires are the following:

1. **Higher amount of sipes**: The number of sipes in a studless winter tire is comparatively more to allow a better grip in the terrain conditions.
2. **Design of the tread pattern**: The tread pattern is designed in such a way that the presence of snow and/or melted water can be automatically squeezed out during the travel of the tire.
3. **Tread depth**: Generally, the depth of tread in a winter tire is higher than an all-season variant. The reason is to lessen the snow buildup at the contacting face to increase the traction.
4. **Rubber compound**: The rubber compound in a winter tire is intended to be comparatively soft than an all-season variant, even in cold weather. Also, the rubber in the tread is generally hydrophilic in nature.

It is apparent from the working of the tire that the tread is the part responsible for contacting the terrain. Generally, winter tires have additional silica in their tread rubber to improve the friction at the surface. Thus, the interaction of the tread with the terrain highly affects tire performance. In such a scenario, the rubber compound of the tread is an area to be focused on given that the compounding technology used for the tread will dictate the performance especially on a low friction terrain like ice. The effect of sipes on the coefficient of friction was studied experimentally by Ripka et al. (Ripka et al., 2012). It shows that the increase in the number of sipes proves to be a booster for the friction coefficient up to a limit after which it acts as a detractor as shown in Figure 2-3.

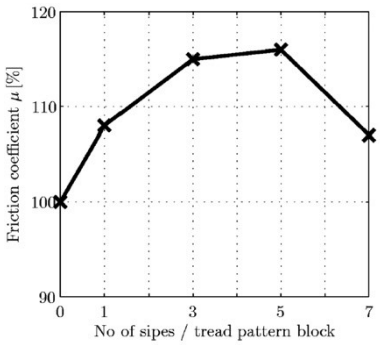

Figure 2-3: Effect of number of sipes on the coefficient of friction (Ripka et al., 2012)

2.3 Effect of Rubber/Tread Compound on friction on ice

To understand the impact of rubber compounds on the performance of tire on ice, we first need to understand other efforts in this field as well as the field of rubber friction. Persson (Persson, 2006) analyzed the effect of the flash temperature on rubber friction. Flash temperature basically is the localized increase of temperature in the contact patch. The authors have shown that when velocities are of the order of 0.01 m/s or more, the flash temperature will play a crucial role in the friction between rubber and asphalt. The flash temperature will play a more prominent role in tire-ice friction as a higher flash temperature is bound to increase the height of water film caused by the localized melting of ice.

Persson (Persson, 2011) in his work proposed a rubber friction law. The author has stated that rubber friction depends on previous instances of sliding motion. The proposed friction law is dependent on the flash temperature. In this work, it is stated that the localized heating of rubber, due to viscoelastic energy losses, occurs in the region of energy dissipation. The regions of energy dissipations are shown in Figure 2-4.

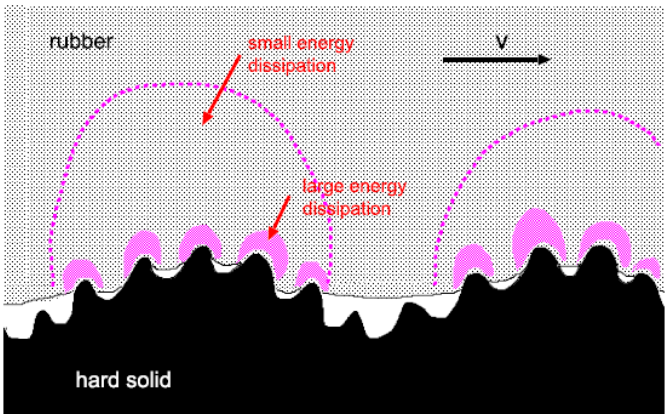

Figure 2-4: Regions of energy dissipation (Persson, 2011)

This work takes into consideration the interaction between tire rubber and road (asphalt). Another point of concern is that the presented calculations in section 4 do not take into consideration the changes in the properties of the tire due to variation in temperature of tire and variation in its inflation pressures. The author has also studied the effects that the tire-road footprint has on the μ-slip curve. For this, they considered 3 types of possible tire footprints but the same pressure and normal load in each condition so that all the footprints have the same area. It was found that the shape of the footprint doesn't have a strong influence on the μ-slip curve which is denoted in Figure 2-5.

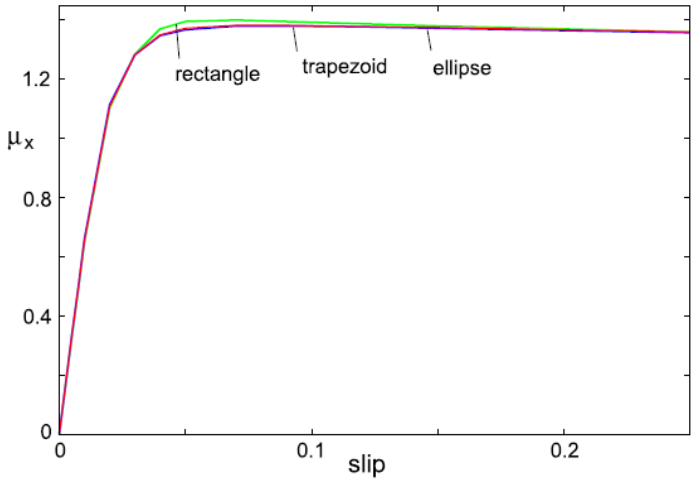

Figure 2-5: Influence of footprint shape on the μ-slip curve (Persson, 2011)

The dependence of the μ-slip curve on the size of the footprint was also studied by the author by assuming a rectangular footprint where the contact pressure was varied due to the change in footprint length. This resulted in a decrease of tire longitudinal stiffness (C_x) which affects the

maxima of the μ-slip curve as shown in Figure 2-6. In real-world scenarios, variation in the inflation pressure of the tire generally causes a change in the contact length but it also leads to a change in the stiffness of the tire body. To nullify the effects of this phenomenon, the normal load and inflation pressure were kept constant throughout the experimental testing of this research work.

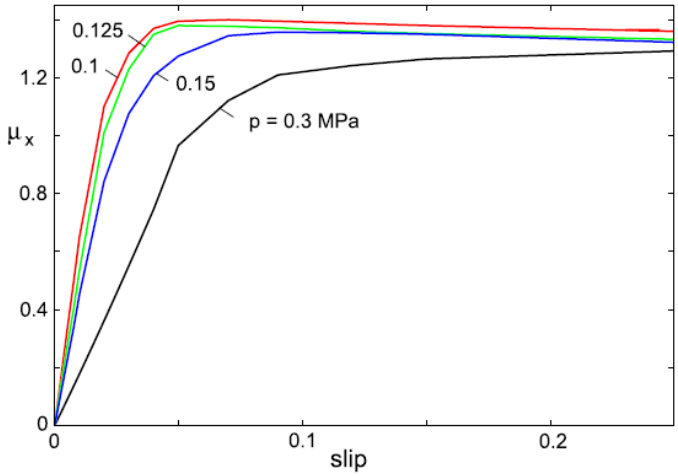

Figure 2-6: Influence of increase in contact pressure on the μ-slip curve (Persson, 2011)

Persson in his work (Persson, 2014) analyzed the role that heating due to friction plays in the phenomena of rubber friction. He has derived his work assuming a non-uniform motion and that some part of the frictional energy is actually produced inside the rubber due to friction between layers of the rubber (internal friction). This corroborates that the mechanical and physical properties of rubber will affect the friction between the rubber block and ice.

The friction of rubber on ice was studied experimentally by Skouvaklis (Skouvaklis et al., 2012). Three different rubber compounds were tested by the authors at 3 different levels of normal load and temperature each. The speed of the sample was varied between 0.1 m/s to 1 m/s. The effect of ice formed from de-ionized water and tap water in the friction coefficient was investigated too by the authors. It was deduced that an increase in the normal load generally decreases the friction coefficient. Increasing the sliding velocity and temperature also seemed to have a reducing effect on the coefficient of friction. The authors concluded that at high velocities and temperatures, the reduction in friction caused due to the presence of the melted water layer has a significant effect on the friction available. At lower speeds, however, the effect of viscoelastic rubber properties is much more noticeable. The softer rubber having lower glass transition temperature

seems to demonstrate a higher level of friction as shown in Figure 2-7. The authors attribute this to the higher real area of contact that a softer rubber can have on the surface.

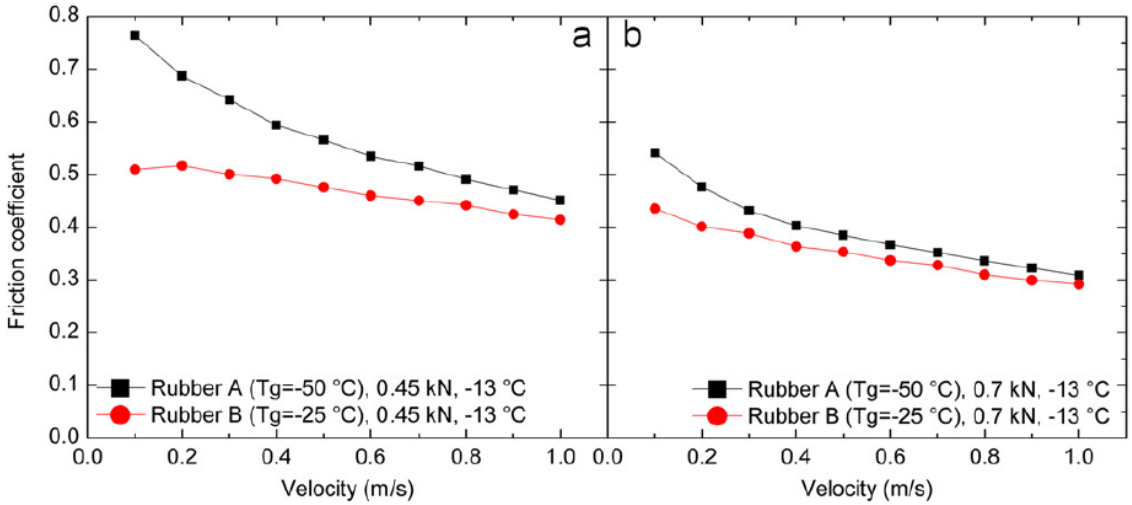

Figure 2-7: Coefficient of friction comparison for two rubbers having different properties (Skouvaklis et al., 2012)

Wiese et al (Wiese et al., 2012) developed an analytical approach to the friction involved in the interaction of rubber on ice. This approach is primarily based on the first law of thermodynamics. For the development of their model, the authors have assumed that the melting of ice, which is caused due to friction between ice and rubber, is solely generated due to the viscous shearing occurring in the liquid layer. This assumption is in consensus with the low friction coefficient present when rubber slides on ice. The model is developed based on the Greenwood-Williamson contact theory (Greenwood and Williamson, 1966). Based on these assumptions, the developed model describes a relation for the change in height of water layer formed with respect to time and with respect to longitudinal distance as described in eqns. (2.1) and (2.2) respectively.

$$\frac{dh(t)}{dt} = \frac{\eta}{\rho L}\frac{v^2}{h(t)} - \sqrt{\frac{\lambda C}{\pi \rho L^2}}\left(\frac{T_m - T_{ice}}{t^{\frac{1}{2}}}\right) \tag{2.1}$$

$$\frac{dh(x)}{dx} = \frac{\eta}{\rho L}\kappa_x\frac{v^2}{h(x)} - \sqrt{\frac{\lambda C}{\pi \rho L^2}}\left(\frac{T_m - T_{ice}}{(v.x)^{\frac{1}{2}}}\right) \tag{2.2}$$

The above 2 equations, especially the eq. (2.2) make us aware of the influence that the roughness parameter 'k_x' will have on the height of water film developed and thus effectively on the friction

coefficient between the 2 surfaces. Conclusively, the work compares the output of the model with the experimental results which are in close agreement with one another.

Klapproth (Klapproth et al., 2016) developed a viscous model for rubber-ice friction. In this work, they have stated that as long as there is no transient behavior, the amount of hysteretic friction will be negligible. They have considered 3 rubber compounds that differ in their stiffness and for which experimental data was available. As a part of this work, the authors have also examined the effect of various parameters like ice temperature, nominal pressure, rubber stiffness, sliding velocity, etc.

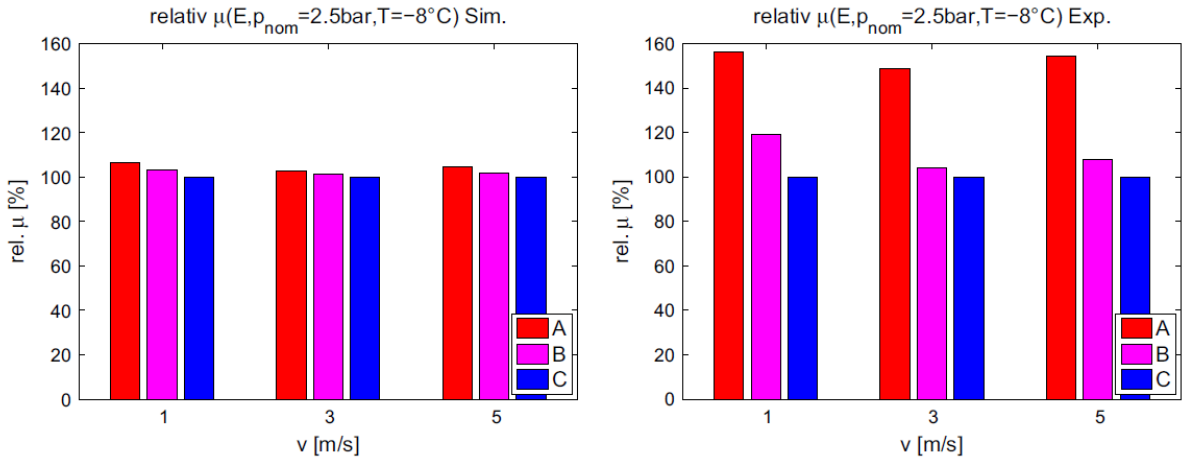

Figure 2-8: Simulated and experimentally measured results for relative friction coefficients of 3 compounds (Klapproth et al., 2016)

In conclusion, the authors have been successful in qualitatively modeling the effect on the rubber-ice friction due to variations in the rubber compound stiffness.

Lorenz et al. (Lorenz et al., 2013) had studied the friction between a rubber block of tire tread compound and the road (asphalt surface). They determined that the friction between the two surfaces majorly depends on the area of contact and asperity deformation, depending on the sliding velocity. Though negative asphalt temperature was considered by the authors in this study, the replacement of asphalt by ice may vary the results at large as the temperature affects the ice properties, especially near the melting point.

Isitman et al. (Isitman et al., 2017) studied the tribological performance of rubber on ice based on rubber stiffness and surface roughness. They concluded that the dynamic coefficient of friction is inversely proportional to rubber stiffness. The impact of filler material was also

examined and proves to be a ground for further studies to analyze its impacts on tire performance as a whole.

The effect of siping edges on the friction between tire and ice depending on the temperature and velocity was studied by Yamazaki et al. (S. Yamazaki, M. Yamaguchi, E. Hiroki, T. Suzuki, 2000). One of the conclusions of their study was that if the velocity is less and the temperature is in the vicinity of the melting point of ice, the effect of sipes is negligible. Thus, this effect was neglected by us as the tires tested in our study were identical in design.

The interaction between tire and ice was studied by Zhang et al. (Zhang et al., 2018). A term called rubber ratio was defined by them signifying the area of the rubber sample that will be in actual contact with the ice as compared to the apparent cross-sectional area. For superior friction on ice, the optimal rubber ratio was found to be in the range of 0.64-0.76. This ratio supports the design of tread generally found in winter tires but the actual to the apparent area of contact with ice needs to be considered by prospective researchers.

The tire performance on the ice was investigated using a finite element approach by Jung et al. (Jung et al., 2018). The authors performed a finite element analysis of a winter tire. The authors determined that the compound of the tread has a considerably high effect on the performance of tire in comparison to the compounds of the undertread of the tire. The frictional force at the contact is also found to be reduced when the temperature of ice nears the melting point of ice as shown in Figure 2-9.

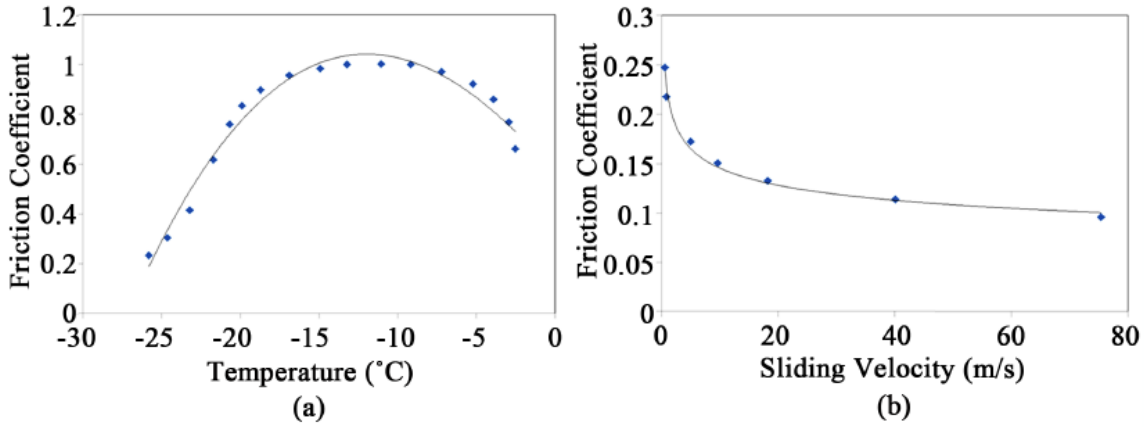

Figure 2-9: Variation of friction coefficient with temperature and sliding velocity (Jung et al., 2018)

2.4 Effect of ambient temperature on tire performance on ice

A study on the friction of rubber on icy asphalt pavements was conducted by Tan et. al (Tan et al., 2020). In this, it was found by the authors that the effect of velocity on the friction on the icy surface is not as significant as the effect of the ambient temperature when comparisons are made to a dry surface. It was also validated that a rise in the ambient temperature decreases the coefficient of friction. This shows the importance of the ambient temperature in the experimental and modeling-based studies of tire-ice interaction. A point of importance to be noted here is that the ambient temperature during these studies was negative.

The effect of ambient temperature on the performance of tire on ice was also investigated by Bhoopalam (Bhoopalam, 2015). It was found that the drawbar pull coefficient of the tires decreased with the reduction in ambient temperature. This could be attributed to two things. One is the effect on the material properties of the rubber due to the reduction in the surrounding temperature. Another is that the presence of a higher ambient temperature affects the ice at the surface especially if the ice temperature is near to its melting point.

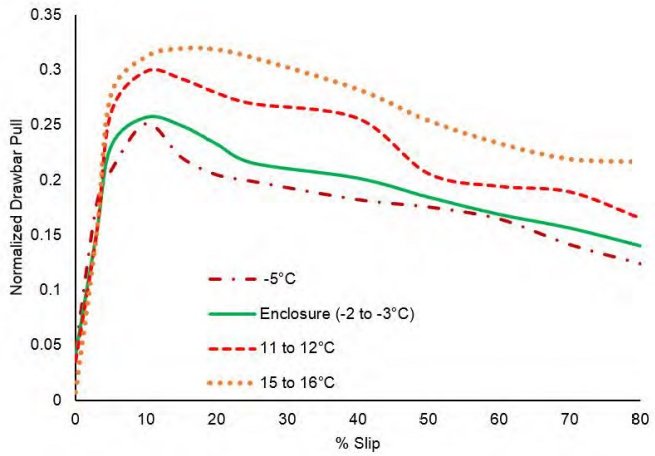

Figure 2-10: Drawbar pull performance of tire with respect to changes in the ambient temperature (Bhoopalam, 2015)

2.5 Various approaches to modeling Tire-Ice Friction

To have a detailed understanding of the phenomenon of friction occurring at the tire-ice interface, the role of tire traction models in the estimation of friction is increasing by the day. Several models have been created over the years which take various generalized parameters like the normal load, the dimensions of the contact patch, the temperature of ice, etc. into consideration.

2.5.1 General models from experimental studies

Experimental studies are conclusive pieces of evidence for the demonstration of a phenomenon under study. A model was developed by Higgins et al. (Higgins et al., 2008) to find the time required for the temperature of the ice surface to reach the melting point. This model is based on the unsteady heat flow equation. A slightly modified formulation was presented by the authors in their work (Skouvaklis et al., 2012) as shown in eq. (2.3).

$$\mu = \frac{\Delta T}{2v\sigma_n}\sqrt{\lambda C_p \rho}\sqrt{\frac{\pi}{t_c}} \tag{2.3}$$

where μ is the coefficient of friction, v is the sliding velocity, C_p is the specific heat capacity, ΔT is the difference in the initial and melting temperature of the ice, ρ is the density of ice, λ is the thermal conductivity of the ice and t_c is the duration for which the rubber slides against a specific position on the surface of the ice. A drawback of this model is the assumption that all the heat generated at the contact is used up and absorbed by the ice, which stems from the fact that the conductivity of ice is an order of magnitude greater than the conductivity of the rubber sample.

Lahayne et al. (Lahayne et al., 2016) had developed models for the macro and micro scale based on an experimental investigation in which three different rubber compounds were tested with four different ice surfaces with 4 levels of ambient temperature, 3 levels of nominal pressure and a constant speed of sliding. The macroscopic model proposed by the authors consists of 8 coefficients which are fitted to the experimental data for estimation of their values. An advantage of this model though is the incorporation of the parameter for the roughness of ice which affects

the friction of the rubber-ice pair in contact as shown in Table 2-2 for one of the rubber compound (R_1) in one level of ambient temperature (-13°C) and nominal pressure (p_1 = 0.15 MPa).

Table 2-2: Coefficient of friction values depending on ice surface roughness. Adapted from (Lahayne et al., 2016)

Ice type	Measured coefficient of friction
I_1	0.377
I_2	0.301
I_3	0.395
I_4	0.510

2.5.2 Estimation of Friction based on presence of winter aggregate and ambient temperature

A lot of research has been done previously to evaluate the effect of the presence of winter aggregate and changes in ambient temperature on the coefficient of friction at the tire-ice interface. One such classical model was proposed by Navin et al. (Navin et al., 1996) which estimates the coefficient of friction as shown in eq. (2.4) and (2.5). The *'A'* in the equation refers to the application of aggregates in gm/m^2 whereas *'T'* refers to the temperature in °C. The model is valid when the ambient temperatures are negative which is the condition in reality but cannot always be ensured in the experimental setup at TMVS laboratory. Secondly, a drawback of the model is that even if the accuracy of the model is assumed to be high, it would predict similar friction coefficients in similar conditions even if the tires were different. Lastly, by virtue of the equations of this model, similar friction coefficients would be estimated if the ambient temperature and the aggregate application would be same but it does not take into consideration the effect that different aggregates can have as their individual interaction with ice could have a different effect on the melting of ice.

$$f_x(ice, car) = 0.11 - 0.0052\,T + 0.0002\,A \quad (2.4)$$

$$f_x(ice, truck) = 0.10 - 0.0052\,T + 0.00016\,A \quad (2.5)$$

This last drawback is highlighted in the testing done by Bhoopalam (Bhoopalam, 2015). The effect of different types of aggregate material on the performance of the tire is as shown in Figure 2-11. The presence of a slush-soil mixture on the ice greatly enhanced the performance of the tire in comparison to salt or dry soil on ice.

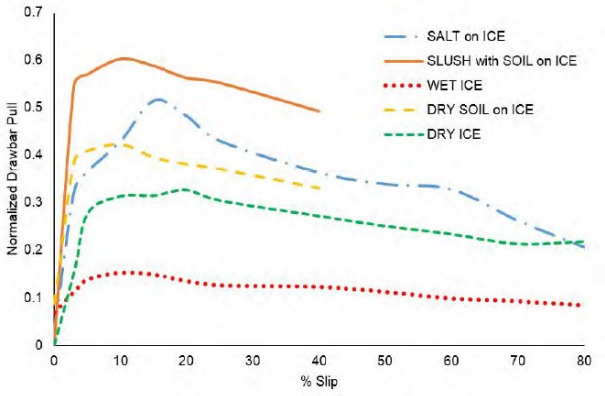

Figure 2-11: Effect of various aggregates on the performance of tire on ice (Bhoopalam, 2015)

2.5.3 Evan's model

One of the earliest attempts to develop an analytical model for the friction on an icy surface was realized by Evans et al (Evans et al., 1976). Though the experimental testing was carried out for ice skating, the concepts proposed by the model are relevant. It was suggested that the heat generated due to force of friction (F_f) is due to the contributions of three parts namely, the heat conducted through the body (F_r - rubber/tire in our case), the heat conducted through the ice (F_i) and the heat required to melt the ice (F_m) as shown in eq. (2.6). The heat carried by the water film after the melting of ice was assumed to be part of F_m as its value is comparatively very low.

$$F_f = F_r + F_i + F_m \tag{2.6}$$

On deriving further, a detailed form of this is as presented in eq. (2.7). In this, *'A'* and *'B'* are constants. *'A'* is dependent on the area of the contact, geometry of the material and its surface whereas *'B'* is dependent on the thermal properties of the ice and the dimensions of the contact patch. *'L'* is the normal load applied, *'T_m'* and *'T_o'* are the melting and ice surface temperatures respectively.

$$\mu = \frac{Ak(T_m - T_o)}{Lv} + \frac{B(T_m - T_o)}{Lv^{\frac{1}{2}}} + \mu_m \qquad (2.7)$$

The variable μ_m was found to have a maximum value of about 0.005 considering a reasonable range of variation in other variables, thus making a negligible contribution. The concept of components of friction being derived from conduction into the 2 materials and heat required to melt the water was an important finding, although the process of evaluation of the constant *'A'* is not clear.

2.5.4 Model by Hayhoe and Shapley

A theory to analytically evaluate the coefficient of friction of a tire on ice was proposed by Hayhoe and Shapley (Hayhoe and Shapley, 1989). It was proposed that the contact patch could be assumed to be composed of two different regions, one which is dry sliding in the front part of the contact patch and the other being a region having a film of water leading to viscous friction. Some of the major assumptions in the formulation of this model are stated below and the concept of transition point is as shown in Figure 2-12.

1. A smooth tire surface is assumed.
2. The pressure in the contact patch is assumed to be constant.
3. As the thermal conductivity of rubber is an order of magnitude less than the thermal conductivity of ice, it was assumed that all the heat generated flows into the ice.
4. Heat flow into the ice from the interface is linear in the vertical direction.

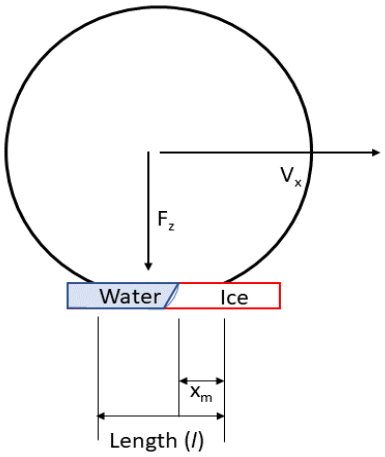

Figure 2-12: Separation of the dry and wet sliding regions of tire on ice. Adapted from (Hayhoe and Shapley, 1989)

The change in temperature at the tire-ice interface based on the conduction between two solids is given by eq. (2.8). In this work, it is further assumed that conductivity of rubber is zero, and change in temperature is only dependent on the numerator of eq. (2.8). If this were to be assumed true, with all other parameters nearly equal, the friction predicted by the model won't be able to highlight the differences arising due to changes in the tread rubber compounds. To avoid, this we decided not to neglect this effect and as the axle velocity is constant, we get eq. (2.10) by substituting eq. (2.9) into eq. (2.8). To find the point where initiation of melting begins, the change in temperature at that point needs to be equated with the difference between the melting point of ice and the bulk temperature of ice. By assuming the melting point to be 0°C, this temperature is equal to the bulk ice temperature, albeit with a positive sign, to get eq. (2.11). The estimation of friction forces in both regions is performed separately before they are added to compute the cumulative friction force.

$$\Delta T = \frac{\frac{2\,\dot{Q}_s}{k_{ice}} \cdot \left[\frac{\alpha_{ice} \cdot t}{\pi}\right]^{0.5}}{\frac{k_{rubber}}{k_{ice}} \cdot \left[\frac{\alpha_{ice}}{\alpha_{rubber}}\right]^{0.5} + 1} \tag{2.8}$$

$$x = v.t \tag{2.9}$$

$$\Delta T = \frac{\frac{2\,\dot{Q}_s}{k_{ice}} \cdot \left[\frac{\alpha_{ice}}{\pi \,.\, v}\right]^{0.5} \cdot x^{0.5}}{\frac{k_{rubber}}{k_{ice}} \cdot \left[\frac{\alpha_{ice}}{\alpha_{rubber}}\right]^{0.5} + 1} \tag{2.10}$$

$$x_m = \left[\frac{k_{ice} \,.\, T_b}{2\,\dot{Q}_s} \cdot \left(\frac{k_{rubber}}{k_{ice}} \cdot \left[\frac{\alpha_{ice}}{\alpha_{rubber}}\right]^{0.5} + 1\right)\right]^2 \cdot \frac{\pi \,.\, v}{\alpha_{ice}} \tag{2.11}$$

2.5.5 Models by Peng et al

Two analytical models were developed by Peng et al (Peng et al., 1999) (Peng et al., 2000) in consecutive years to estimate the friction in a tire-ice interaction. A majority of the assumptions of both the models are similar to the ones mentioned in section 2.5.4. Both the models were developed for rectangular as well as elliptical contact patch shapes. For the purpose of explanation and implementation in this work, equations pertaining to the rectangular contact patch are considered. The earlier model required estimation of the height of water film by solving a 4th-degree polynomial equation. This estimated height is then utilized for the prediction of the average coefficient of friction in the contact patch. A drawback of this method would be that though the height of water film is estimated and follows an expected trend with an increase in the slip ratio, a single value of the height of water film does not make physical sense even when compared to the parent model for this work which was explained in section 2.5.4. This model calculates the transition point from the rear of the contact patch as shown in Figure 2-13 and thus the calculation of transition point is done as shown in eq. (2.12). The value of the transition point is then used to calculate three constants shown in eq. (2.13) where 'H' is the latent heat of fusion and 'ρ' is the density of ice. Estimation of the height of water film is done by solving eq. (2.14) and the estimated height is used to find the average friction coefficient by eq. (2.15).

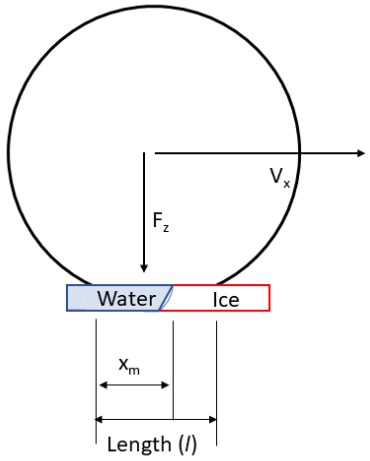

Figure 2-13: Transition point from dry sliding to melted water film under a tire moving on ice. Adapted from (Peng et al., 1999)

$$x_m = length - \left(\frac{\pi V}{\alpha_{ice}}\right)\left(\frac{T_b k_{ice} C}{2\dot{Q}_s}\right)^2 \tag{2.12}$$

$$C_1 = \eta V_{sliding}^2 \; ; C_2 = 2T_b(C_t + C_{ice})\left(\frac{U}{x_m}\right)^{\frac{1}{2}}; \quad C_3 = \frac{p_{avg}\rho H}{\eta . width^2} \tag{2.13}$$

$$C_1 - C_2 h - C_3 h^4 = 0 \tag{2.14}$$

$$\mu_{avg} = \mu_s\left(1 - \frac{x_m}{l}\right) + \frac{\eta V_{sliding}}{h\,.\,p_{avg}}\left(\frac{x_m}{l}\right)^2 \tag{2.15}$$

In the latter work developed by the authors, this step of estimation of the height of water film was bypassed. The characteristics of the contact patch, sliding velocity, the bulk temperature of the ice, and thermal properties of ice and tread are utilized for estimating the value of transition point, fluid friction coefficient, and the average coefficient of friction in this model. The calculation of the transition point in this model is based on eq. (2.16), and the point is calculated from the leading edge of the contact patch, whereas the fluid frictional resistance and the average value of the coefficient of friction are estimated using eq. (2.17) and (2.18) respectively. In the equations, the constant 'C_b' is dependent on the thermal properties of the rubber and the tread.

$$x_m = \left[\frac{\pi C_{ice} C_b T_b}{4\mu_d p_{avg} V_{sliding}}\right]^2 V_{axle} \tag{2.16}$$

$$\mu_f = \frac{C_{ice} C_b T_b}{p_{avg}\sqrt{length\,.\,V_{sliding}}} \tag{2.17}$$

$$\mu_{avg} = \mu_d\left(\frac{x_m}{l}\right)^2 + (C_{ice} + C_{tread})T_b\left(1 - \frac{x_m}{l}\right)^{\frac{3}{2}}\left(\frac{l}{V}\right)^{-\frac{1}{2}}\left(P_{avg}.V_{sliding}\right)^{-1} \tag{2.18}$$

Chapter 3 Experimental approach and design of experiments

The focus of this chapter is to introduce the reader to the experimental setup at the Terramechanics, Multibody and Vehicle Systems (TMVS) laboratory. The testing was conducted in the winter of 2020 to have a lower ambient temperature which has an effect on the performance of the tire. In real-life scenarios, the ambient temperature is generally in the negative range which cannot be enforced in the indoor testing setup at the laboratory. Thus, efforts were made to ensure the same ambient temperature for testing of all the tires.

3.1 Testing Setup

This section focuses on the description of the experimental setup, the system used to collect the pressure distribution of the tire and the procedures followed for preparation of the ice bed.

3.1.1 Description of the Indoor Test Rig

The Terramechanics Rig at TMVS lab was conceptualized (Sandu et al., 2008) with the intention of testing a single wheel on different terrains like soil, ice, etc. The operational conditions like the inflation pressure of the tire, slip ratio, camber angle, toe angle, normal load on the tire, etc. are some other parameters that can be varied (Sandu et al., 2008). Various improvements were made to the rig over time, the most recent being the one by (Khan, Aamir K., Sandu, 2017) which allowed the capability to test free rolling and braking conditions.

The rig is equipped with two motors. One of the motors provides the longitudinal movement of the carriage and in turn to the tire at a constant speed. The longitudinal speed of the carriage is 6 cm/s. The other motor is the wheel motor which provides additional torque to the tire through means of a clutch mechanism. This is utilized to apply various slip ratio conditions as well as testing the free-rolling condition by the disengagement of the clutch. The slip ratios are applied by using the PicPro software to set a rotational speed for the wheel motor.

The normal load is applied to the carriage and in turn the wheel through air springs fitted on top of the carriage. The springs are controlled by means of a proportional valve and controlled

by using NI Labview software. This Active Normal Load Controller system was developed by Naranjo (Naranjo, 2013). The proportional valve is dependent on the feedback from the Kistler measurement system in a closed-loop. The change in the voltage through the software controls the valve to increase/decrease the normal load on the system at a rate of about 0.05V for 75 N.

The applied normal load though is not constant throughout the run but in a precise range of the desired value. This was also shown by Mousavi et al. (Mousavi et al., 2019) by the implementation of the central limit theorem as shown in Figure 3-1. In Figure 3-1, the targeted value of the normal load was 5600 N.

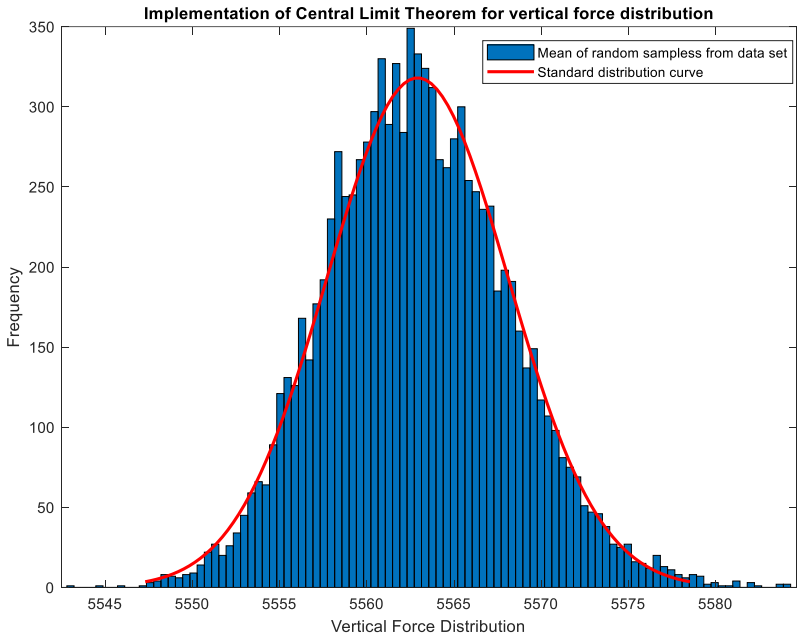

Figure 3-1: Histogram depicting the precise implementation of normal load by the active normal load controller system (Mousavi et al., 2019)

The measurement system of the rig consists of the Kistler P650, a 6-axis force transducer that records the data, most importantly of the forces and moments in 3 mutually perpendicular directions that act on the tire. It also records the rotational velocity and angular position of the tire. The Kistler hub has a sampling frequency of 160 Hz which is quite high and thus filtration of noise and averaging of the data may be required for postprocessing.

Depending on the procedure used for calibration of the Kistler hub, the force in the longitudinal direction can be the drawbar pull or net tractive effort which is the difference between the tractive and resistive forces similar to what is experienced by the tires of a vehicle in real-world

scenarios. A process of calibrating the hub when the tire is rotating on the ice was used by Mousavi et al. (Mousavi and Sandu, 2020b) which led to the removal of a significant amount of resistive forces acting on the tire and providing a better understanding of the tractive forces only.

3.1.2 Description of pressure measurement instrumentation

The Tekscan 3150 pressure measurement system is a system which consists of a pressure pad and supporting hardware to connect with the software. The pressure pad has a cumulative total of 2288 sensels in a matrix-like arrangement to give a cumulative pressure sensing area of 160759.92 mm^2 and a spatial resolution of 1.4 sensel/cm^2 (Tekscan Inc., 2018). In preparation of the pressure pad, the system needs to be equilibrated through the equilibration setup. This is done to ensure that all the sensors of the pressure pad sense equally well when uniform pressure is applied to the pad. It also is a vital process for the detection of faulty rows or columns of sensors which could occur due to overuse or shearing action over time.

The pressure pad is then calibrated with a certain amount of known load, preferably near the region of the required normal load. A multi-point per sensel calibration methodology was developed by Misiewicz et al. (Misiewicz et al., 2015) for the calibration of some other similar pressure measurement products by Tekscan. It was shown by the authors that the multi-point calibration methodology was useful to reduce the bias errors and statistical error range of measurement to about 1/3rd of the error when calibration was performed according to proprietary standards. The pressure measurement as a part of this study though was performed using the proprietary methods recommended.

3.1.3 Description of procedures to be followed for ice testing

The ice bed was created by following the steps detailed below:

1. Placement of the metal U-channels on the brackets of the top level of the chamber. Two layers of the plastic tarp were spread on top and affixed to the frame of the chamber.
2. A layer of insulation foam was placed on top of this by custom cutting it to the inner dimensions of the chamber and fixed with tape to prevent relative motion between the foam

sheets. An additional layer of plastic tarp was then placed on the foam and fixed with the chamber frame.

3. The tubular heat exchanger system from Custom Ice Rinks was then rolled and placed on top in such a way as to ensure the maximum of the tubes being placed adjacent to each other. The connections to the chiller are completed through the inlet and outlet pipes.
4. Rockwool was used to cover the piped connections between the heat exchanger mat and the chiller to prevent a reduction in efficiency.
5. The agent used for heat exchange in the system is ethylene glycol and the chiller mechanism has a feedback by means of a thermocouple which needs to be placed on the surface of the ice.
6. After all the connections are made and the system is warmed up, water is sprayed at a rate of about 2 mm every 2 hours for about 5-6 days to have an ice bed of about 3 inches thick. It was found that this rate ensured an optimal strength of the ice instead of creating a water pool and allowing it to freeze slowly in previous efforts made in the lab (Bhoopalam, 2015) (Jimenez, 2018).
7. The ice surface was cleared of any residual amount of ice flakes or traces of the previous run by using the tools available in the lab. This step is essential to have an almost identical texture of ice and its need is explained in section 2.5.1.

3.2 Design of Experiments

A design of experiments was developed in order to focus on the parameter under study i.e. the tread rubber compound.

3.2.1. DOE for experimental testing on ice

The design of experiments was created in order to focus only on the intended differentiating factor which was the tread rubber compound. The nominal value of normal load and inflation pressure chosen were 4000 N and 28 psi respectively. Thus, all the other parameters of testing were kept constant for all the tires. The ice temperature was chosen to be -1°C as this will create

scenarios of wet friction similar to most real-world scenarios. It was previously found that at lower temperatures of ice like -10℃, the testing of tires is a case of dry friction (Bhoopalam, 2015). As the tread rubber compound was the point of focus and constraints of time, the effect of camber and toe angles could not be tested. The slip ratios were applied in groups of 3 which led to the final two slip ratios to be tested in a single group. This design of experiments is as shown in Table 3-1. All the configurations mentioned were tested twice to ensure the repeatability of the test data.

Table 3-1: Design of Experiments for experimental testing on ice

	Rubber compound A		**Rubber compound B**		**Rubber compound C**		**Rubber compound D**		**Rubber compound E**		**Rubber compound F**		**Rubber compound G**		**Rubber compound H**	
Tire	Tire A1	Tire A3	Tire B1	Tire B3	Tire C1	Tire C3	Tire D1	Tire D3	Tire E1	Tire E3	Tire F1	Tire F3	Tire G1	Tire G3	Tire H1	Tire H3
Load (kN)	4	4	4	4	4	4	4	4	4	4	4	4	4	4	4	4
Infl. Pres. (psi)	28	28	28	28	28	28	28	28	28	28	28	28	28	28	28	28
Slip ratio	0%, 2%, 4%, 6%, 8%, 10%, 12%, 15%, 20%, 25%, 30%, Free Rolling															

3.2.2. DOE for pressure distribution measurement

The design of the experiments table created for testing on ice was modified as the Tekscan pressure measurement system even after affixing perfectly faced issues for dynamic testing at higher slip ratios which can damage its sensels especially due to shearing. This modified design of experiments is shown in Table 3-2.

Table 3-2: Design of Experiments for pressure distribution measurement

	Rubber compound A		**Rubber compound B**		**Rubber compound C**		**Rubber compound D**		**Rubber compound E**		**Rubber compound F**		**Rubber compound G**		**Rubber compound H**	
Tire	Tire A1	Tire A3	Tire B1	Tire B3	Tire C1	Tire C3	Tire D1	Tire D3	Tire E1	Tire E3	Tire F1	Tire F3	Tire G1	Tire G3	Tire H1	Tire H3
Load (kN)	4	4	4	4	4	4	4	4	4	4	4	4	4	4	4	4
Infl. Pres. (psi)	28	28	28	28	28	28	28	28	28	28	28	28	28	28	28	28
Slip ratio	0%, 2%, 4%, 6%, 8%, 10%, 12%, 15%, Free Rolling, Static															

3.3 Preliminary steps and testing methodology

Before commencing the testing phase some steps were undertaken to prepare the tires instead of using them in a brand-new condition. This section details these steps, the importance of the method of estimating the rolling radius, and the steps involved in the testing of tires.

3.3.1. Preparation of tires for testing

The preparation of the tires for testing involved two steps. The first was to have a uniform wear on the tires and the second was to affix thermocouples in the grooves of the tire to experimentally measure the rise in temperature during testing.

a. Wearing of tires

A total of 16 tires of 8 different rubber compounds were identified and tested as a part of this study. Three of these tires were previously tested in the preceding winter. For the remaining tires, the vent spews were removed by using tools available in the lab. All the remaining tires were mounted on a vehicle and run for a total of 100 kms each with tire rotation after every 25 km as shown in Figure 3-2. The tires were left undisturbed for at least 3 days after this process.

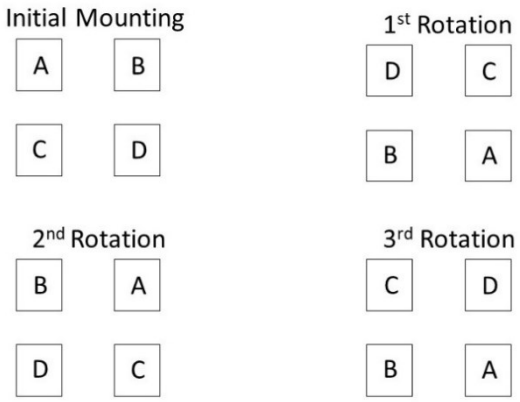

Figure 3-2: Rotation of tires for uniform wear during the preparatory stage

b. Attaching of thermocouples in the groove of the tires

K-type thermocouples which are compatible with the in-house data loggers available were chosen. As the tread pattern of the candidate tires isn't plain like an SRTT (Jimenez, 2018)

but typical to that of a winter tire, there was a risk of damage by having longer thermocouples and bending them manually. So smaller thermocouples of the size ϕ3 mm * 20 mm were chosen and are depicted in Figure 3-3. The disadvantages of this measurement system are that K-type thermocouples are accurate up to ± 2.2 ℃ and the minimum rate of transmission by the data logger is 10 seconds, both of which are a huge trade-off given the temperature of ice employed during the testing conducted for this study.

Figure 3-3: K-type thermocouple to attach to the grooves of the tire

The thermocouples were then fixed to the tire grooves by using white and clear silicone and the procedure described by Jimenez (Jimenez, 2018) and are shown in Figure 3-4.

Figure 3-4: Thermocouples fixed in the grooves of the tires

3.3.2. Estimation of effective rolling radius

The effective rolling radius (r_{eff}) is the ratio of the speed in the longitudinal direction of a tire (V_x) to the angular speed of rotation of the tire (ω) as shown in eq. (3.1). The accurate

estimation of the effective rolling radius is important as it is used in the estimation of slip and the corresponding value required as input for the wheel motor.

$$r_{eff} = \frac{V_x}{\omega} \tag{3.1}$$

Though the application of higher normal loads tends to decrease the radius of the tire in the loaded condition, the effective rolling radius is fairly constant as found in Figure 3-5.

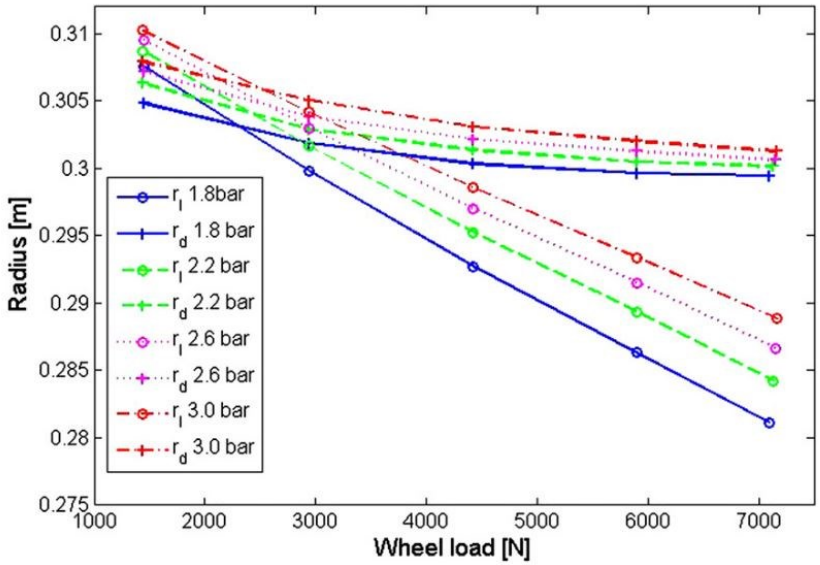

Figure 3-5: Variation in effective and loaded rolling radius with respect to normal load (Tuononen, 2011)

In a prior research study conducted in the TMVS Lab, benchmarking of various methods used for estimation of the effective rolling radius was performed (Mousavi et al., 2019). Tests were conducted on an SRTT and measurements were taken as a part of this study which focused on this goal. One of the methods was the estimation of the effective radius by eq. (3.1). Another method involved the measurement of the length traveled by the tire in one complete rotation with the notion that if a point on the circumference of a tire travels that length (L) in one rotation, the effective radius can be found by the circumference formula as shown in eq. (3.2). The third method involved a formulation commonly found in the literature (Rajamani, 2012) which involves estimation of the effective rolling radius by measurement of the loaded radius (r_L) and the free radius (r_f) of a tire and is as shown in eq. (3.3).

$$r_{eff} = \frac{L}{2\pi} \tag{3.2}$$

$$r_{eff} = \frac{\sin\left(\cos^{-1}\left(\frac{r_L}{r_f}\right)\right)}{\cos^{-1}\left(\frac{r_L}{r_f}\right)} * r_f \tag{3.3}$$

The study proved to be useful as the results indicated that the methods described by eqns. (3.2) and (3.3) were far more accurate in estimation of the effective rolling radius as shown in Figure 3-6. The methods 1, 2, and 3 in Figure 3-6 are as described by eqns. (3.1), (3.2) and (3.3) respectively. This does not imply that the method related to eq. (3.1) is incorrect but in the current experimental setting, the accuracy of the method is not implicit. One of the reasons for the same could be that the measurement system does not aggregate the angular position of the tire but restarts from 0^0 after every rotation. This leads to the value of angular velocity seeing a sharp decline at several points during a run and if the accurate estimation of the effective rolling radius is to be performed by this method, then the part of the results (in time) used for the computation is important. Another way of improving the usage of this method would be to aggregate the angular positions using a code and estimation of its derivative with respect to time to find the value of the angular speed of rotation of the tire. As 16 tires were tested for this research work, it would have been a tedious process to accurately measure the length travelled by every tire in a complete rotation and hence the method described by eq. (3.3) was chosen as the loaded radius was the only parameter required to be measured.

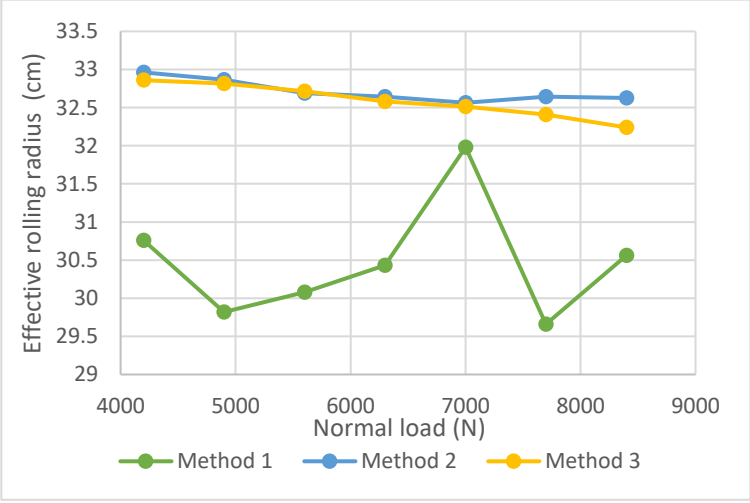

Figure 3-6: Estimation of the effective rolling radius by 3 different methods against the variation of the normal load. Adapted from (Mousavi et al., 2019)

Once the estimation of the rolling radius is completed the input values for the concerned slip ratios are calculated using the equation for the theoretical slip ratio (s, in percentage) as in eq. (3.4).

$$s = 1 - \frac{V_x}{r_{eff} * \omega} \tag{3.4}$$

Chapter 4 Experimental Results

This chapter presents and discusses the results from the experimental testing conducted on the tires according to the design of experiments described in Table 3-1. Efforts were made to ensure a constant ambient temperature throughout the testing of various tires, as the effects of change in the ambient temperature could skew the results either in favor of or against a certain rubber compound. The ambient temperature during the testing of nearly all the tires was about 10-11 ℃ except for one tire each of rubber compound F and rubber compound H which is detailed in the relevant subsection of this chapter.

4.1 Material Properties

The exact composition of the tread rubber compound was not known but relevant physical and thermal properties of the tread rubber compounds were provided and are listed below.

a. Thermal conductivity: The thermal conductivity of all the rubber compounds was assumed to be a constant having a value of 0.3 $Wm^{-1}K^{-1}$
b. Density of the rubber compound: The density property available of the rubber compounds is shown in Table 4-1. Rubber compound H had the highest density whereas rubber compound C had the lowest.

Table 4-1: Density of the 8 different rubber compounds

Name of Compound	Density (kg/m^3)
A	1105
B	1103
C	1094
D	Not Provided
E	1104
F	1139
G	1137
H	1158

c. Specific heat capacity (J/ (g.K)): The specific heat capacity of only 5 of the rubber compounds were available listed in Table 4-2.

Table 4-2: Specific heat capacity of different rubber compounds at various temperatures

Temp. (°C)	A	B	C	D	E	F	G	H
-5	Not Provided	1.84	2.03	2.09	Not Provided	2.18	2.09	Not Provided
0		1.88	2.14	2.26		2.28	2.26	
5		1.92	2.18	2.29		2.30	2.29	
10		1.94	2.21	2.32		2.33	2.31	
15		1.96	2.23	2.35		2.36	2.34	
20		1.99	2.26	2.37		2.38	2.36	
25		2.02	2.29	2.40		2.42	2.39	
30		2.05	2.32	2.43		2.45	2.42	
35		2.07	2.35	2.47		2.47	2.45	
40		2.09	2.37	2.49		2.50	2.47	
45		2.11	2.39	2.50		2.52	2.49	
50		2.12	2.40	2.52		2.53	2.51	
55		2.13	2.42	2.53		2.55	2.52	
60		2.16	2.44	2.55		2.57	2.54	
65		2.18	2.46	2.58		2.60	2.56	
70		2.20	2.49	2.60		2.63	2.59	
75		2.23	2.52	2.63		2.66	2.62	
80		2.26	2.55	2.65		2.69	2.65	

d. Properties related to stiffness: The storage modulus, loss modulus, tangent of the phase difference, and the dynamic modulus was provided at various temperatures for the rubber compounds and are listed in Table 4-3, Table 4-4, Table 4-5 and Table 4-6 respectively.

Table 4-3: Storage modulus of different rubber compounds at various temperatures

Temp. (°C)	E' (in MPa)							
	A	**B**	**C**	**D**	**E**	**F**	**G**	**H**
-11.2	Not Provided	4.002	5.12	Not Provided	Not Provided	Not Provided	7.421	9.101
-8.3		3.697	4.916				6.628	8.366
-5.6		3.495	4.556				6.489	7.977
-2.7		3.401	4.197				6.184	7.568
0.4		3.137	4.153				6.03	7.115
30.9								5.371

Table 4-4: Loss Modulus of different rubber compounds at various temperatures

Temp (°C)	E'' (in MPa)							
	A	**B**	**C**	**D**	**E**	**F**	**G**	**H**
-11.2	Not Provided	1.106	1.205	Not Provided	Not Provided	Not Provided	1.508	2.255
-8.3		0.946	1.044				1.24	1.914
-5.6		0.808	0.839				1.115	1.669
-2.7		0.765	0.771				0.992	1.54
0.4		0.587	0.762				0.983	1.328
30.9								0.767

Table 4-5: Tangent of phase difference for various rubber compounds at various temperatures

Temp. (°C)	Tan – D							
	A	**B**	**C**	**D**	**E**	**F**	**G**	**H**
-11.2	Not Provided	0.276	0.235	Not Provided	Not Provided	Not Provided	0.203	0.248
-8.3		0.256	0.212				0.187	0.229
-5.6		0.231	0.184				0.172	0.209

-2.7		0.225	0.184				0.16	0.204
0.4		0.187	0.184				0.163	0.187
30.9								0.143

Table 4-6: Dynamic Modulus of different rubber compounds at various temperatures

Temp. (°C)	**E* (in MPa)**							
	A	**B**	**C**	**D**	**E**	**F**	**G**	**H**
-11.2		4.152	5.26				7.573	9.377
-8.3		3.816	5.025				6.743	8.582
-5.6		3.587	4.633				6.584	8.149
-2.7		3.486	4.268				6.263	7.723
0.4	4.21	3.191	4.222		5.26	4.87	6.11	7.238
30.9	3.08				3.84	3.56		5.425

4.2 Effect on the tire performance based on changes in the tread rubber compound

As multiple slip ratios (a maximum of three) were tested in one run, the data acquired by the system needed to be filtered in order to separate the effect of every specific slip ratio. An equi-ripple filter was used for filtering the data. The post-processed performance curves of all the tires based on the drawbar pull coefficient are presented in this section. The curves show the average value of both the runs with an error bar signifying the values in which the drawbar pull coefficient of a specific slip ratio occurs. Before the experimental testing, every tire was cooled down in a freezer to temperatures much lower than the ice surface. Considering the rise in temperature during the removal from freezer, mounting of tire on the Kistler hub and the subsequent calibration process, it led to the temperature of the tire being slightly less or nearly equal to the ice temperature. This was done in order to replicate real-world conditions in which the tire is at temperatures similar to the ice surface.

At higher slip ratios on ice, an intermittent sticking of the tire to the ice occurs. This effect is perceptible when testing a single tire on the Terramechanics Rig. Except for the tires of rubber compound A, this effect was seen for all the tires. This may be attributed to the adhesive interaction of the specific tread rubber compound with ice. All the tires except tires F1 and H3 were tested at an ambient temperature of about 10-11°C whereas tire F1 and tire H3 were tested at an ambient temperature of approximately 6°C. As explained further in this section, the results of tire 1 and tire 3 of a specific rubber compound are not exactly identical in all the cases which may be due to change in the ambient temperature, change in the roughness of the rubber surface and/or the aging of the tire and hence the results are presented separately for tire 1 and tire 3 in the case of all the rubber compounds.

4.2.1. Testing Results of the tires

1. Rubber compound A

Both the tires of rubber compound A displayed nearly identical performance in the experimental testing conducted. The maximum value of the drawbar pull coefficient occurred at about 6% slip ratio and averaged about 0.24. The results for tires of rubber compound A are presented in Figure 4-1 and Figure 4-2.

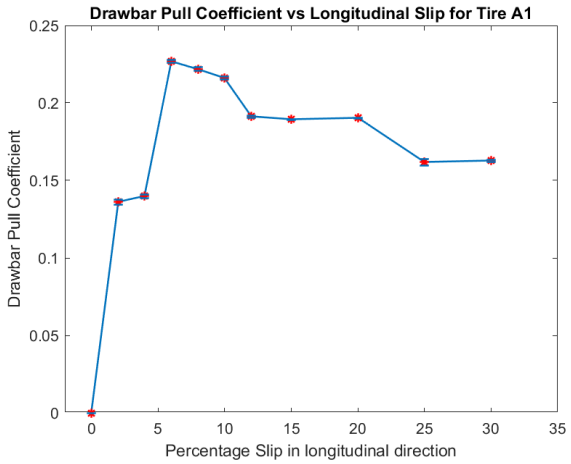

Figure 4-1: Drawbar Pull Coefficient vs Percentage Slip plot for tire A1

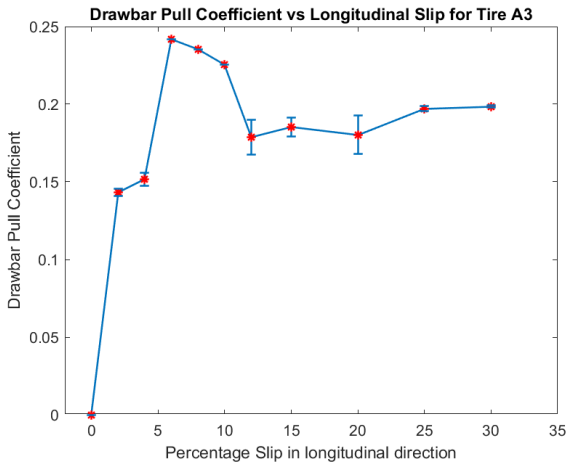

Figure 4-2: Drawbar Pull Coefficient vs Percentage Slip plot for tire A3

2. Rubber compound B

The tires of rubber compound B too displayed a peak value of drawbar pull at about 6% slip ratio and a plateau after that. The average of the peak values was about 0.27 and the performance of the tires is displayed in Figure 4-3 and Figure 4-4.

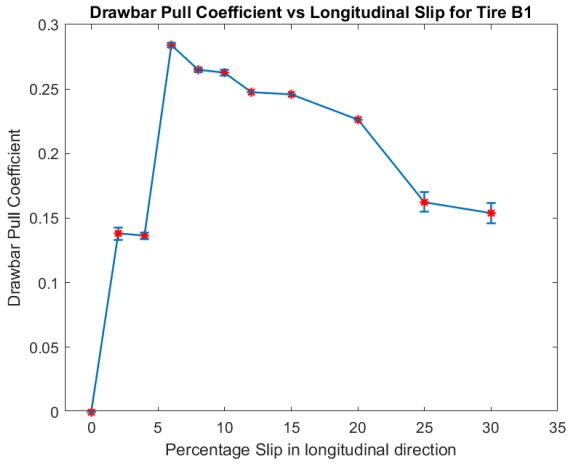

Figure 4-3: Drawbar Pull Coefficient vs Percentage Slip plot for Tire B1

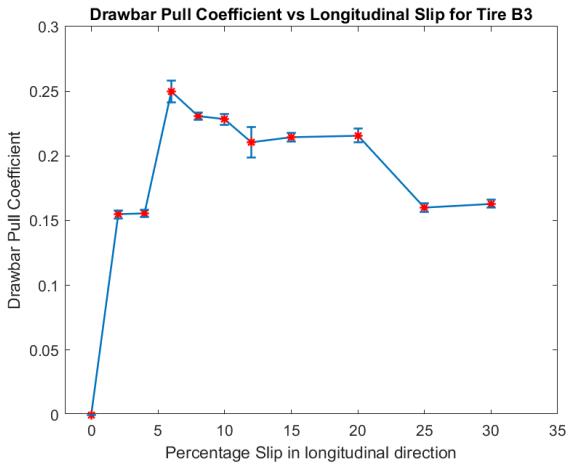

Figure 4-4: Drawbar Pull Coefficient vs Percentage Slip plot for Tire B3

3. Rubber compound C

The tires of rubber compound C had an average peak drawbar pull coefficient of about 0.16 and the results are presented in Figure 4-5 and Figure 4-6.

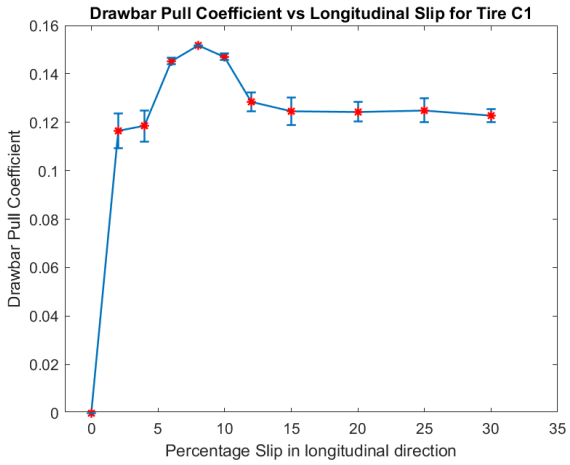

Figure 4-5: Drawbar Pull Coefficient vs Percentage Slip plot for Tire C1

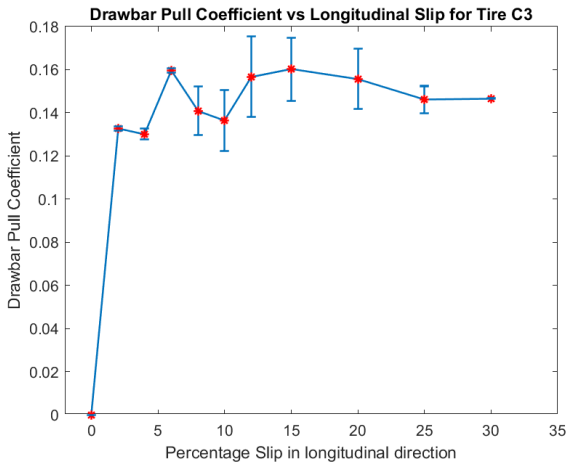

Figure 4-6: Drawbar Pull Coefficient vs Percentage Slip plot for Tire C3

4. Rubber compound D

The tires of rubber compound D averaged a maximum drawbar pull coefficient of about 0.29. A deviation in the behavior of both the tires was observed in the sense that one of them had the peak drawbar pull at 6% slip ratio whereas another one had a peak drawbar pull at 12% slip ratio. This anomaly was evident after several rounds of retesting, as shown in Figure 4-7 and Figure 4-8. As the exact constituents are not known for the tires, a valid justification cannot be proposed for these results and there exists a possibility that the rubber compound in both the tires may not have been exactly identical.

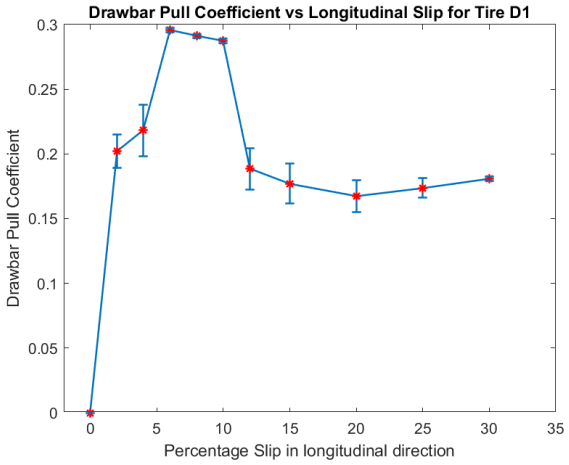

Figure 4-7: Drawbar Pull Coefficient vs Percentage Slip plot for Tire D1

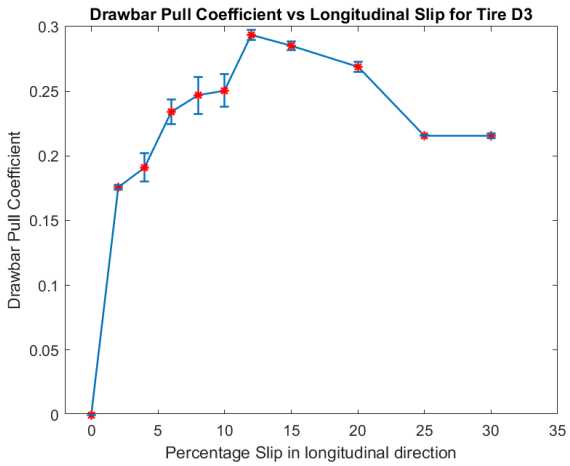

Figure 4-8: Drawbar Pull Coefficient vs Percentage Slip plot for Tire D3

5. Rubber Compound E

The tires of rubber compound E had an average value of the peak drawbar pull coefficient of about 0.2. In the case of tire E1, an upward trend was observed at 12% slip ratio in both the runs of the testing. There is a possibility that this could be because of the rubber compound itself or slight variation in the ambient temperature for the runs of 12-15-20 slip ratios. Due to this, except for these three slip ratios, the performance of both the tires is nearly identical as presented in Figure 4-9 and Figure 4-10.

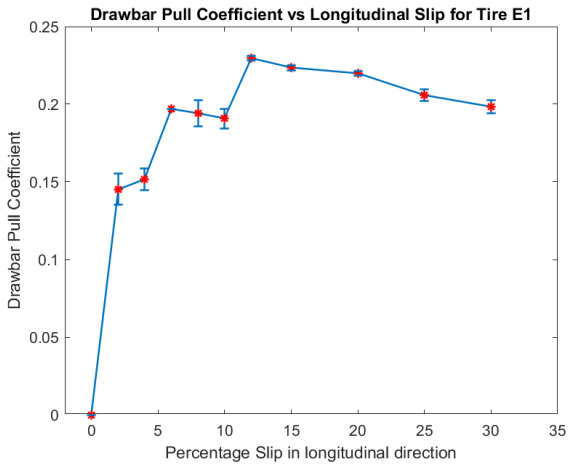

Figure 4-9: Drawbar Pull Coefficient vs Percentage Slip plot for Tire E1

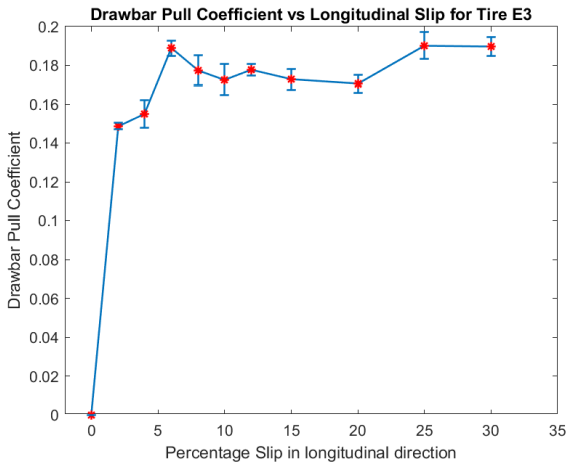

Figure 4-10: Drawbar Pull Coefficient vs Percentage Slip plot for Tire E3

6. Rubber Compound F

Due to constraints of the testing setup, the ambient temperature during the test cannot be controlled and hence adds uncertainty to the results. In the case of rubber compound F, both the tires could not be tested at the same ambient temperature. The ambient temperature during the testing of tire F1 was about 6°C whereas it was about 10°C during the tests conducted for tire F3. The results are shown in Figure 4-11 and Figure 4-12 for tire F1 and tire F3 respectively.

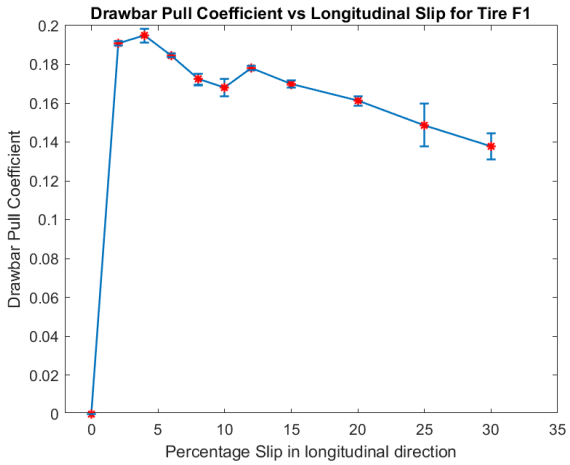

Figure 4-11: Drawbar Pull Coefficient vs Percentage Slip plot for Tire F1

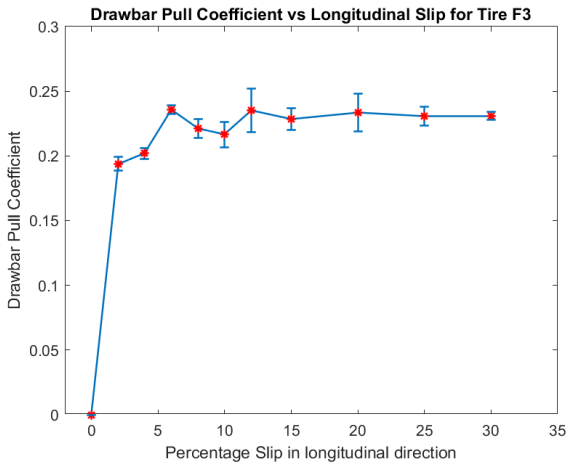

Figure 4-12: Drawbar Pull Coefficient vs Percentage Slip plot for Tire F3

7. Rubber Compound G

In the case of the tires of rubber compound G, both the tires performed nearly identical peaking at 6% slip ratio for and averaging a drawbar pull coefficient of about 0.19 as shown in Figure 4-13 and Figure 4-14.

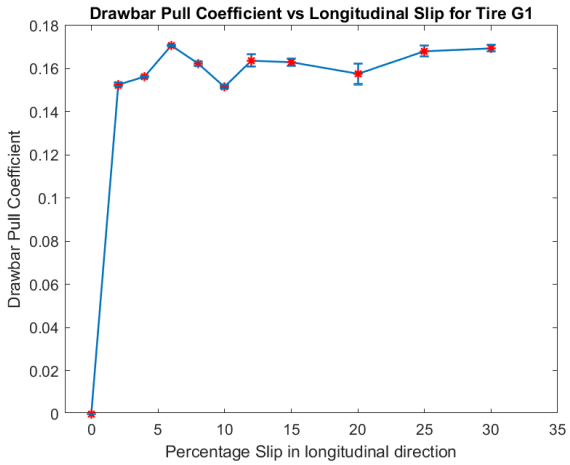

Figure 4-13: Drawbar Pull Coefficient vs Percentage Slip plot for Tire G1

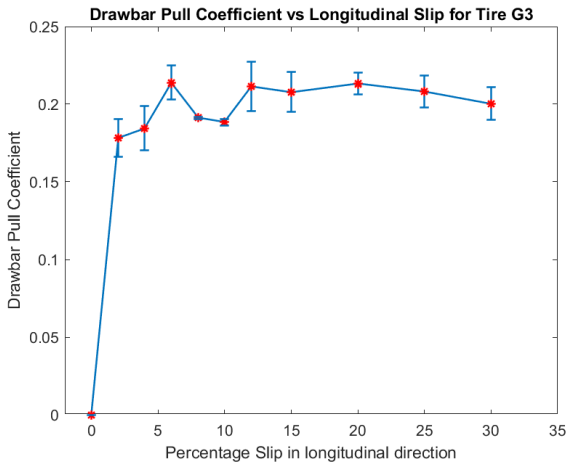

Figure 4-14: Drawbar Pull Coefficient vs Percentage Slip plot for Tire G3

8. Rubber Compound H

Tires of rubber compound H, too, could not be tested at the same ambient temperatures. The ambient temperature during experimental testing of tire H1 was about 11℃ while tire H3 was tested in the ambient temperature of about 6℃. Due to a temporary failure of the testing setup, even the latter part (slip ratio ≥12%) of tire H1 could not be tested at the same ambient temperature as the earlier part of the tire and was tested at about 8℃. This factor affected the results in the plateau (unstable) region. To account for this, the arrows in Figure 4-15 estimate the plausible value of the drawbar pull coefficient if the latter part, too, would have been tested at the same ambient temperature. The performance curve for tire H3, which has a lower ambient temperature, is shown in Figure 4-16.

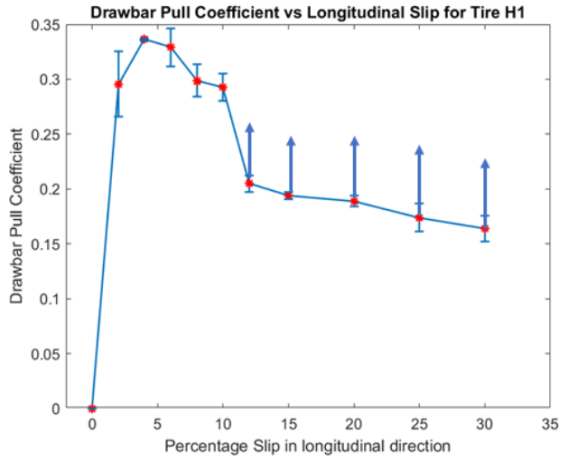

Figure 4-15: Drawbar Pull Coefficient vs Percentage Slip plot for Tire H1

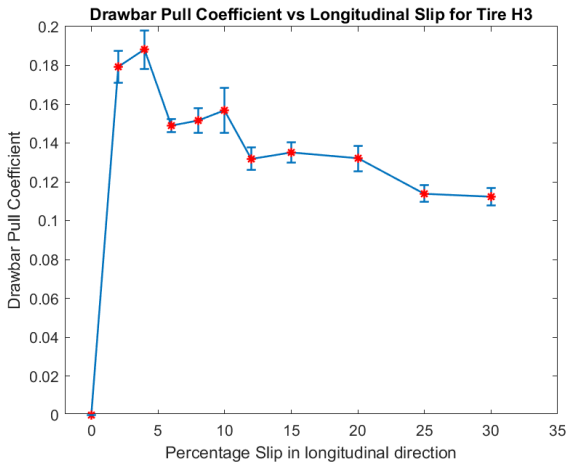

Figure 4-16: Drawbar Pull Coefficient vs Percentage Slip plot for Tire H3

4.2.2. Comparative results for change in rubber compounds in identical conditions

The average value of the drawbar pull coefficient for all the rubber compounds was plotted as a histogram for every slip ratio for comparative analysis of the effect of the rubber compound. For the averaging purpose in the case of rubber compounds F and H, the runs of tire F1 and tire H3 have been discarded as there was a difference in the ambient temperature. The plots for comparison of the equivalent coefficient of friction (vertical load normalized value of the resistive forces measured during free rolling) are shown in Figure 4-17. With consideration of the values of specific heat capacity available for 5 of the rubber compounds and discarding rubber compound B, it is noticeable that a decrease in the specific heat capacity results in an increase in the equivalent coefficient of friction which signifies the resistive forces in the free-rolling condition. As the peak drawbar pull coefficient occurred at 6% slip ratio for the majority of the tires, the relevant plot of comparison is shown in Figure 4-18. Additional results for the remaining slip ratios are presented in Appendix A.1.

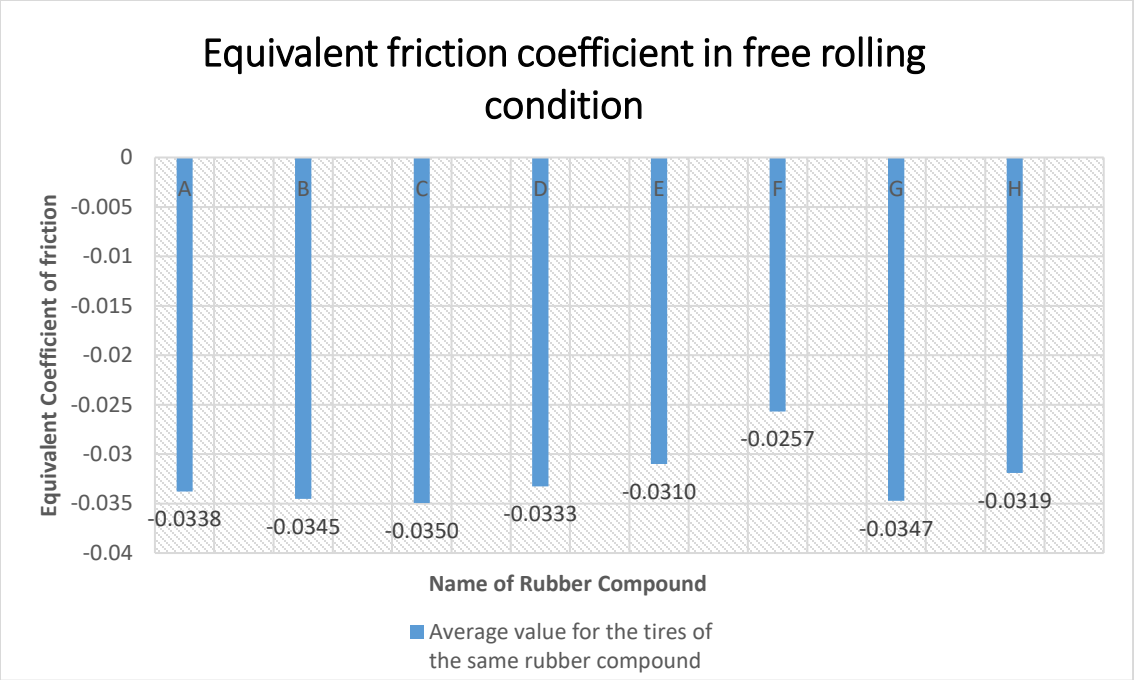

Figure 4-17: Plot of the average value of the equivalent coefficient of friction for comparative analysis for the effect of rubber compounds

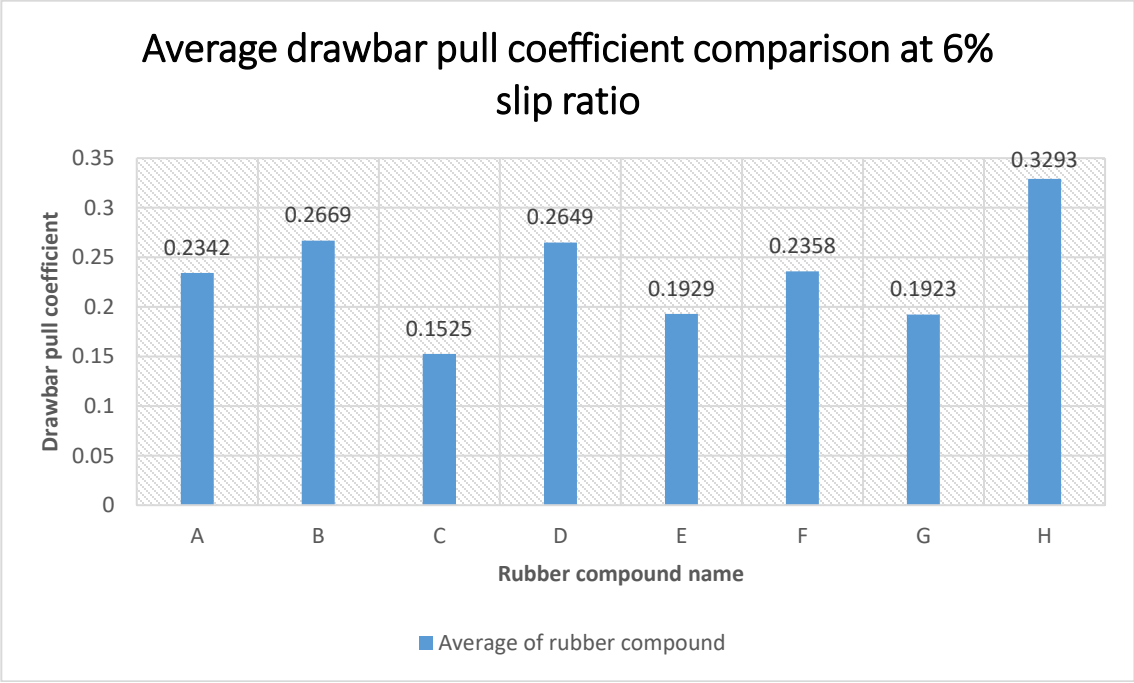

Figure 4-18: Plot of the average value of drawbar pull coefficient for comparative analysis for the effect of rubber compounds

As can be inferred from the performance curves of the tires and the comparison plots for the rubber compounds, tires of rubber compound C had the highest amount of resistive forces per unit normal load as well as the lowest amount of drawbar pull coefficient generated. Thus, it can

be postulated that the rubber compounds of tire C won't be an ideal candidate if the enhancement of tire performance on the ice was the goal. The next to the worst performance in both the aspects were displayed by rubber compound G. Another point of significance is that the drawbar pull coefficient for all 16 tires lies in a small range of each other in the higher slip ratio region whereas the effect of variation in the tread rubber compound is the most prominent in the stable/low slip ratio region which is also the region of maximum operation in real-world scenarios. The order of performance, from the best to the worst, of the tires based on the experimental investigation, with the drawbar pull coefficient as the criteria, is as follows:

H > D > B > A > F > E > G > C

A point worth noting is that this order of performance is based on the drawbar pull experienced by the tires at low velocities but replication of the same order of performance at higher velocity needs to be investigated. As described in Chapter 2, it was found that the reduction in the stiffness of the rubber sample led to an increase in the friction but as can be noted after comparing the material properties with the results above, we can deduce that this cannot be a singling out factor when analysis of the entire tire is concerned. The rubber compound H had a higher dynamic modulus and density in comparison with the other rubber compounds but the best performance was still yielded by rubber compound H. Thus, it can be deduced that the material properties provided cannot be the only significant factors and further investigation into other properties may be required to have a generalized conclusion.

4.3 Effect of the ambient temperature

The ambient temperature during the experimental investigation of the tires of rubber compounds F and H was different and the performance curves were shown earlier in section 4.2.1. The effect of the change in ambient temperature on the normalized resistive forces in the free-rolling condition is shown in Figure 4-19. It can be noticed that the ambient temperature also affects the resistive forces experienced by the tires. The effect of change in ambient temperature is more prominent in the case of tires of rubber compound H that rubber compound F. Even in the case of the peak value of the drawbar pull coefficient it is evident that for rubber compound H, this value is nearly halved when the two tires H1 and H3 are compared. This behavior, based on the properties available, could be due to the dynamic modulus of the rubber compounds. Rubber

compound H has a higher dynamic modulus and thus the effect of the reduction in ambient temperature on the stiffening of the rubber compound is more pronounced.

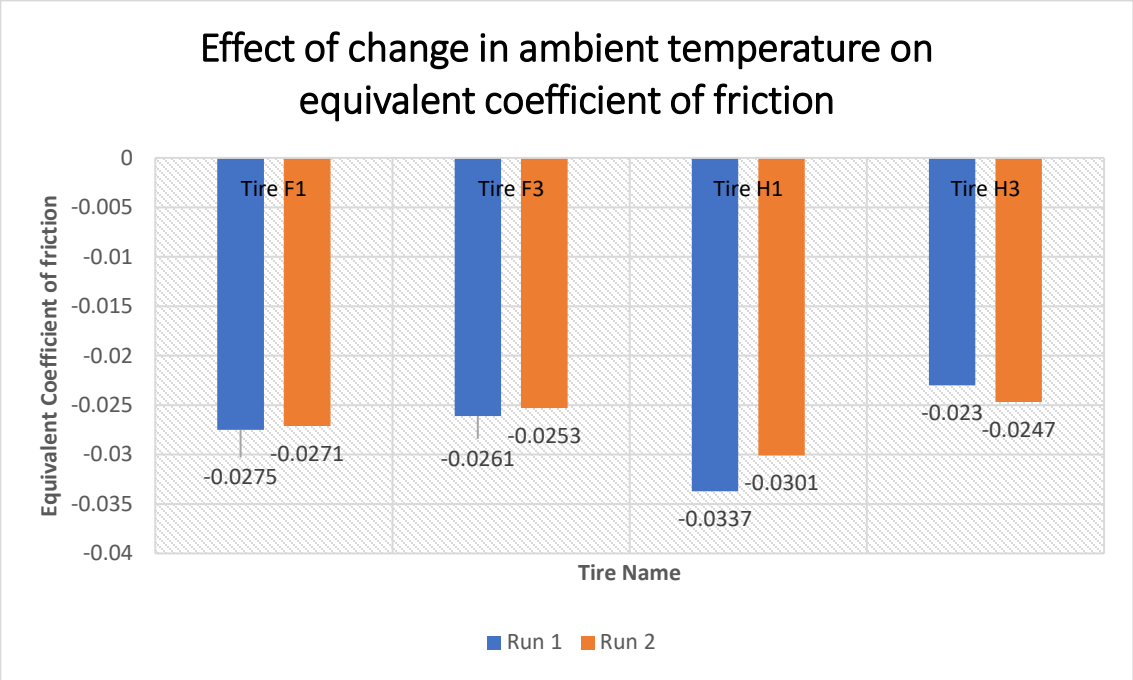

Figure 4-19: Effect of change in ambient temperature on the equivalent coefficient of friction

4.4 Effect of aging of a rubber compound

Three of the tires were tested in the previous winter, namely tires B3, C3, and G3. The conditions of the normal load and inflation pressure, as well as the method of the calibration, were different and hence a direct comparison was not feasible with the results of the previous year. It was thought upon that as the rubber compounds are identical, the tires tested earlier could be considered as aged more than the tires tested for the first time. The performance curves of the tires of these three rubber compounds were presented in Figure 4-3, Figure 4-4, Figure 4-5, Figure 4-6, Figure 4-13, and Figure 4-14.

Generally, we expect a reduction in the performance of the tire with aging, over a period of time. In the current scenario, it can be stated that this is evident only in the case of rubber compound B. In the cases of rubber compounds C and G, the aged tire performed better which is in contradiction to several studies found in the literature. This could be due to reasons related to uncertainty in the test rig, minor changes in the ambient temperature, etc. It is also possible that as

the tires were run only for 100 kms and then kept unused the effect of aging wasn't that prominent. Lastly, as in the case of rubber compound D, there is a possibility that this behavior could be an attribute of the rubber compound and thus the comparison of two tires, in this way, may not be entirely logical to arrive at a fair conclusion.

4.5 Experimental measurement of the rise in temperature in the tread region

All the tires were affixed with thermocouples in the grooves to measure the rise in temperature experimentally. The data was sent to the computer by the use of dataloggers transmitting data every 10 seconds through the network. The rise in temperature was plotted as a histogram by the averaging method (by discarding tires F1 and H3). The average rise in temperature, measured for a duration of 20 seconds during testing in the free-rolling condition is shown in Figure 4-20. The rise in temperature measured for the rubber compound H may be significantly high due to the lesser accuracy of the K-type thermocouples. Additional results are presented in Appendix A.2. Based on the available specific heat properties of 5 rubber compounds, it can be stated that a lower value of specific heat capacity implies a higher value of rise in temperature in the experimental data, which will also affect the water film formation at the interface. In most of the results, the rubber compound H had a higher value of average temperature rise and on similar lines of thinking, it can be speculated that rubber compound H will have the lowest specific heat capacity. Thus, it can be recommended that the tread rubber compound should have a higher specific heat capacity to reduce the height of the water film but more investigation with an even accurate measurement of temperature rise needs to be performed.

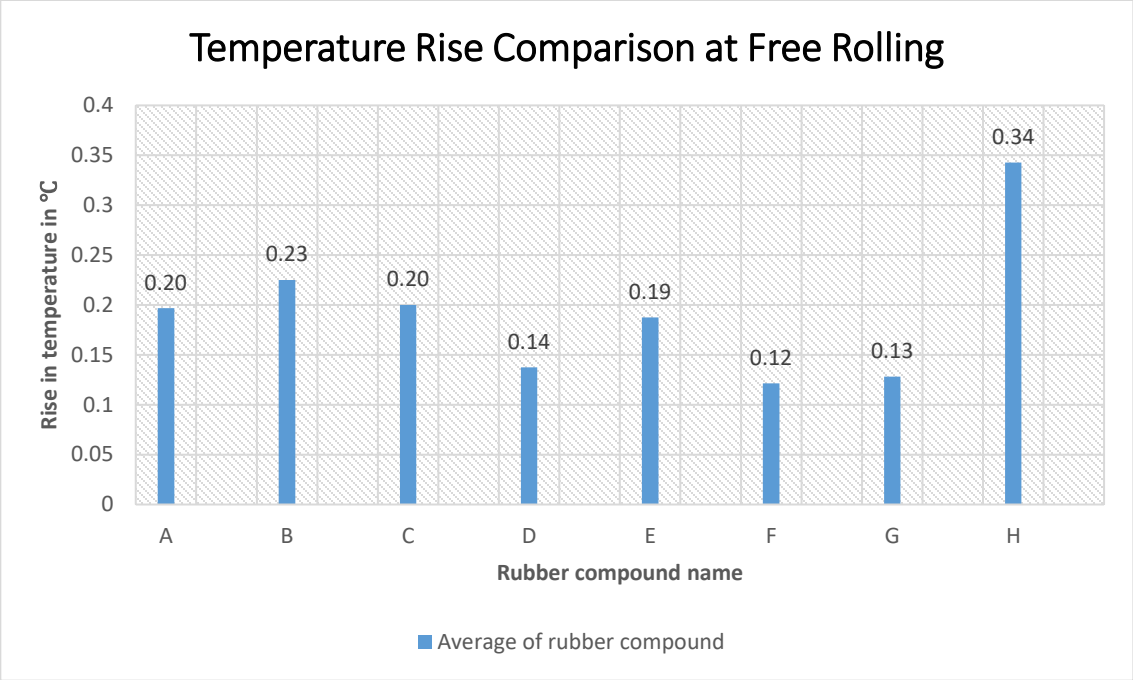

Figure 4-20: Comparison of the experimental rise in temperature for all rubber compounds during free rolling tests conducted on ice

Chapter 5 Modeling and Parametrization

Analysis of the pressure distribution data measured for all the tires with several classical analytical models was performed to compare the predictions against the in-house developed model ATIIM 2.0. An attempt to parametrize the Pacejka Magic Formula tire model (Pacejka and Bakker, 1992) was performed on the experimental results of all the tires to see the extent to which the magic formula parameters are affected by the tread rubber compound and the ambient temperature.

5.1. Simulation results of the predicted rise in temperature and height of water film from ATIIM 2.0

ATIIM 2.0 is a model developed by Mousavi et al. (Mousavi and Sandu, 2020a), with further improvements to ATIIM, to incorporate more properties related to the rubber compound like the roughness of the rubber and incorporation of a time-independent method for estimation of height of water film. The collected pressure distribution needs to be zero-padded in the areas apart from the contact patch to remove the noise/disturbances sensed by the pressure sensors in those regions. Occasionally, it is possible that an array of sensors in the lateral direction of tire movement may be faulty and/or not detect the pressure in the region, as shown in Figure 5-1. In such a case interpolation of data is used to estimate the values that could have been recorded by the sensor. The emergence of this fault generally occurs over repeated use of a pressure pad. It could be due to the squeezing of the pressure pad that occurs at high slip ratios, as shown in Figure 5-2. The best way to delay the fault emergence employed during this work is to have the protective film fixed as tight as possible against the direction of tire motion and avoiding the pressure pad to stay in the apparatus when not in use as it gets stuck to the Photodon 6HS Tempered Glass protective film, possibly due to the high pressures during testing.

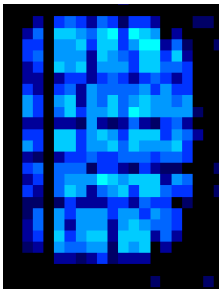

Figure 5-1: Array of pressure measurements missing in a specific run of a tire over the pressure measurement system

Figure 5-2: Squeezing of the pressure distribution setup when a tire is rotating with 12% slip ratio

5.1.1. Results for the rise in temperature

The rise in temperature in the contact patch by ATIIM is calculated using Jaeger's formulation. The finite difference formulation of the same is detailed by Fujikawa et al (Fujikawa et al., 1994). For rubber compounds, A, E, and D, the specific heat properties of rubber compound G were used. As the only properties required for temperature rise simulations were the specific heat and density (thermal conductivity being constant), it was assumed that rubber compound D had a density equivalent to rubber compound F and specific heat equivalent to rubber compound G. The results of the simulations run for 4% slip ratio are presented in Table 5-1. The assumed static coefficient of friction was 0.1, similar to the procedure followed during the experimental investigation. A point of significance observed was that the emergence of wet regions, due to a rise in temperature overcoming the difference between bulk ice temperature and melting point, did not start till the slip ratio equaled or exceeded 10% slip ratio. The direction of motion of the tire is from left to right for the simulations presented. The point of the highest rise in temperature

generally is observed as the tread progresses from the leading to the trailing edge of the contact patch. Another point of significance observed is that in many cases throughout the simulations of all the configurations, the point of highest temperature rise was also observed on tread blocks near the periphery of the contact patch in the lateral direction. Additional results for the rise in temperature simulation are shown in Appendix B. 1.

Table 5-1: Rise in temperature simulation for all the tires at 4% slip ratio using ATIIM

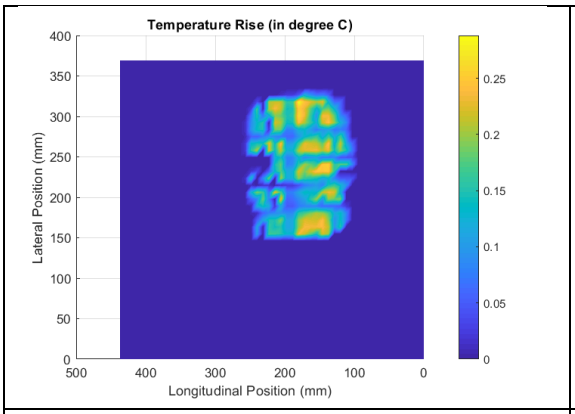	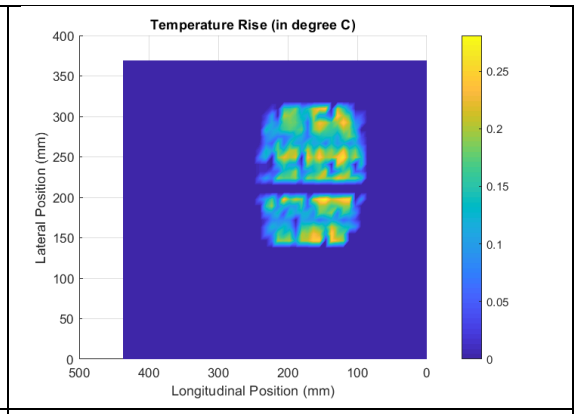
Tire A1	*Tire A3*
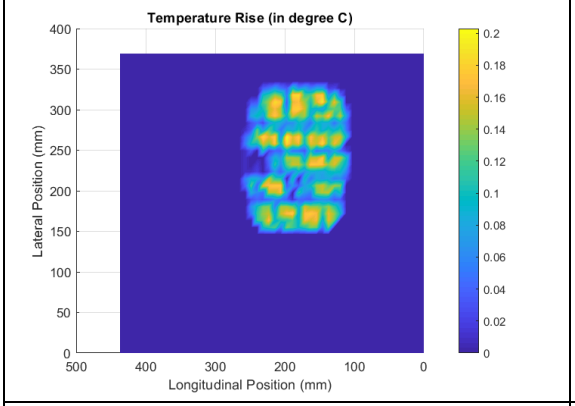	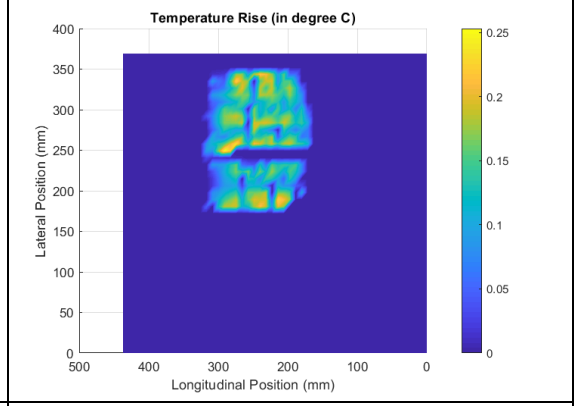
Tire B1	*Tire B3*
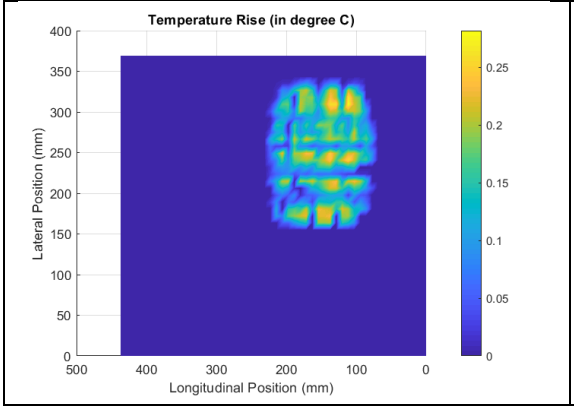	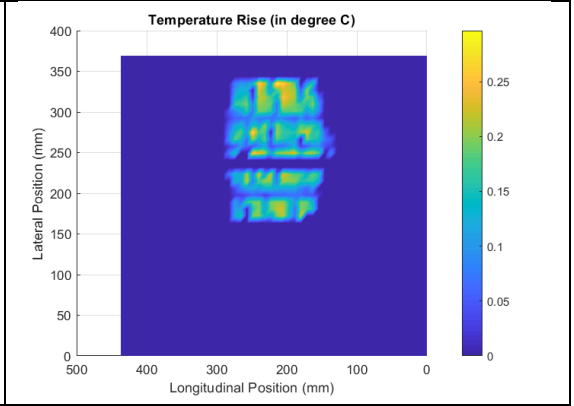
Tire C1	*Tire C3*

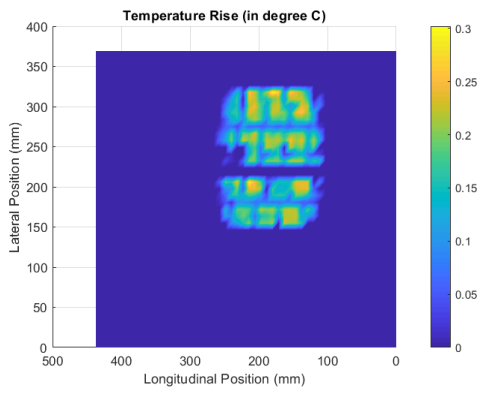

Tire D1

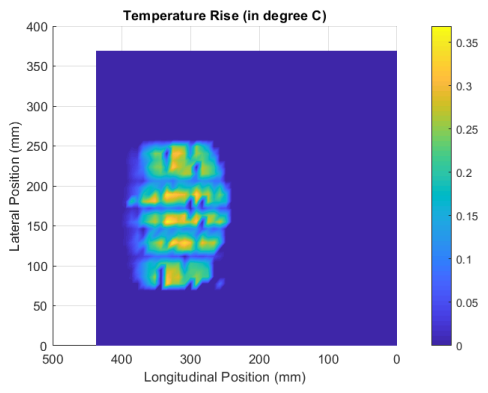

Tire D3

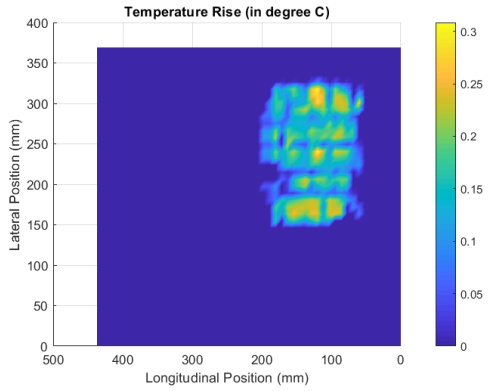

Tire E1

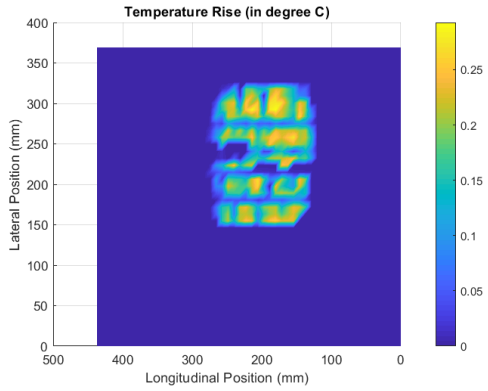

Tire E3

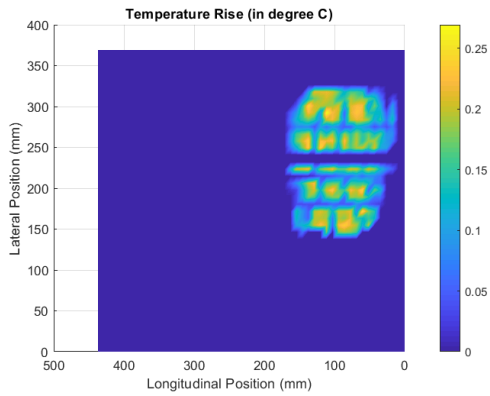

Tire F1

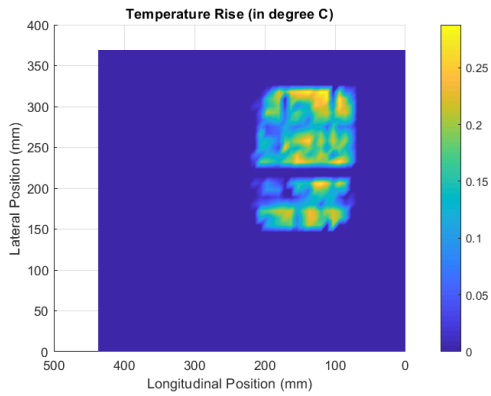

Tire F3

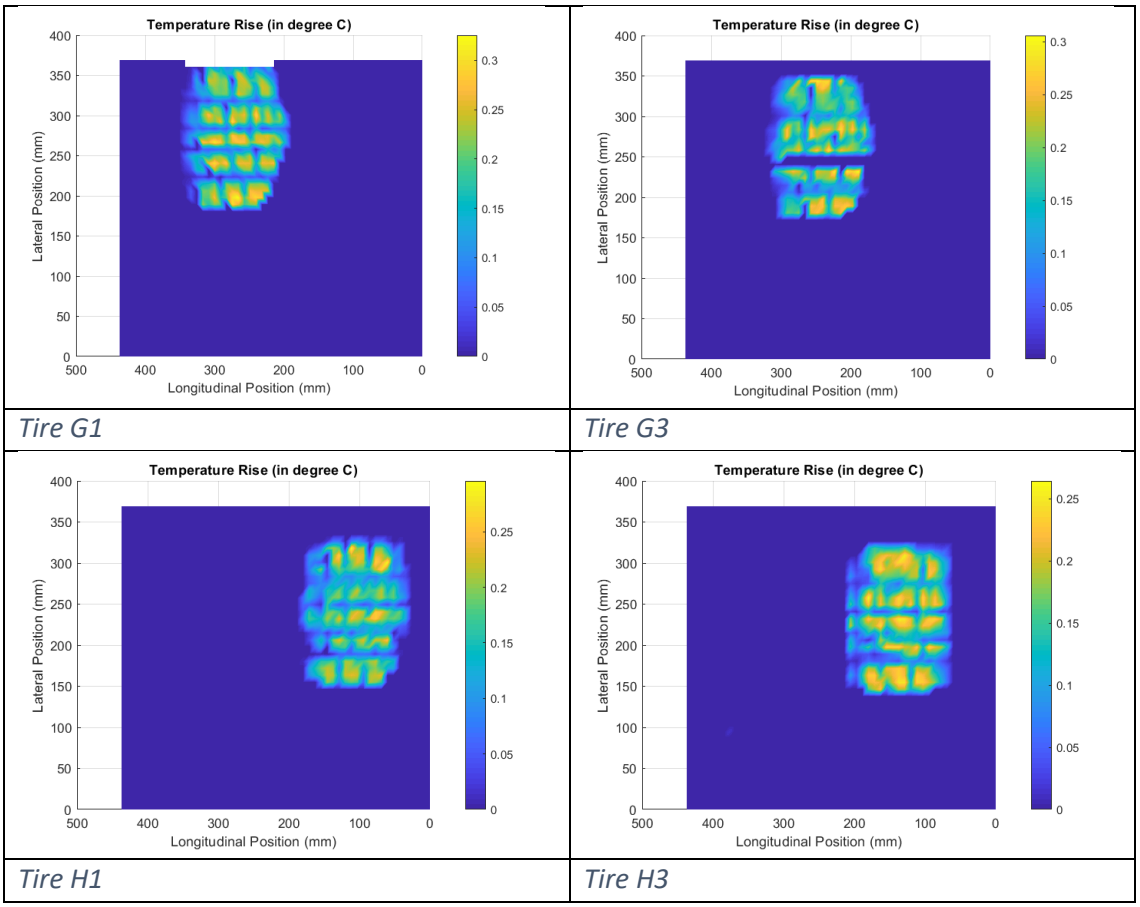

5.1.2. Results for the height of water film

The estimation of the height of water film was performed using ATIIM 2.0. The specific heat properties of rubber compound G were used for simulation of the rubber compounds A, E, and H, as their properties were not available. As the physical properties of rubber compound D were not available, the simulations for rubber compound D were not run. The values of the mean root square gradient ($\nabla z = 0.35$) and the roughness parameter (l_r = 6.5 µm) were taken from the literature (Wiese et al., 2012). The estimated height of water film for all the tires in the 4% slip ratio configuration is shown in Table 5-2. Additional results for estimation of height of water film are presented in Appendix B. 2. Some of the generalized conclusions from the simulations are:

- The water film height increased as the slip ratio increases in the conditions of all the tires. The differences in the rubber compound do not affect this generalized trend though the average height and maxima get affected.

- The predicted height of the water film was found to be higher in the case of tire 3 in many configurations. This effect could be attributed to some of the assumptions related to the properties of the rubber compounds, roughness, etc. or due to variations in the measured pressure distribution of the tire.

Table 5-2: Estimated height of water film for all tires simulated using ATIIM 2.0 in 4% slip ratio configuration

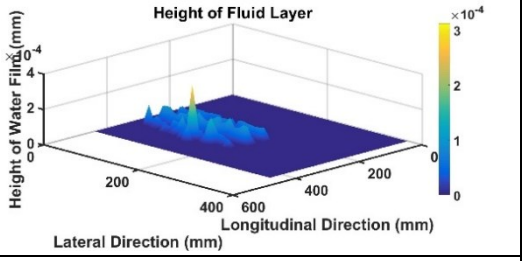	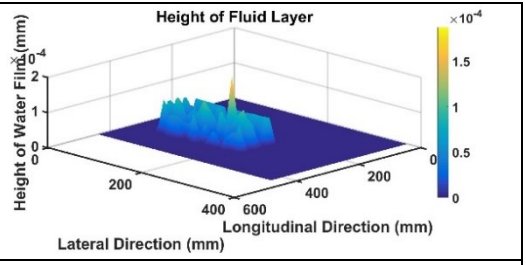
Tire A1	*Tire A3*
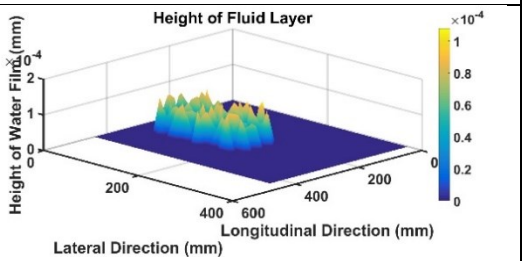	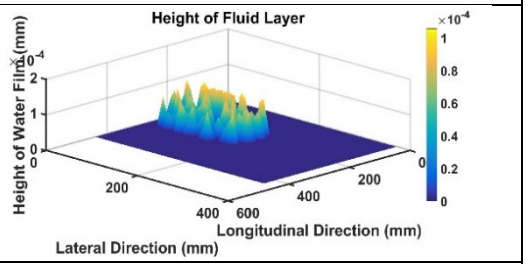
Tire B1	*Tire B3*
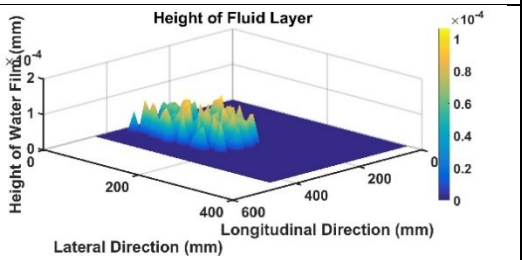	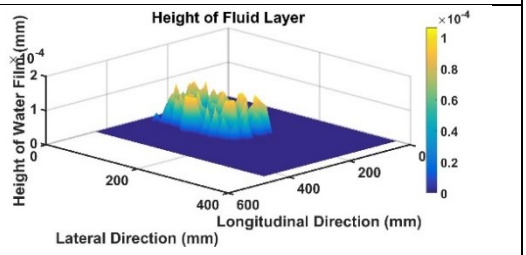
Tire C1	*Tire C3*
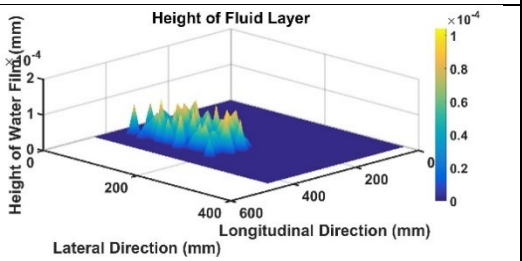	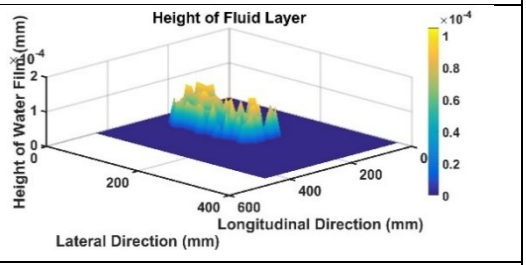
Tire E1	*Tire E3*

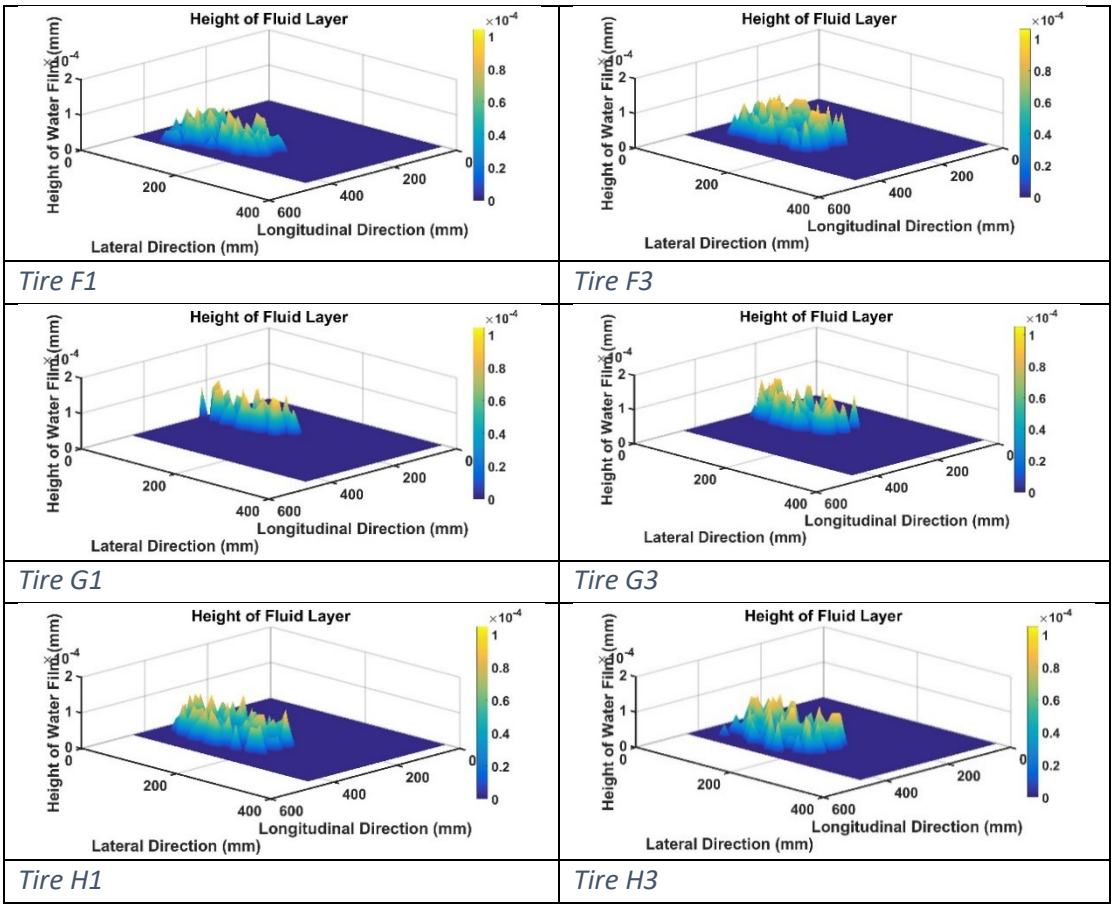

5.2. Capabilities of Classical Tire-Ice Models and of the ATIIM2.0

Some of the classical friction models for modeling the tire-ice contact were described in sections 2.5.4 and 2.5.5. The only inputs required for these models from the experimental data are the dimensions of the contact patch which could be obtained from the preprocessed pressure pad data, and the material properties. The specific heat properties for rubber compounds A, D, E and H were assumed to be same as rubber compound G whereas the density of rubber compound D was assumed to be equivalent to rubber compound F. Though the static coefficient of friction measured during the experimental testing on ice was 0.1, the static coefficient of friction assumed for the simulations in this section were 0.15, which is equivalent to the pressure measurement system (Jimenez, 2018).

5.2.1. Predictions from Hayhoe and Shapley model

As explained in section 2.5.4, this model assumes no heat flows into the tire for estimation of the temperature rise and the point of transition. As this would nearly nullify the effect of the rubber compound, it was overridden as explained in section 2.5.4. Due to these, sometimes the point of transition occurred outside the length of the contact patch, which implies the non-occurrence of melting. The value of the fluid friction coefficient in such a scenario was assumed to be zero as it wouldn't be logical to calculate friction occurring from fluid without melting of ice. The occurrence of the point of transition from the leading edge in all the cases is as shown in Figure 5-4. As can be inferred, with a rise in slip ratio the transition point moves towards the leading edge of the contact patch, thus implying more area being under fluid friction which lowers the overall value of the friction experienced by the tire, which can be seen in Figure 5-3. The rise in temperature for rubber compound B in all the cases is presented in Figure 5-5. It can be inferred that this model does capture the effect of more rise in temperature in the rear of the contact patch and the slip ratio having a direct effect on the rise in temperature. The variation of temperature rise in the lateral part of the contact patch cannot be captured and even the effect of the tread pattern, which is a characteristic of winter tires, will not affect the predictions of this model which are drawbacks of the assumptions made during the modeling process. One of the conclusions which is similar to the experimental results is that with an increase in slip ratio the variance in the coefficient of friction experienced by the various tires decreases as compared to the variance in the lower slip region. Another point worthy of interest is that even though the ranking of the predicted friction coefficients differs from the observed ranking from experimental results, the highest-ranked (rubber compound H) is the same, which reinforces the fact that the density of the rubber compound plays a huge role in the contact of the tire-ice phenomenon. The predicted order of total coefficient of friction is as follows:

H>F>D>G>A>E>C>B

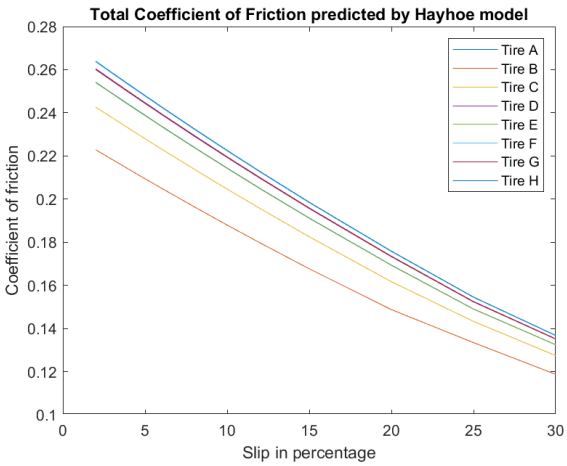

Figure 5-3: Total coefficient of friction prediction by Hayhoe and Shapley model

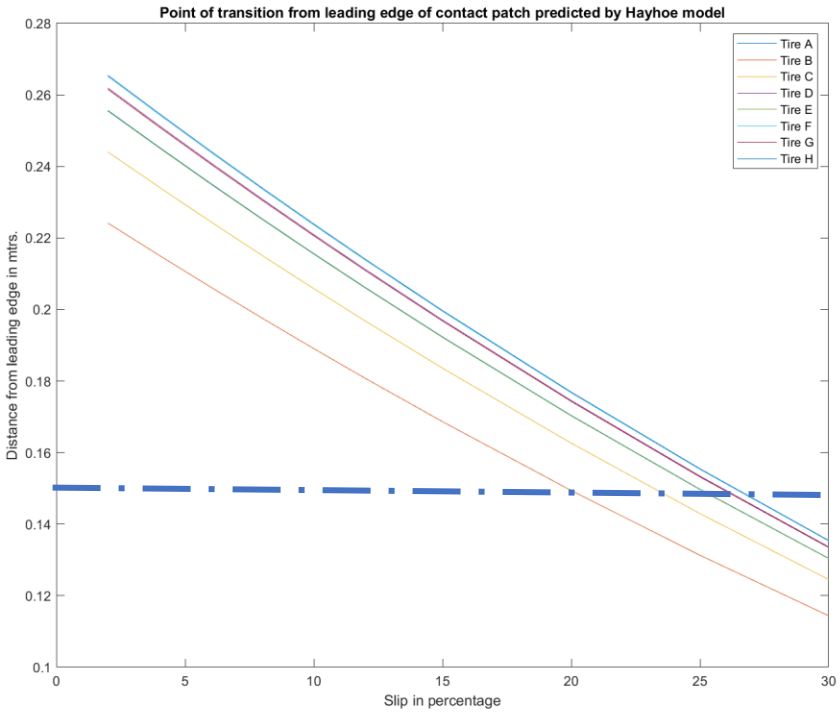

Figure 5-4: Variation in point of transition for all tires with a change in slip ratio for Hayhoe and Shapley model

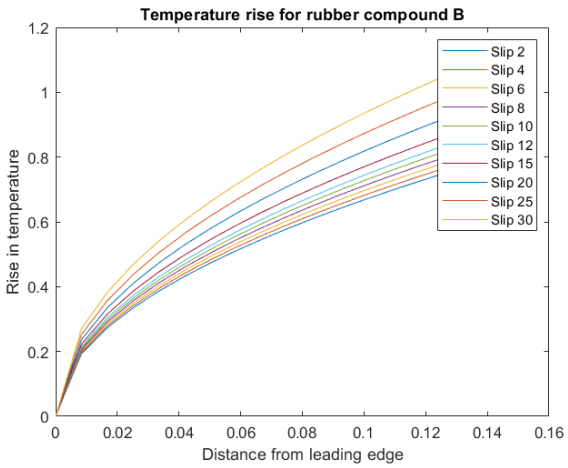

Figure 5-5: Temperature rise for rubber compound B by simulation using Hayhoe and Shapley model

5.2.2. Predictions from 2nd Peng model

The 2nd Peng model bypasses the step of estimating the height of water film for calculation of the friction coefficients. With the assumed static coefficient of friction, the point of transition still occurred outside the contact patch in some cases. A condition was enforced to eliminate the effect of the coefficient of the fluid frictional resistance in such cases. Similar to the predictions of the Hayhoe model, the point of transition moved from the trailing to the leading edge, as presented in Figure 5-7, implying an increase in the area where fluid friction takes effect but the coefficient of fluid friction saw a decrease in its value with an increase in slip ratio as shown in Figure 5-6. This behavior does not make sense in comparison to other studies in this area where the fluid friction increases with an increase in slip ratio. The average value of the friction coefficient decreased with an increase in slip ratio, as shown in Figure 5-8. The order of the predicted average coefficient of friction is as follows:

H>F>D>G>A>E>C>B

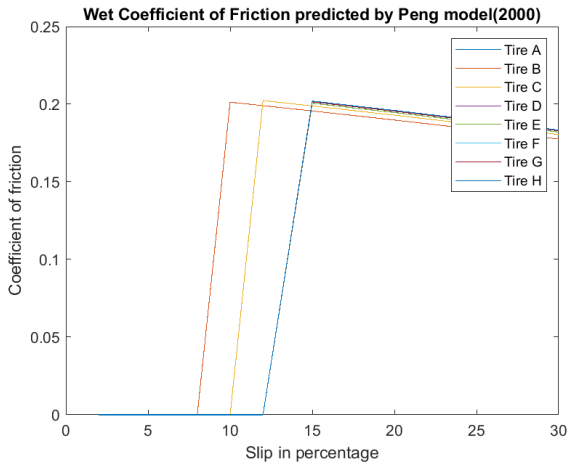

Figure 5-6: Coefficient of fluid friction predicted by the 2nd Peng model

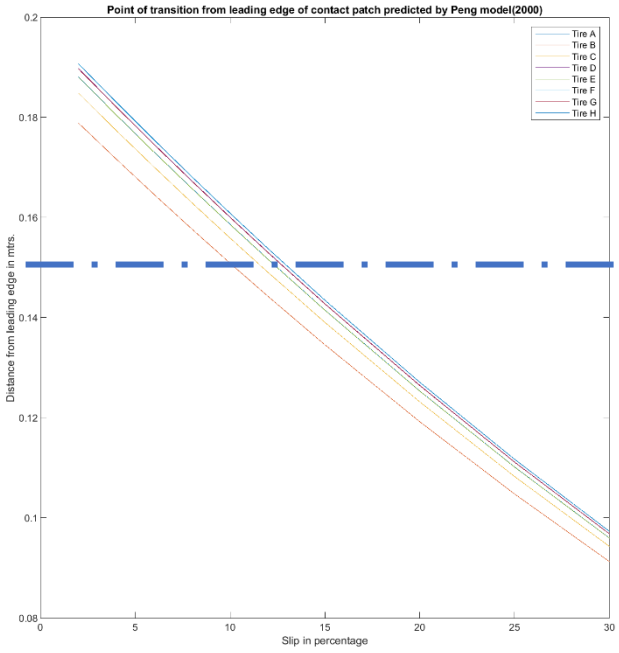

Figure 5-7: Point of transition prediction by 2nd Peng model

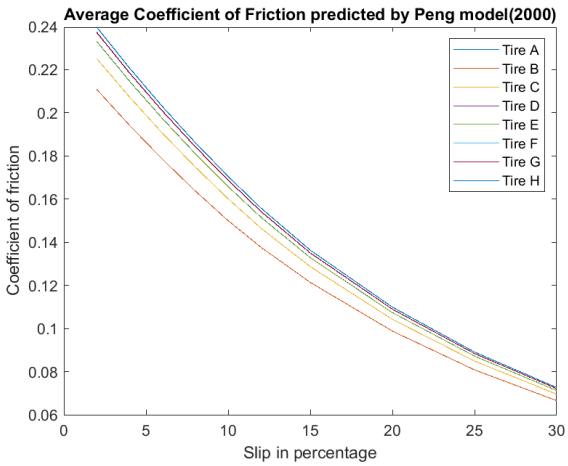

Figure 5-8: Average coefficient of friction predicted by 2nd Peng model

5.2.3. Predictions from 1st Peng model

The 1st Peng model as explained in section 2.5.5, calculates the phase transition location from the trailing edge of the contact patch. With the properties of the compounds available, the occurrence of the phase transition location being negative signifies that there is no melting in the contact patch, as shown in Figure 5-12. One of the similarities in both the Peng models is that even though the method to calculate the point of transition is different both the models predict initiation of melting in the 8-12 % slip ratio range, summarizing all the rubber compounds. The 2nd half of the right-hand side of eq. (2.15), can be considered as the contribution from the wet regions to the average coefficient of friction. In the cases where melting does not occur, the height of fluid film and the wet friction coefficient is considered to be zero and is presented in Figure 5-9 and Figure 5-10. Though even in this model, we see that the wet friction coefficient reduces with increase in slip ratio which may not be realistic, as we expect the value to increase as the wet region increases, the values of the fluid friction coefficient predicted by this model seem far more realistic than the 2nd Peng model when compared with similar studies. The predicted height of water film increases with slip ratio and the order of magnitude of the water film is in nanometers which is comparable to the order of magnitude of the water film height predicted by ATIIM 2.0. The predicted value of the average coefficient of friction predicted using this model is shown in Figure 5-11. The order of the predicted average coefficient of friction is as follows:

H>F>D>G>A>E>C>B

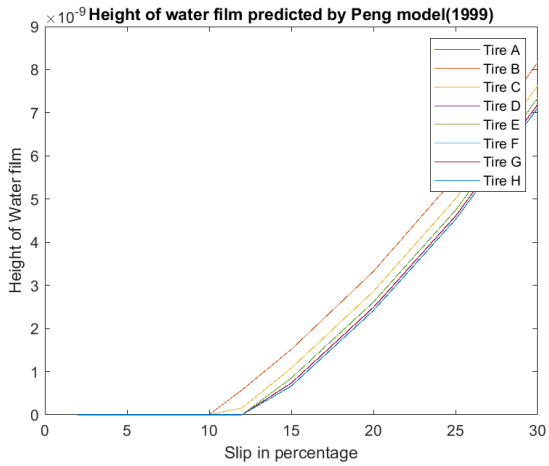

Figure 5-9: Estimated height of water film varying with the slip in the 1st Peng model

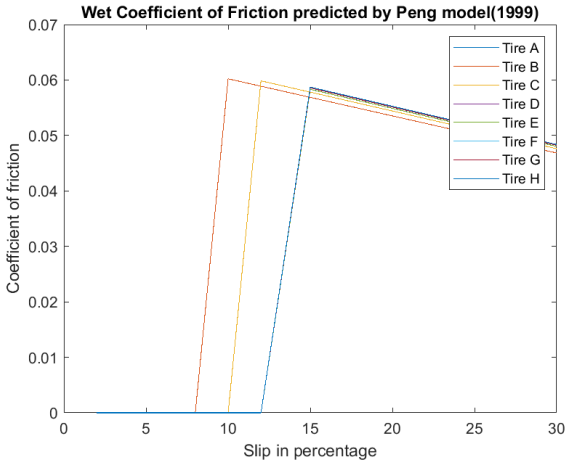

Figure 5-10: Predicted wet coefficient of friction from 1st Peng model

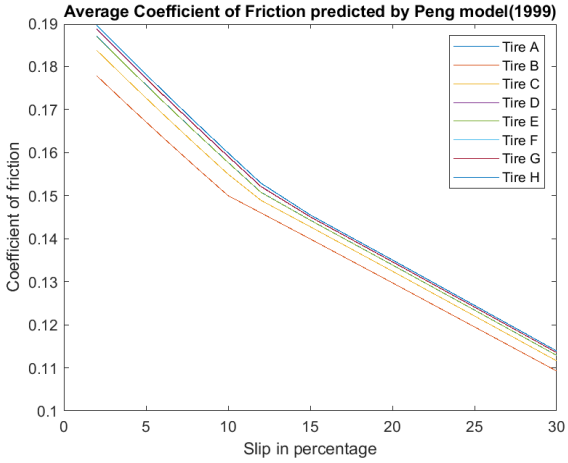

Figure 5-11: Average coefficient of friction predicted by 1st Peng model

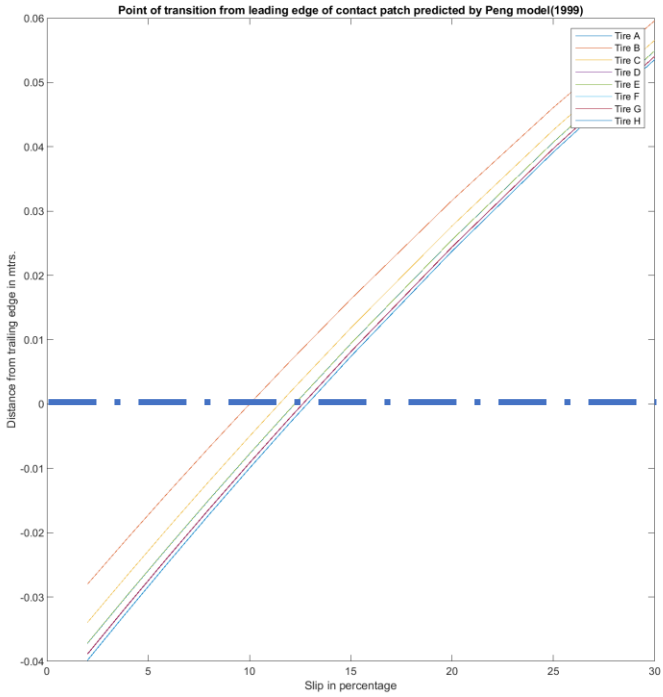

Figure 5-12: Point of transition variation with slip ratio for all rubber compounds by 1st Peng model

Thus, in conclusion, it can be stated that the classical models may have their advantages to some extent but fail to capture the holistic picture regarding the tire-ice phenomenon. It can be also noticed that the prediction of the initiation of melting is overestimated by the Hayhoe model where melting is initiated near the 20% slip ratio range whereas the estimation of the range at which melting initiates is nearly the same in case of both the Peng models and the simulation presented in section 5.1.1. This can be considered as a drawback of the Hayhoe model which leads to an overestimation of the slip ratio at which melting initiates in case of most of the tires. Another drawback of all the three classical models, especially the Hayhoe model, is the neglect of the variation of pressure in the lateral directions. Based on the simulations presented in Table 5-1, it is deductible that the variation in the lateral direction saw the points of highest temperature rise. This could be due to several reasons, one of which is the small number of material properties considered. Another drawback is neglecting the effect in the lateral direction of the contact patch and assuming uniform pressure throughout the contact patch which is not the real-life scenario and cannot even capture the variations due to tread patterns which are a characteristic of winter tires. As ATIIM and ATIIM2.0 consider the effects of variation of pressure in the lateral direction, it is

found that the prediction of the temperature rise and water film height at the contact patch respectively is much more accurate in the case of these models, especially in the case of winter tires which have a characteristic asymmetric tread pattern. ATIIM2.0 also considers the effect of the roughness of the rubber which maybe different even if the tread rubber compound is same and is affected by various factors especially the abrasion due to use. The radii of spherical asperities of the rubber and its distribution are two more parameters considered by ATIIM2.0 to predict the height of water film which is found to have an effect on the friction experienced by the tires and are thus of vital importance especially in the analysis of the tread rubber compound effect.

5.3. Parametrization of the Pacejka Magic Formula Tire Model

One of the most popular empirical tire models used for estimation of the force and moment characteristics of the tire is the *'Magic Formula Tire Model'* developed by Pacejka and Bakker (Pacejka and Bakker, 1992). The capabilities of the general formulation of this model include the estimation of the longitudinal force, the lateral force, and the aligning moment characteristics. Based on the focus of this work, only the estimation of longitudinal force in the pure slip condition is considered. In the case of the pure slip, the formula estimates the longitudinal force for a prescribed value of the slip, *'s'* and the camber angle, *'γ'* as shown in eqns. (5.1) - (5.3).

$$F_x(s) = D\sin(C * \tan^{-1}(B * s - E(B * s - \tan^{-1}(B * s)))) \tag{5.1}$$

where

$$F_{long.}(S) = F_x(s) + S_v \tag{5.2}$$

$$s = S + S_h \tag{5.3}$$

where 'S_v' and 'S_h' are the vertical and horizontal shifts at the origin.

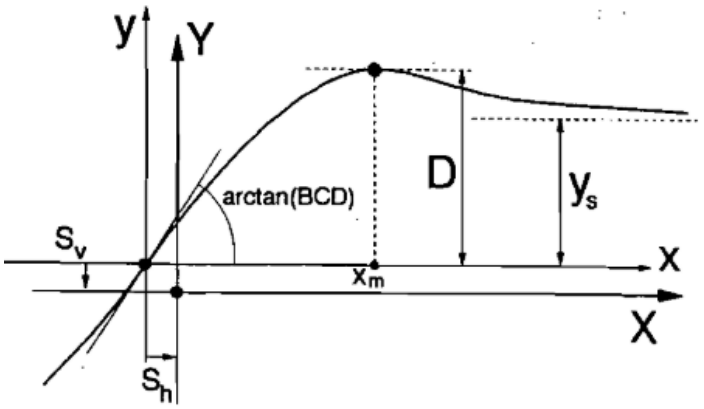

Figure 5-13: A standard curve resulting from the magic formula tire model (Pacejka and Bakker, 1992)

The shifts were assumed to be zero as a part of this work. Amongst, the coefficients presented in eq. (5.1), *'B'* is called the stiffness factor, *'C'* is referred to as the shape factor, *'D'* is the factor describing the peak value and *'E'* is the curvature factor. The peak value factor is the measure of the expected theoretical peak with respect to the slip-axis. The shape factor controls the extent to which the argument of the sine function can vary and thus is an important influence on the final curve. The stiffness factor controls the slope at the origin which is determined by the product of the stiffness factor, the peak value factor, and the shape factor. The curvature factor controls the curvature in the peak region of the curve as well as the slip value at which the peak occurs, in case the peak exists. The estimation of the factors based on Figure 5-13 can be explained by eqns. (5.4) to (5.7).

$$D = y_m \; if \; C \geq 1 \tag{5.4}$$

$$C = 1 \pm (1 - \frac{2}{\pi}\sin^{-1}\frac{y_s}{D}) \tag{5.5}$$

$$B = \frac{\tan(\tan^{-1}(BCD))}{CD} \tag{5.6}$$

$$E = \frac{B*x_m - \tan\left(\frac{\pi}{2C}\right)}{B*x_m - \tan^{-1}(B*x_m)} \; if \; C > 1 \tag{5.7}$$

Generally, the data to parametrize the Magic Formula is collected at high speeds of rotation of tires, which is not possible in the Terramechanics rig in the lab. As was found by Van Oosten (Van Oosten, 1999), an accurate portrayal of the Magic Formula parameters with the inclusion of camber effects during steady state cornering requires conducting about 159 experiments on each tire. Considering these facts, the results presented in this section can be considered as an attempt

to see the effects on individual parameters but the accuracy of the obtained parameters in comparison with data collected in real-life scenarios or through finite element modeling has not been validated and is a limitation of the results obtained.

Various algorithms have been devised and widely used for the parametrization of models from data. The least-squares optimization technique is one of the simplest techniques commonly used in optimization. Newton's method, Gauss-Newton method, and Levenberg-Marquardt technique are some of the algorithms used for solving non-linear optimization problems as in this case. One of the drawbacks of the least-squares method is its sensitivity to outliers. Another drawback is the dependency on the initial guess provided. A perceptible change in the value of the initial guess for the parameters can altogether change the final value estimated by the algorithm. In the case of the methods mentioned above, this could be attributed to the Taylor series approximation used, which is very efficient for local convergence but may not achieve the global minima (Hansen et al., 2012).

In the case of the Genetic Algorithm (GA), the sensibility to the initial guess is mostly relaxed although a reasonable range of bounds needs to be provided to the algorithm. Extensive work on GA was developed by Goldberg (Goldberg, 1989). A prior effort to parametrize and model the effect on the Magic Formula parameters, due to variation in soil compaction and inflation pressure of the tire was performed by He (He, 2019). Genetic Algorithms are based on the principles of genetics and natural selection from the theories of evolutionary biology. It is a combination of the survival of the fittest theory with a randomly generated populace to create an algorithm that will try to achieve the required optimization by creating future generations from the best parents of the previous generation. The algorithm differs from other optimization algorithms as it works with a set of parameters instead of the individual parameters to reach the desired optimization. This is achieved by evaluation using a population of the points (between the upper and lower bounds set) and not by some finite initial guess set by the user. Also, the evaluation or input of the gradient function is not required to have better optimization. The type of genetic algorithm used for optimization in this work is the real-coded genetic algorithm to avoid the drawbacks of the binary-coded genetic algorithm. The working is based on a randomly generated prescribed number of population which is then evaluated against the cost function. Based on the evaluated value of the cost function, the parents are chosen for the next generation for the reproduction phase. In the reproduction phase, the offspring is created by crossing over the

chromosome of the parents, based on a uniform normal distribution. This crossover operation is governed by the crossover probability. After performing the crossover, the mutation module adds some variation to the values of the genes within a small range. Due to this, the probability of mutation should not be too high as it may lead to oscillations in a region that may be far away from the global minima. Optimally, the mutation probability is set to be much lower than the crossover probability. The individuals of the new generation (offspring) are then evaluated against the cost function to find the best individuals for selection and reproduction in the next iteration/generation. Sometimes during the entire reproduction phase, it is possible that the parameters of an offspring may go beyond the bounds. To avoid this a constraint was added to the algorithm enforcing no deviation from the bounds of the individual parameters. The values of the parameters set for the optimization are shown in Table 5-3.

Table 5-3: Value of parameters for Genetic Algorithm

Sr. No.	Parameter of the algorithm	Set Value
1	Number of iterations	40000
2	Crossover probability	0.4
3	Mutation probability	0.05
4	Population	100
5	Stop condition	5% of F_z

The implementation of the optimization algorithm was performed on the average value of both runs of the specific tire as well as with the minimization of the cost function for both the runs. The values found for the stiffness factor, the shape factor, the peak value factor, and the curvature factor were close for a specific tire in both the cases with the lower value of the cost function in the optimization run for the average of both the runs. In nearly all the cases the algorithm ran for the total number of iterations, signifying that the stop condition has not been met. This could be due to the stop condition defined as being very stringent. It could also be attributed to the variances and uncertainties in the collected experimental data. The values of the optimized parameters for all the tires, when optimization was performed against the average value of the runs is shown in Table 5-4.

Table 5-4: Parameters of the Magic Formula found for average runs of all the tires

Sr. No.	Tire Name	(B)	(C)	(D)	(E)	Final value of the cost function (kN)
1	Tire A1	0.1715	1.6822	0.8521	0.1046	0.0664
2	Tire A3	0.2056	1.4604	0.8721	-0.7359	0.0845
3	Tire B1	0.1044	1.9875	1.0765	-0.0922	0.0973
4	Tire B3	0.1635	1.8886	0.9223	0.5535	0.0780
5	Tire C1	0.3819	1.5159	0.5599	0.6140	0.0324
6	Tire C3	2.8855	0.8303	0.6395	0.8012	0.0330
7	Tire D1	0.1915	1.7578	1.1277	-0.6180	0.1133
8	Tire D3	0.5147	0.7461	1.1266	-0.5194	0.1036
9	Tire E1	0.5355	0.8554	0.9090	0.5036	0.0540
10	Tire E3	1.5428	0.5446	0.9859	0.3642	0.0321
11	Tire F1	0.9888	1.6929	0.7726	0.8855	0.02
12	Tire F3	1.5521	0.7556	1.0173	0.5239	0.0279
13	Tire G1	3.6132	0.8672	0.6740	0.6060	0.0211
14	Tire G3	3.8437	0.4147	0.8845	0.6732	0.0337
15	Tire H1	0.2980	1.8271	1.3976	-0.0627	0.0651
16	Tire H3	0.7007	1.6795	0.7308	0.5614	0.0309

As can be seen in the case of tires of rubber compound A, which were tested in the same conditions and of the same age, the optimized value of the parameters is nearly equal in both the cases even though the final value of the cost function differs. The plot of the estimated performance curve versus the average of measured values curve for the tire A1 and the reduction in cost function with the number of iterations is shown in Figure 5-14 and Figure 5-15. In the case of some tires like tire E3 where the experimental data at higher slip ratios has more uncertainty, the predicted curve by the optimized algorithm appears more like a curve of the tire brush model than the Magic Formula model, as shown in Figure 5-16. One of the reasons for this is that the algorithm tries to minimize the cost function over the entire range. One of the solutions to avoid this could have been optimization with respect to the stable region of the Magic Formula model but it would be logically

incorrect as it would literally mean the eradication of all the uncertainties of the remaining slip ratios.

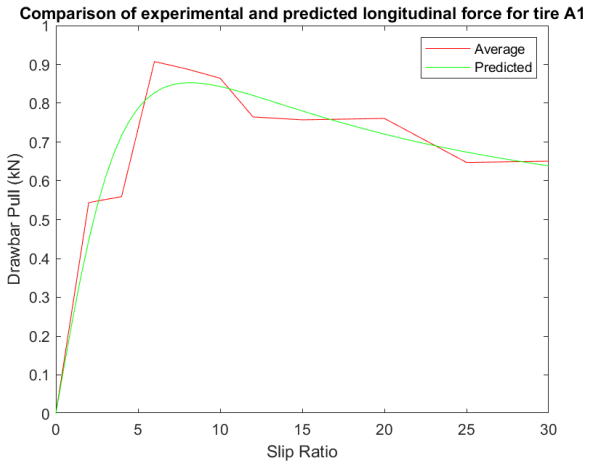

Figure 5-14: Comparison of parametrized Magic Formula model to the average value of experimental data of tire A1

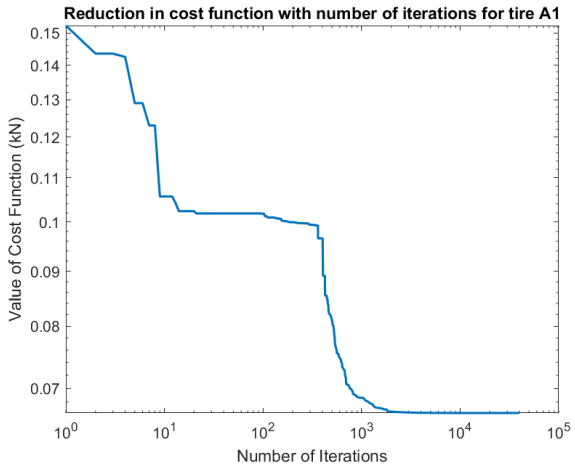

Figure 5-15: Value of the cost function against the number of iterations for the average value of experimental data of tire A1

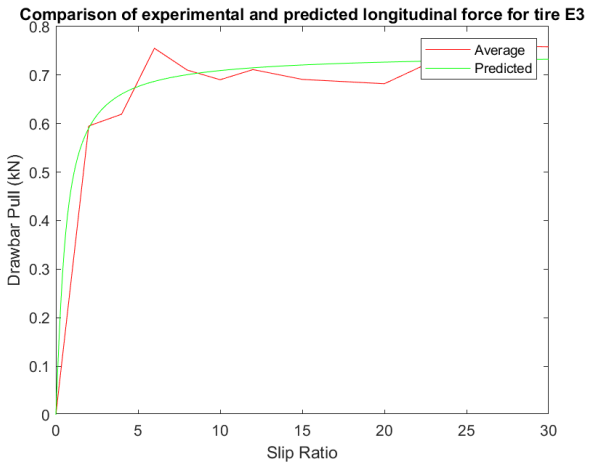

Figure 5-16: Comparison of parametrized magic formula model to the average value of experimental data of tire E3

In the case of optimization where both the runs of the same tire were considered, the value of the optimized parameters is as shown in Table 5-5. It can be observed that the absolute value of the parameters for all the tires in Table 5-4 and Table 5-5 is nearly comparable and it does not affect the results of the algorithm significantly. Another point that can be noted from both the tables is that, in the cases of tires of rubber compounds F and H which were tested at different ambient temperatures, the effect is evident on not only the peak value factor but also the stiffness factor. In the case of the tires of rubber compound F, it may seem that the shape factor is affected by this but it cannot be a concrete statement as tire F3 does not have a discernible plateau after the peak region which can affect the shape and curvature factors. Additional results of the optimized genetic algorithm are presented in the Appendix B. 4.

Table 5-5: Parameters of the Magic Formula found for both runs of all the tires

Sr. No.	Tire Name	(B)	(C)	(D)	(E)	Final value of the cost function (kN)
1	Tire A1	0.1711	1.6769	0.8529	0.0725	0.0665
2	Tire A3	0.2086	1.4572	0.8698	-0.6831	0.0874
3	Tire B1	0.1044	1.9775	1.0772	-0.1326	0.0985
4	Tire B3	0.1634	1.8942	0.9223	0.5625	0.0808
5	Tire C1	0.3829	1.5136	0.5597	0.6111	0.0364

6	Tire C3	2.2198	0.9243	0.6192	0.8176	0.0523
7	Tire D1	0.1917	1.7584	1.1275	-0.6103	0.1212
8	Tire D3	0.5404	0.5772	1.3182	-0.9837	0.1082
9	Tire E1	0.5629	0.8074	0.9312	0.4754	0.0579
10	Tire E3	1.0662	0.9462	0.7405	0.6589	0.0388
11	Tire F1	0.6686	1.8879	0.7716	0.9318	0.0257
12	Tire F3	1.5725	0.7465	1.0243	0.5199	0.0445
13	Tire G1	3.5299	0.7835	0.7	0.4508	0.0225
14	Tire G3	2.9349	0.6237	1.0138	0.6594	0.0530
15	Tire H1	0.2945	1.8227	1.4010	-0.1173	0.0840
16	Tire H3	0.6291	1.6589	0.7353	0.3998	0.0405

In the case of the tires of rubber compounds B, and C, where the aging effect can be considered, it is found that the aged tire in all two cases had a higher value of stiffness factor after optimization and a higher value of the angle at the origin as is evident from Table 5-5.

5.4. Benchmarking of predicted friction coefficient from Genetic Algorithm with the friction coefficient calculated from experimental results

The concept of drawbar pull, the drawbar pull coefficient, and other similar equivalent terms are explained in detail by He et al. (He et al., 2019), basically as the difference between the tractive and resistive forces acting on the traction element, the tire in our case. Due to the method of calibration of the Kistler sensor followed, the Kistler force hub detects the drawbar pull in the longitudinal direction. An attempt was made to find the experimental values of the coefficient of friction experienced by the tires. For this, the tractive force was calculated based on the power of the wheel motor, the value of the effective radius, and the rotational speed. It was assumed that the only loss of power occurs due to friction in the direction opposite to the motion of the tire. The loss that could occur due to other interacting elements within the system was assumed to be small and neglected. Thus, the tractive force and resistive force are calculated according to eqns. (5.8) and (5.9) respectively. The value of the coefficient of friction was found using eq. (5.11).

$$F_{tractive} = \frac{Torque}{R_{eff}} \tag{5.8}$$

$$F_{resistive} = \mu . F_z \tag{5.9}$$

$$DPC = \frac{F_{tractive} - F_{resisitve}}{F_z} = \frac{Torque}{F_z \, . \, R_{eff}} - \mu \tag{5.10}$$

$$\mu = \frac{Torque}{F_z \, . \, R_{eff}} - DPC \tag{5.11}$$

The value of the coefficient of friction was also estimated for the intermediate values of the slip ratios by using the parametrized curve for every tire. The results for the tires of every rubber compound are presented from Figure 5-17 to Figure 5-24. It can be seen that the adherence of the experimental values computed and the values computed based on the parametrized curve is higher and a gradual reduction in the value of friction coefficient is observed as the slip ratio progresses with all of them nearly converging in a coefficient of friction range of about 0.15 to 0.2 at slip ratio 30%. On comparison of all the values at a certain slip ratio in the linear region, say 5%, we see that the coefficient of friction in the case of rubber compounds C and G is higher than others which is contradictory to our findings in the earlier part of this work. This is only because of the assumptions made for the computations of this section detailed earlier and the fact that rubber does not follow the classical laws of friction in which the resistive forces are considered to be proportional to the applied normal load as assumed in (5.9).

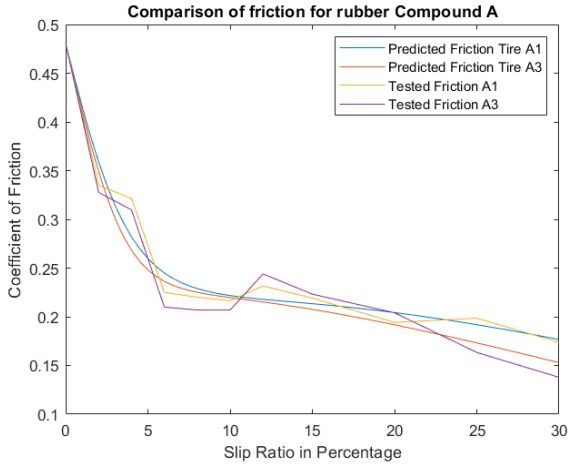

Figure 5-17: Comparison of the experimental value of friction coefficient against the Magic formula parametrized value of friction coefficient for rubber compound A

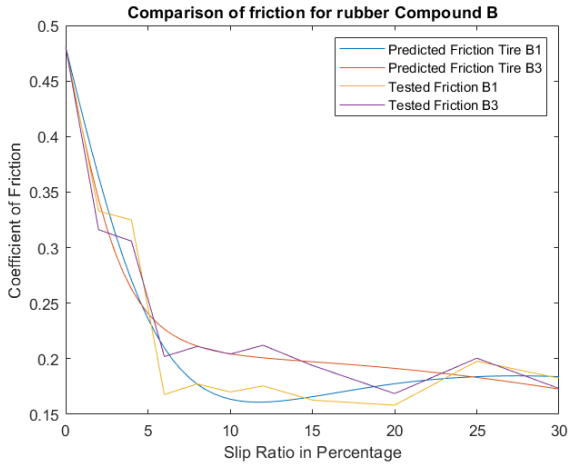

Figure 5-18: Comparison of the experimental value of friction coefficient against the Magic formula parametrized value of friction coefficient for rubber compound B

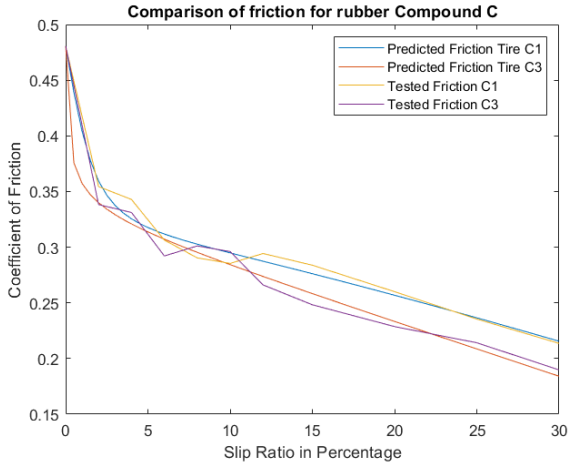

Figure 5-19: Comparison of the experimental value of friction coefficient against the Magic formula parametrized value of friction coefficient for rubber compound C

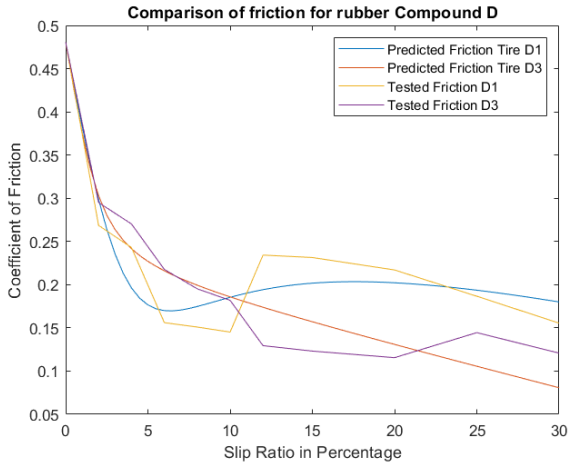

Figure 5-20: Comparison of the experimental value of friction coefficient against the Magic formula parametrized value of friction coefficient for rubber compound D

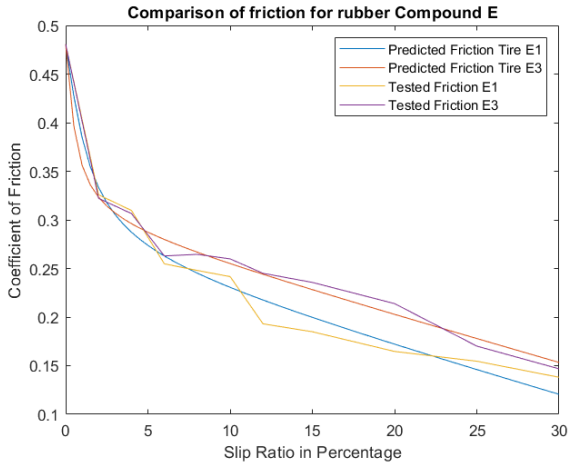

Figure 5-21: Comparison of the experimental value of friction coefficient against the Magic formula parametrized value of friction coefficient for rubber compound E

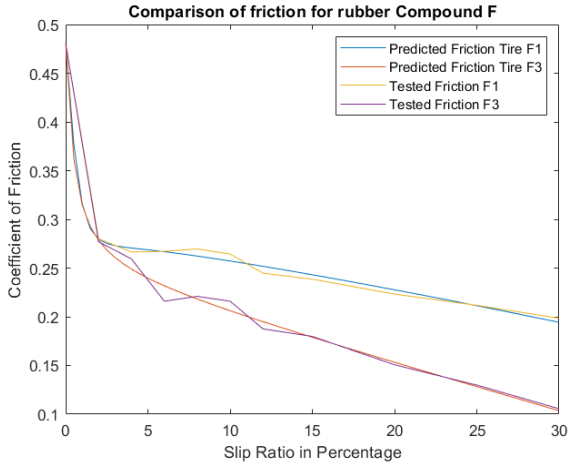

Figure 5-22: Comparison of the experimental value of friction coefficient against the Magic formula parametrized value of friction coefficient for rubber compound F

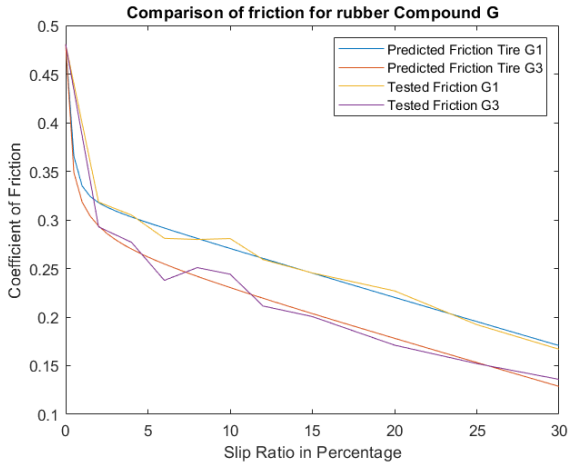

Figure 5-23: Comparison of the experimental value of friction coefficient against the Magic formula parametrized value of friction coefficient for rubber compound G

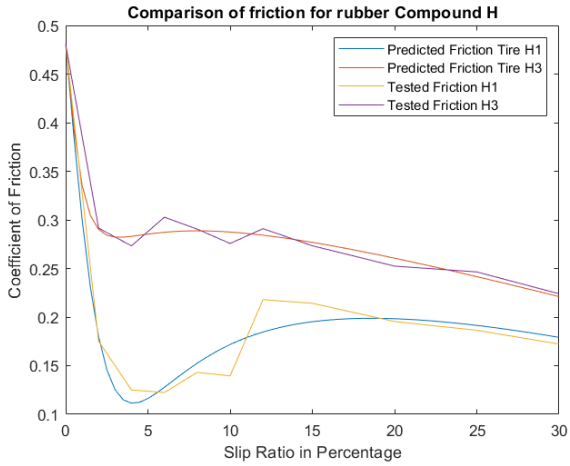

Figure 5-24: Comparison of the experimental value of friction coefficient against the Magic formula parametrized value of friction coefficient for rubber compound H

Chapter 6 Conclusions and Future work

A summary of the research work conducted and the results obtained are presented in this chapter. Findings related to the correlation of tire performance and Magic Formula parameters with respect to the variation in the rubber compound are presented along with a scope for future research in this area.

6.1. Summary of conclusions and outcomes of the research

This project was focused on investigating the effect of variation of the tread rubber compound on the performance of winter tires and modeling the rise in temperature and height of water film estimated to be present in the contact patch due to this effect. As a part of this research work, an extensive experimental investigation of the effect of tread rubber compounds on the performance of the tire on the ice near the melting point was conducted. A varying order of performance was found for all the tires although the order is based on the experimental investigation which was conducted at low speeds, however the same parallel cannot be drawn for higher speeds without testing. Sixteen candidate tires of eight different rubber compounds were chosen for the investigation. As some material properties related to four of the rubber compounds were not available, it was difficult to determine an exact correlation and dependence of individual rubber properties on the performance of the tire; some approximations were involved in order to conduct simulations with ATIIM2.0 for these tires.

A detailed review related to the background and prior efforts in the field of rubber/tire on ice friction was performed. It included not only the works related to the experimental investigation but also various modeling aspects considered in classical models used for simplification of the understanding of the tire-ice phenomenon. Based on prior efforts in this field, a general conclusion was that reduction in the stiffness/dynamic modulus results in the betterment of the available friction for the rubber/tire. Based on the results of the experimental investigation, it was found that this may not necessarily be the case and thus the stiffness or physical properties like the dynamic modulus may not be a singling out factor for a detailed investigation.

In the experimental investigation phase of the project, all the tires were instrumented with K-type thermocouples such that effective distance between them would be enough to capture the

ends of the contact patch. As the ambient temperature, which was positive, could not be controlled efforts were made so that at least one of the tires of every rubber compound was tested at nearly the same ambient temperature to concentrate on the effect of the rubber compound. In the experimental investigation, it was found that a drop of about 5℃ could nearly halve the performance of the tire in the stable region till the peak drawbar pull is experienced by the tire. Another significant finding was that the effect of the rubber compound on the drawbar pull is the most prominent in the stable region of the drawbar-slip curve, which is the region in which most vehicles operate. In the case of the higher slip ratio range, which may occur in critical conditions like emergency braking or sudden maneuvers, the effect due to the variation in tread rubber compound is negligible. The effect of aging in the case of three rubber compounds was also studied during the experimental investigation. Although a reduction in performance with aging is expected, this was seen in the case of only one rubber compound. The rise in temperature measured experimentally was found to be directly dependent on the specific heat capacity, which was available for five of the rubber compounds. It was found that lower specific heat capacity implied a higher temperature rise measured by the thermocouples.

In the next phase, simulations for the rise in temperature and predicted height of water film were run for most of the tires using values of the properties available using an in-house model ATIIM2.0, developed by Mousavi (Mousavi and Sandu, 2020a). The rise in temperature was found to be increasing as the tread progressed towards the rear of the contact patch. In some cases, it was also found that the temperature rise was significant in the lateral periphery of the tire's contact patch. Comparison of predictions of ATIIM2.0 against some of the classical models was performed in this phase. The formulations of these classical models, namely the model by Hayhoe and Shapley, 1st model by Peng et. al., and the 2nd model by Peng et. al., were modified to account for the tread rubber properties wherever applicable. The advantages and drawbacks of these models were highlighted by this. One of the major advantages is the estimation of the transition point, an indication of the slip ratio at which the melting starts. Amongst the major drawbacks is the assumption of a uniform normal pressure in the contact patch which is almost never the case. Another drawback is that as the effect of variation in pressure in the lateral direction of the contact patch is neglected and the limited number of properties considered, the accuracy of the models related to temperature rise, estimation of water film height and in turn the value of friction coefficient in the tire-ice interaction is reduced.

During this stage, the Magic Formula parameters of the tires were calculated based on the experimental data collected and any correlation with the rubber compound properties has been investigated. For this, a genetic algorithm was used for optimization to find the values of the stiffness factor, the peak value factor, the shape factor, and the curvature factor. It was found that a change in the ambient temperature affects the stiffness and peak value factors of the Magic Formula model. It was also found that even though the aged tire did not perform to the expected trend during the experimental investigation, in the case of two of the three rubber compounds, it was found that the absolute value of the stiffness factor and the tangent of the angle at the origin was higher in the case of the aged tire.

6.2. Suggestions for future research

In order to find an actual suitable correlation between the tread rubber compound and performance of the tire, the major contents of the tread rubber should be known in order to analyze the individual and combined effects of the ingredients. From many studies, e.g. (Hiramatsu et al., 1991; Okel and Rueby, 2016; Weng et al., 2020), it is known that the filler material silica and improvements in its dispersion in the rubber matrix can reduce the rolling resistance as well as improve the wet traction. The addition of petroleum resins can improve wet traction but cannot reduce the rolling resistance. Similar other effects of the ingredient variation cannot be judged based simply on the change in the rubber compound properties. Correlation of the free-rolling results can help in generalizing the amount of some ingredient, say silica, but does not give a concrete measure of how much it varies between the rubber compounds. Also, the same effect on the free-rolling results could be possible due to the different combinations of ingredients. Hence, to have a thorough understanding of the tire ice phenomenon, from a material point of view, it is necessary to analyze this effect.

Some of the values used for the modeling and simulation part are taken from the literature. As they were nearly constant in all the cases, the simulations presented in this work were the result of solely the changes in the material properties of the tread rubber compound. The possibility of the variation in the roughness of the tread rubber, the roughness of the ice, the variation in the distances between actual areas of contact, and the actual contact ratio needs to be investigated. It

would also be interesting to investigate if the order of performance gets altered in the case of cornering and the reasons for the same.

A more improved technique for measuring the rise in temperature (based on non-contact sensors) in the contact patch would be helpful, as in the current scenario, the accuracy of K-type thermocouples is not the highest and due to limitations of the datalogger and convection occurring, there are more uncertainties in the measurement. Development of a system/technique to find the contact patch pressure distribution without external aids (like pressure pad) would enhance the model as in that case, the pressure distributions at higher velocities can be captured by the use of a real vehicle.

Lastly, regarding the experimental investigations, control of the ambient temperature would guarantee sole concentration on the changes due to the tread rubber compound. It would also be possible to have the ambient temperature negative to check its effect. Testing a single slip ratio in one run could be possible and hopefully more insightful in such a case.

Appendix A

This appendix provides additional results for relevant measurements and results obtained in the experimental phase of the work.

A.1. Additional results for comparative plots of drawbar pull coefficient at various slip ratios

In this section the plots of the drawbar pull coefficient experienced by the tires of a specific rubber compound are presented from Figure A- 1 to Figure A- 10.

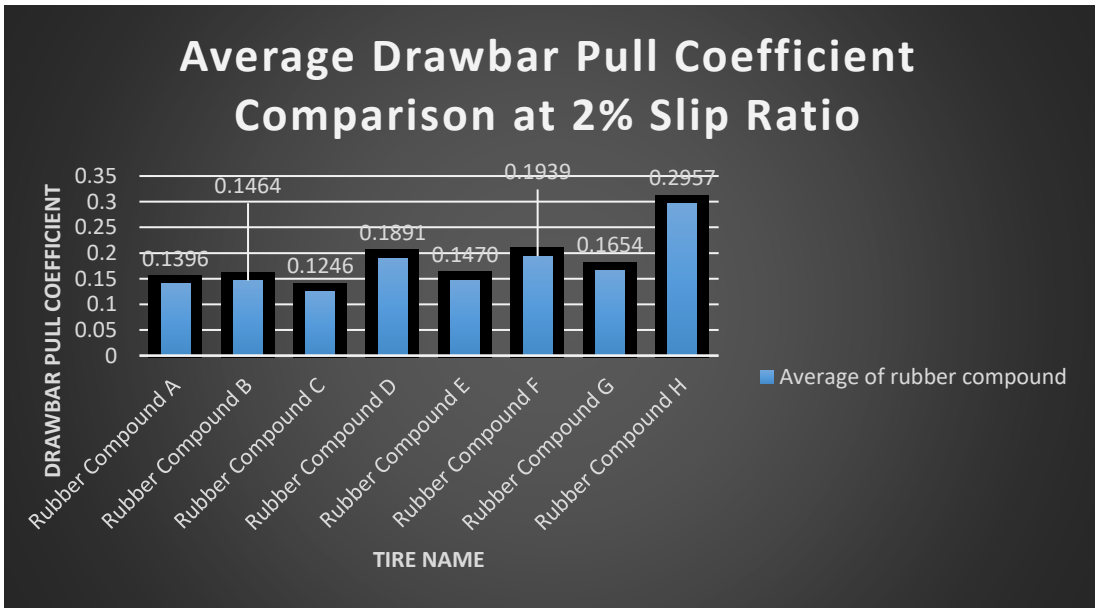

Figure A- 1: Average Value of DPC at 2% slip ratio for all rubber compounds

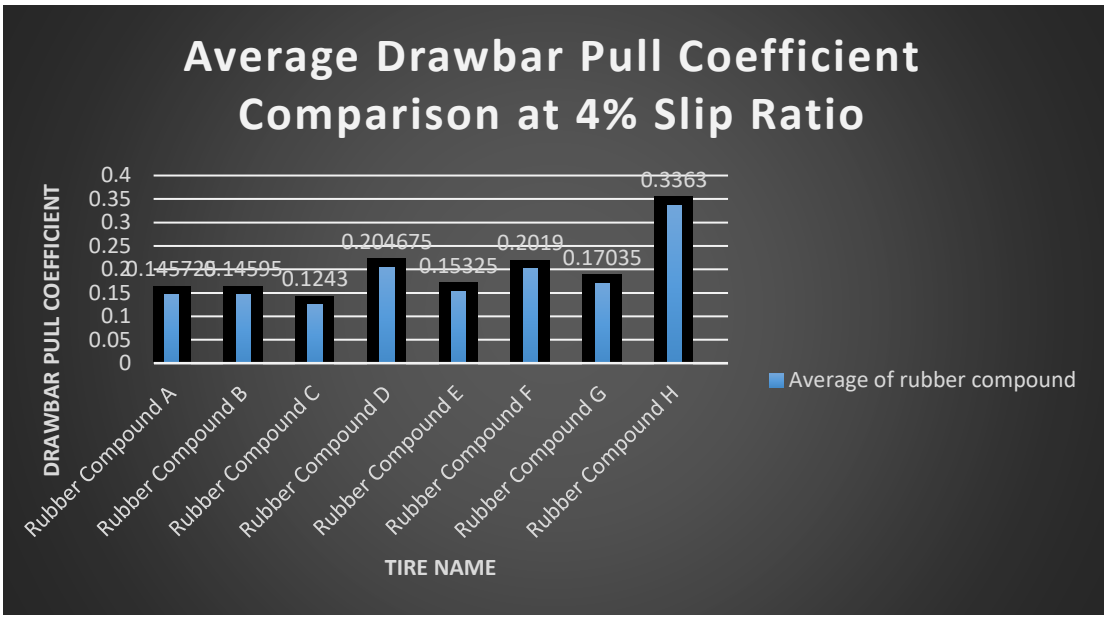

Figure A- 2: Average Value of DPC at 4% slip ratio for all rubber compounds

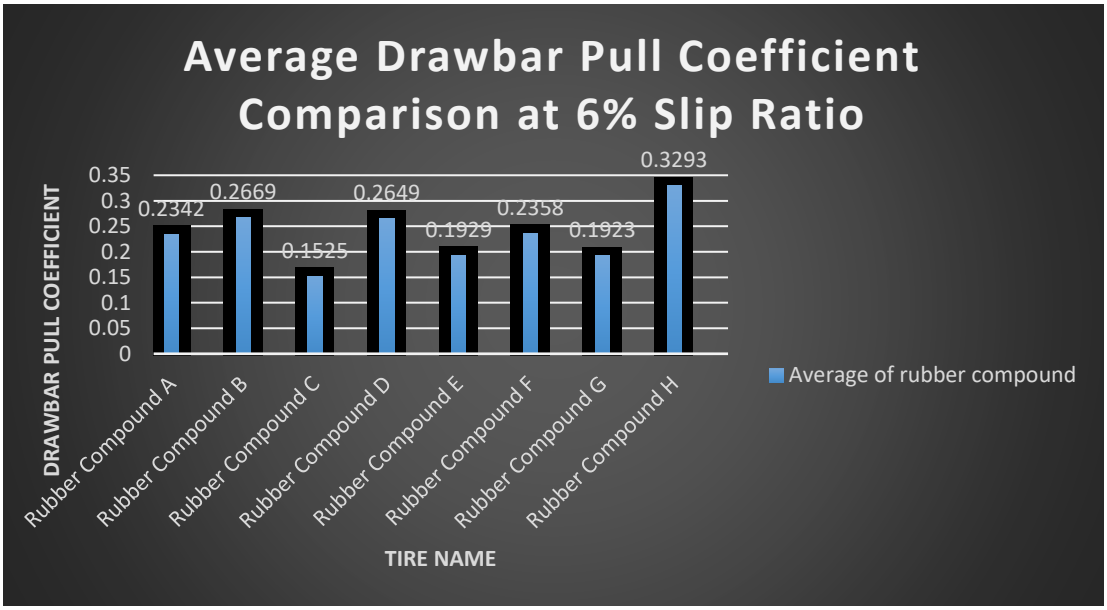

Figure A- 3: Average Value of DPC at 6% slip ratio for all rubber compounds

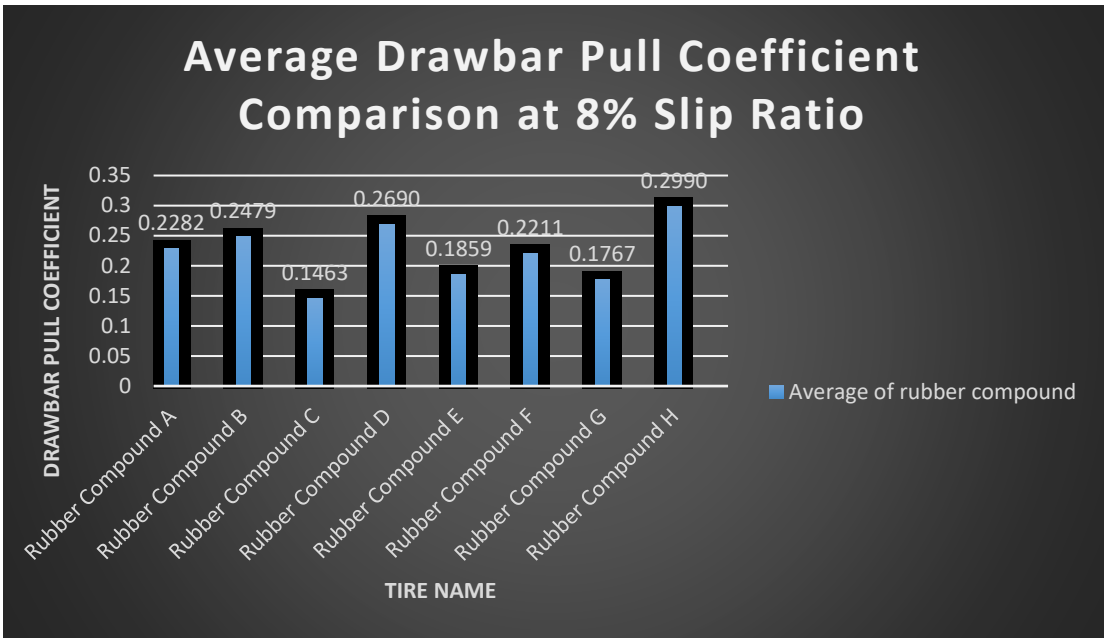

Figure A- 4: Average Value of DPC at 8% slip ratio for all rubber compounds

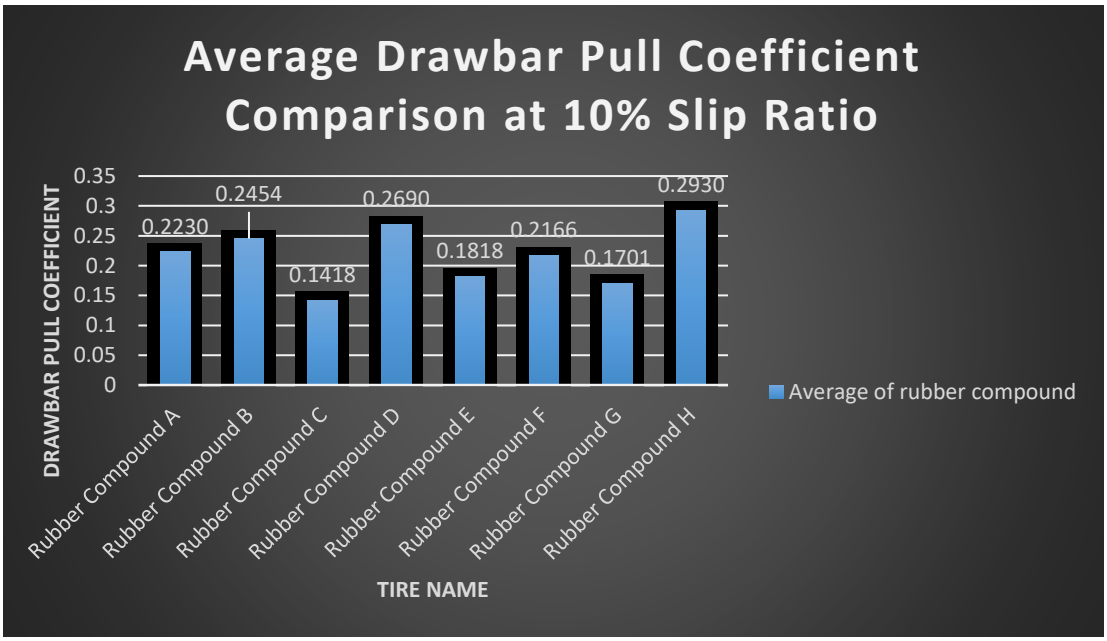

Figure A- 5: Average Value of DPC at 10% slip ratio for all rubber compounds

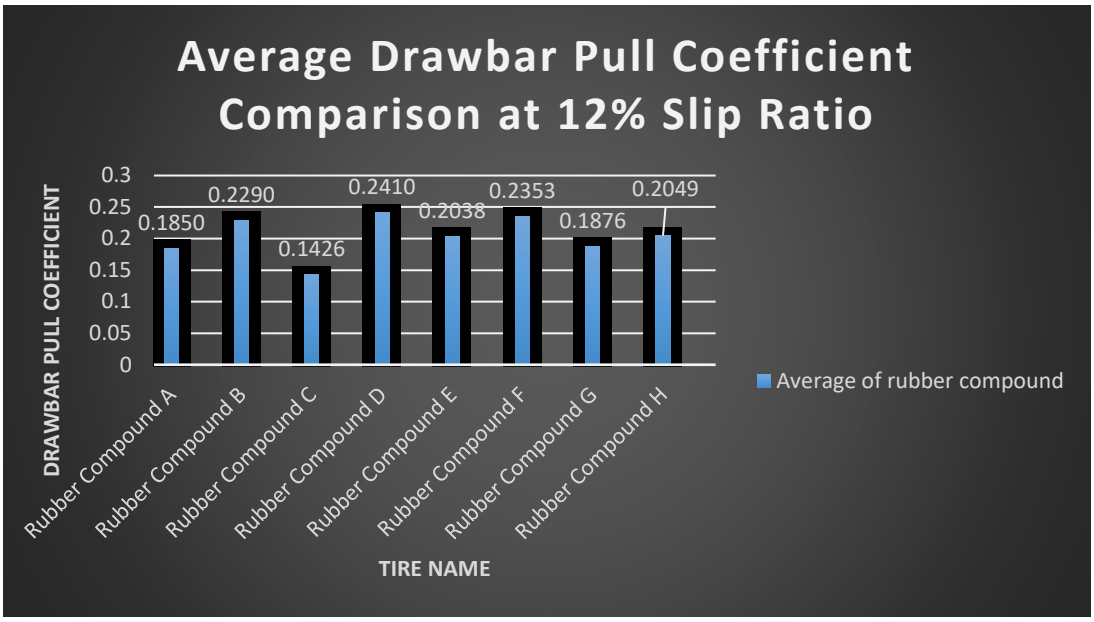

Figure A- 6: Average Value of DPC at 12% slip ratio for all rubber compounds

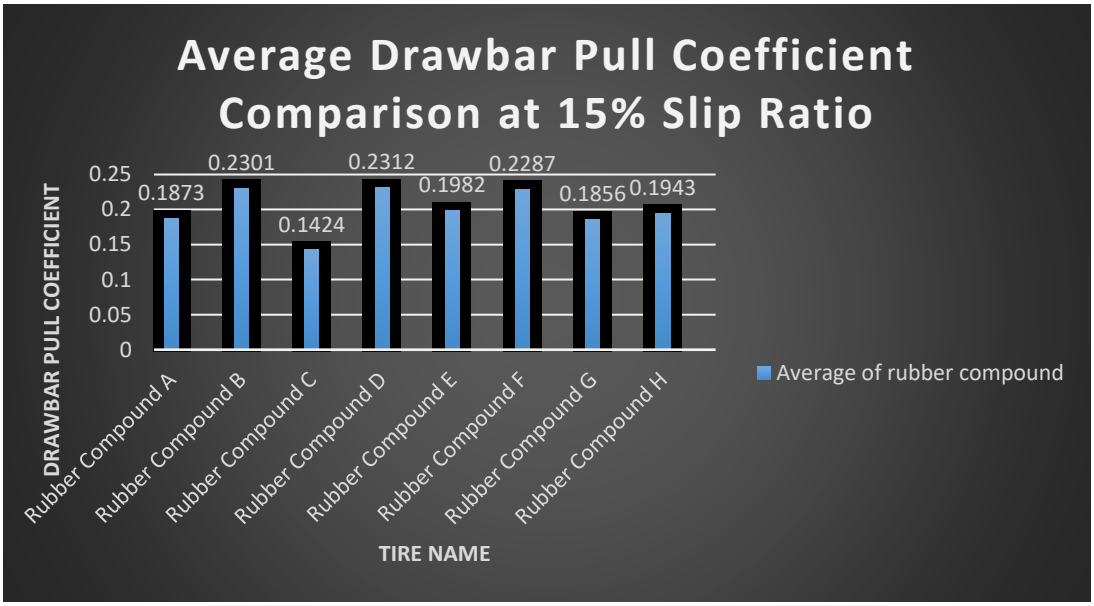

Figure A- 7: Average Value of DPC at 15% slip ratio for all rubber compounds

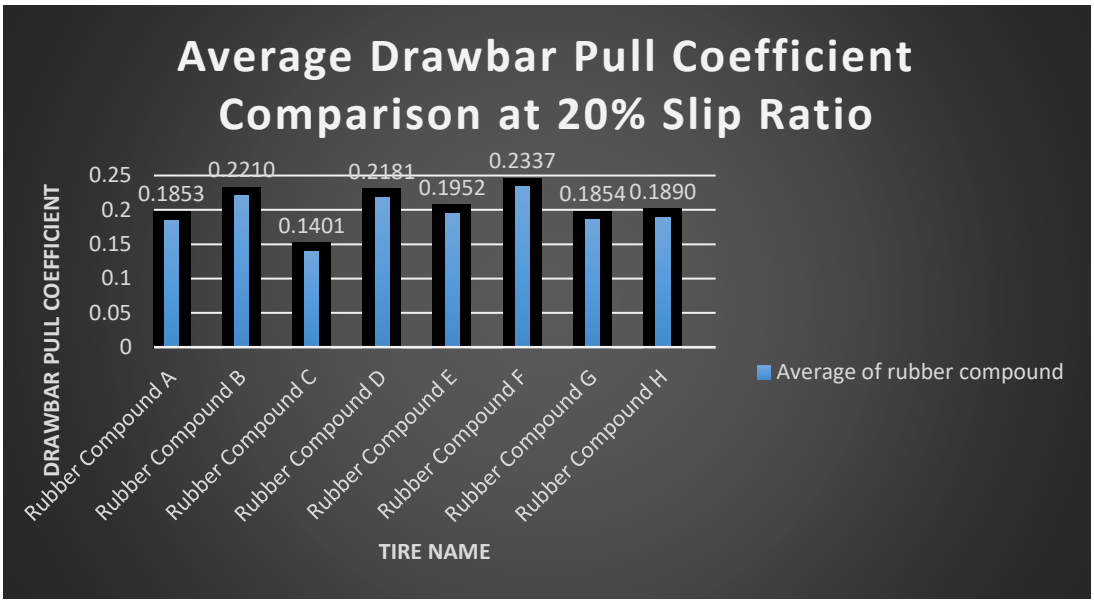

Figure A- 8: Average Value of DPC at 20% slip ratio for all rubber compounds

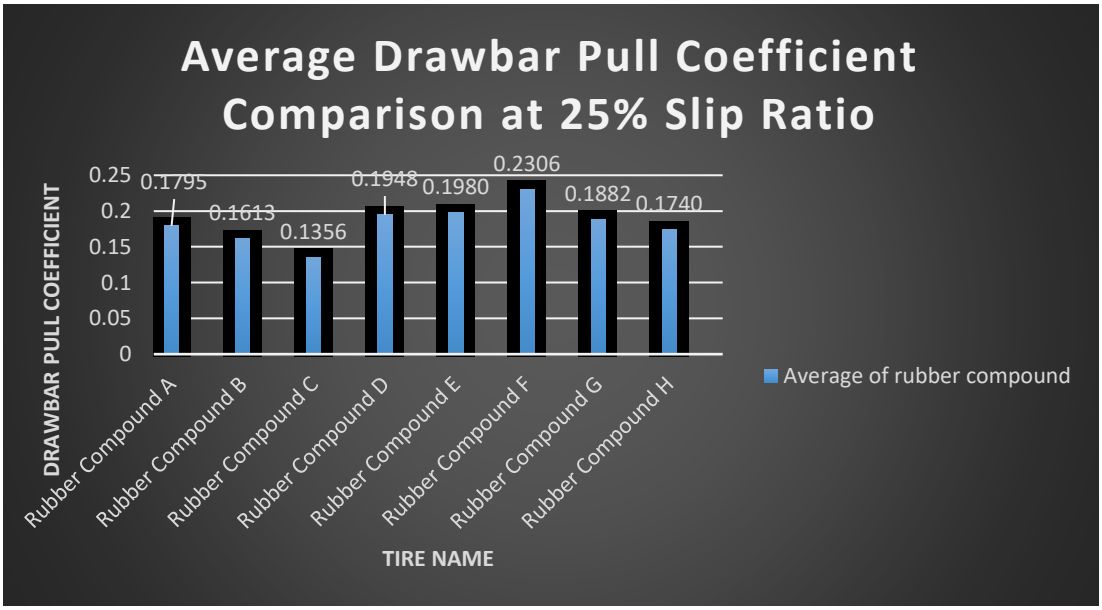

Figure A- 9: Average Value of DPC at 25% slip ratio for all rubber compounds

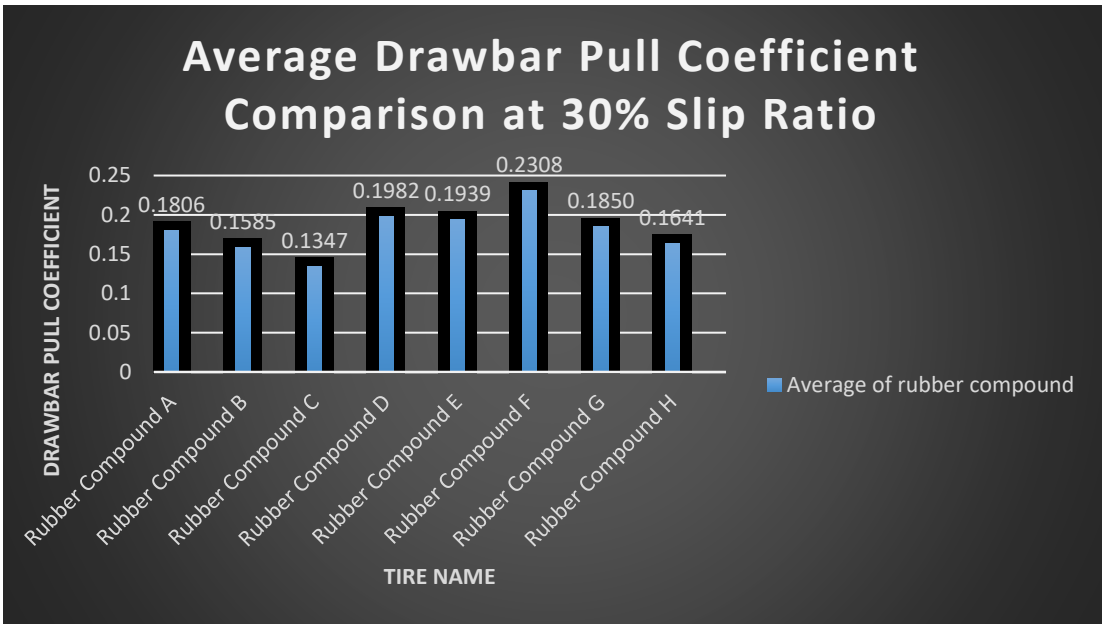

Figure A- 10: Average Value of DPC at 30% slip ratio for all rubber compounds

A.2. Additional results for comparative plots of temperature rise measured by thermocouples at various slip ratios

In this section the comparative plots of measured temperature rise are presented from Figure A- 11 to Figure A- 20.

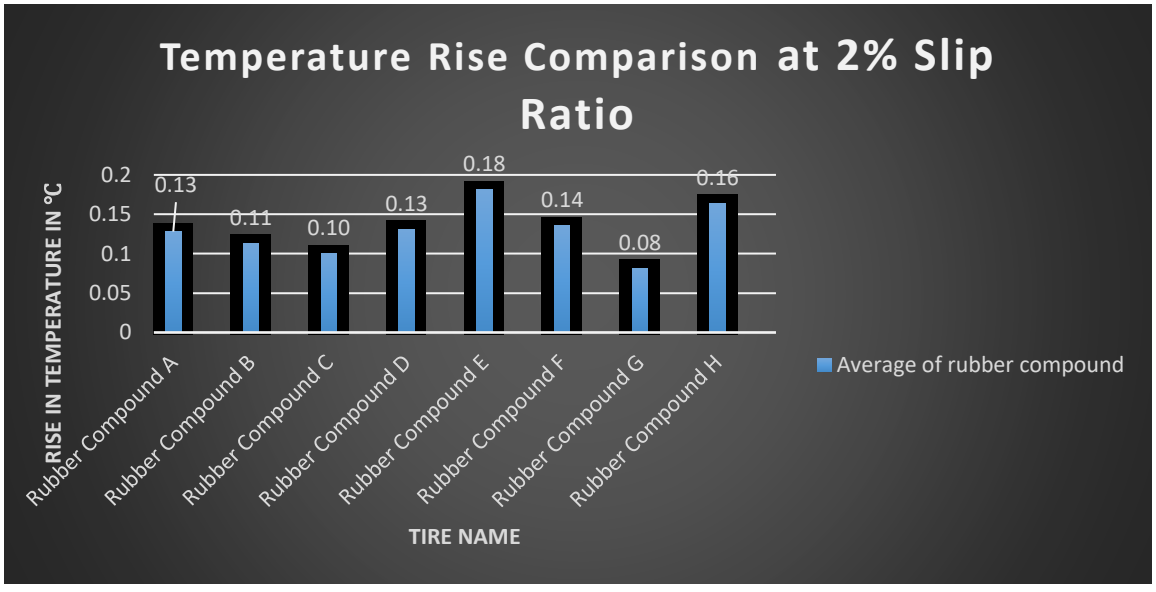

Figure A- 11: Average Value of rise in temperature at 2% slip ratio for all rubber compounds

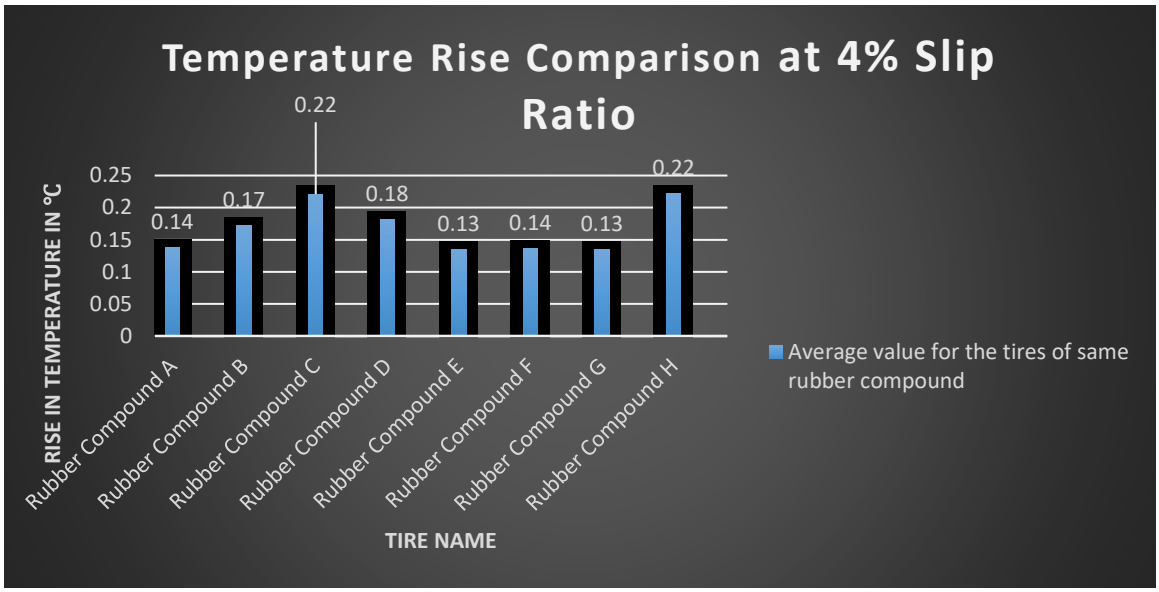

Figure A- 12: Average Value of rise in temperature at 4% slip ratio for all rubber compounds

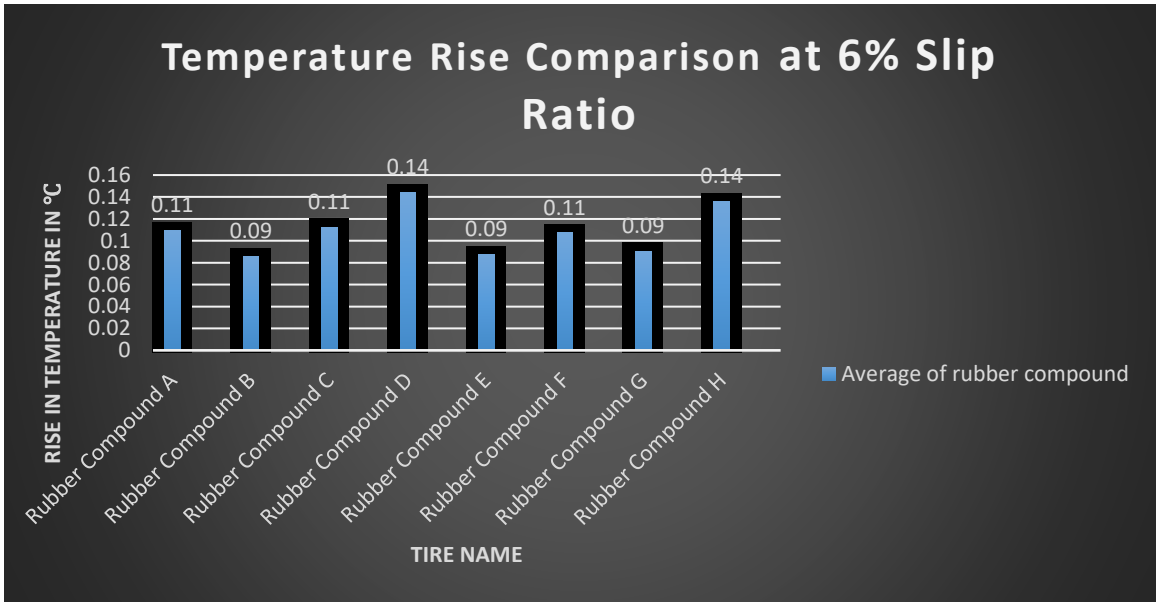

Figure A- 13: Average Value of rise in temperature at 6% slip ratio for all rubber compounds

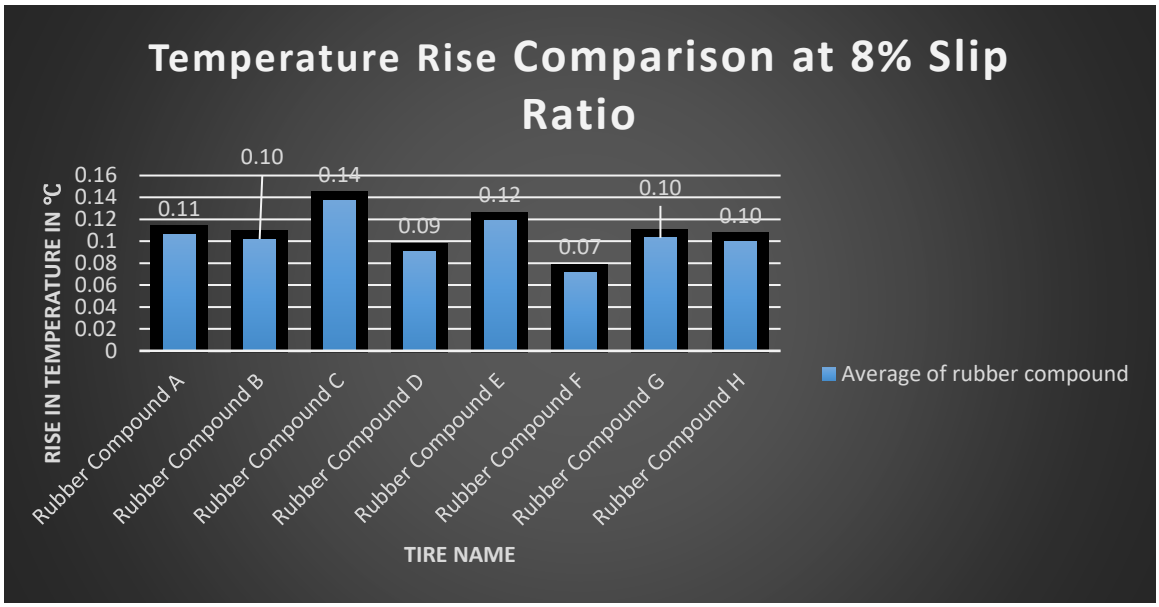

Figure A- 14: Average Value of rise in temperature at 8% slip ratio for all rubber compounds

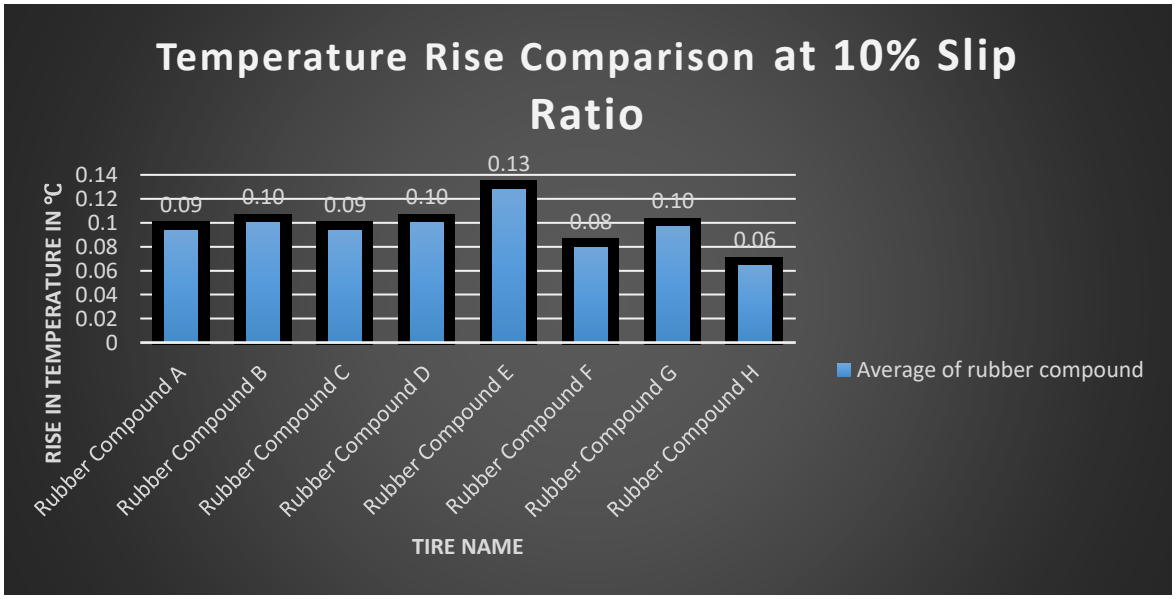

Figure A- 15: Average Value of rise in temperature at 10% slip ratio for all rubber compounds

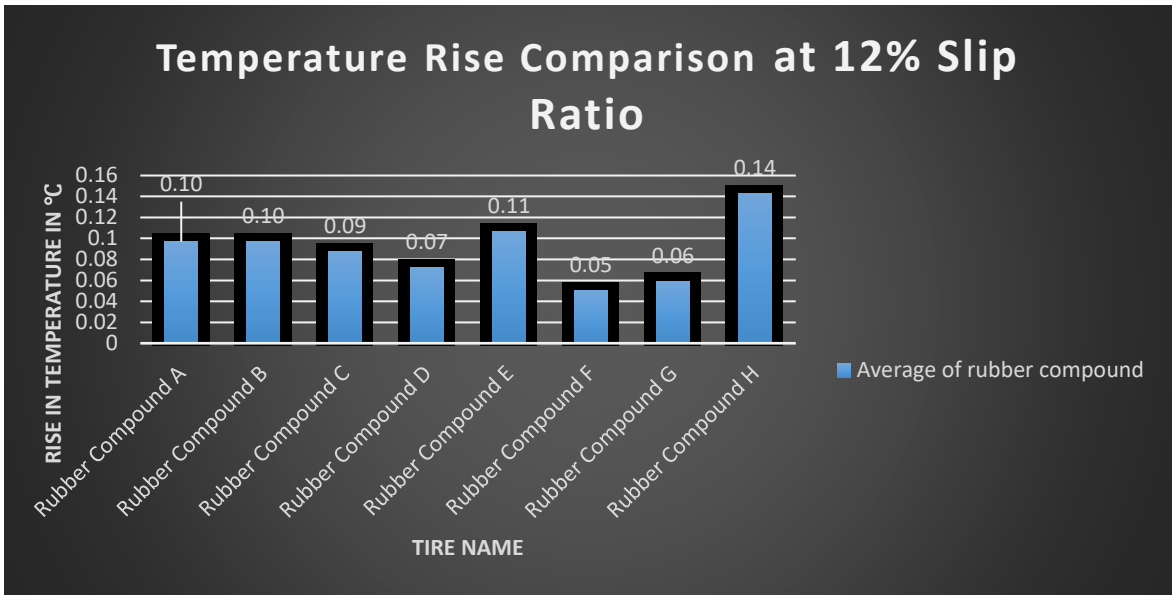

Figure A- 16: Average Value of rise in temperature at 12% slip ratio for all rubber compounds

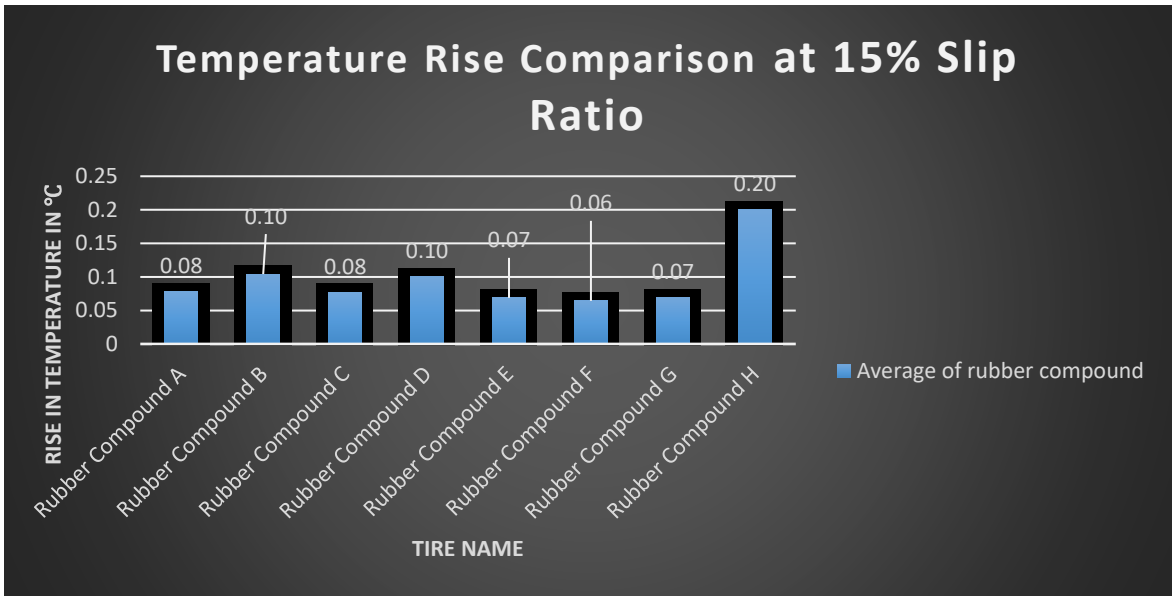

Figure A- 17: Average Value of rise in temperature at 15% slip ratio for all rubber compounds

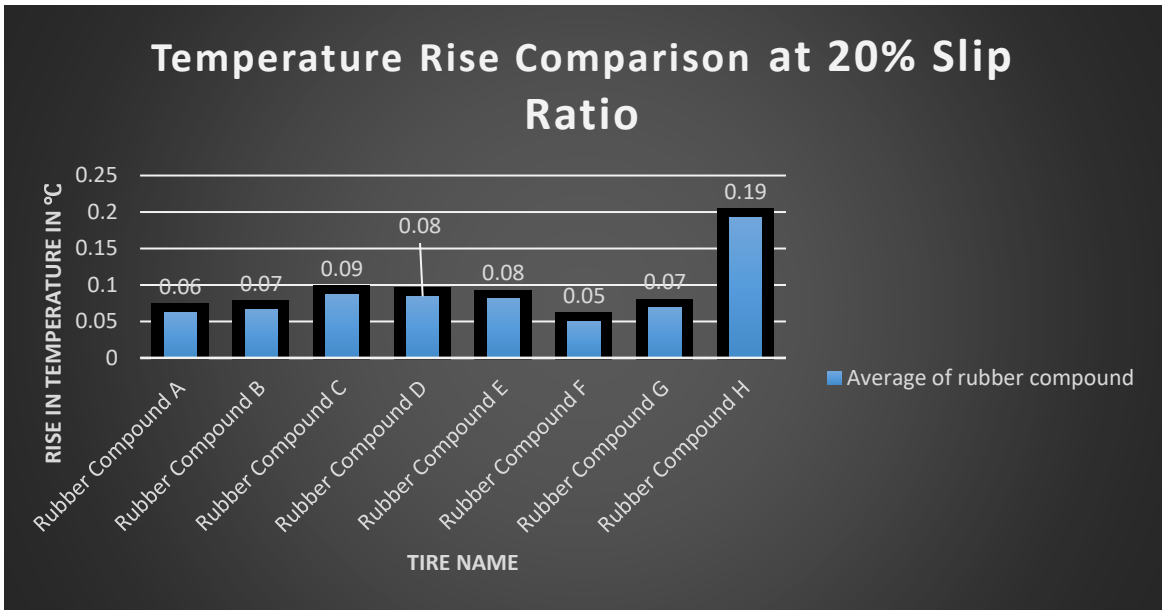

Figure A- 18: Average Value of rise in temperature at 20% slip ratio for all rubber compounds

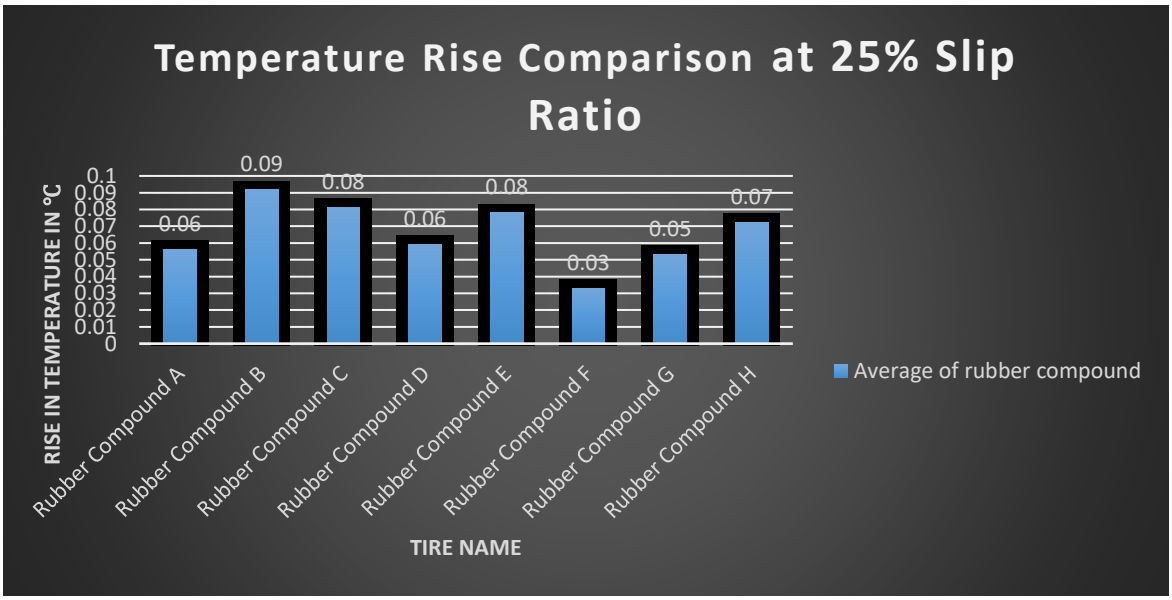

Figure A- 19: Average Value of rise in temperature at 25% slip ratio for all rubber compounds

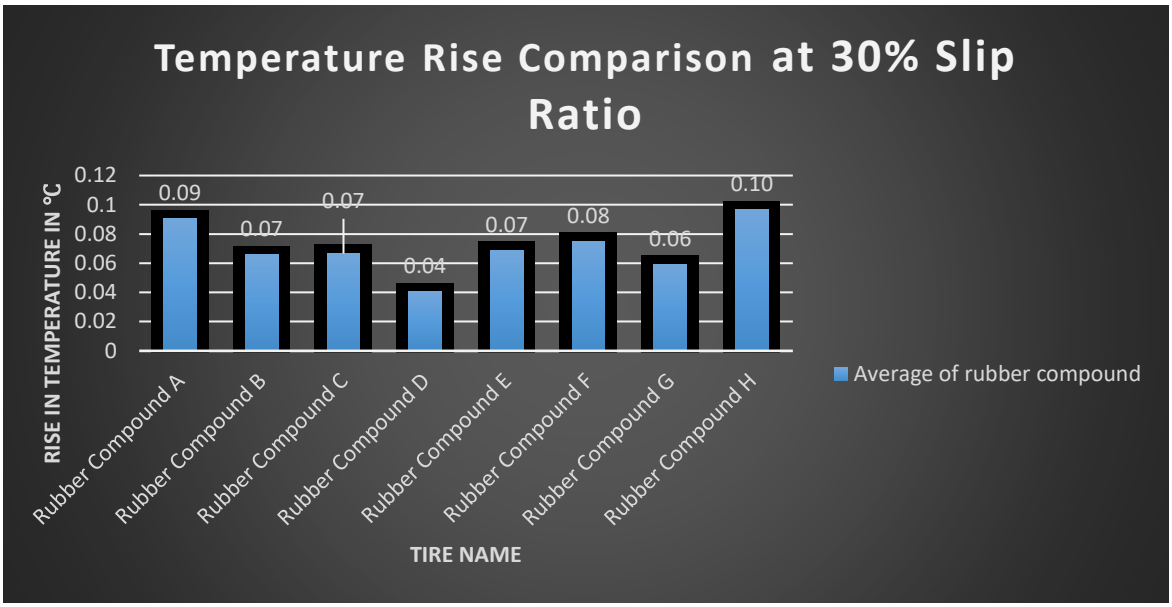

Figure A- 20: Average Value of rise in temperature at 30% slip ratio for all rubber compounds

Appendix B

This appendix provides additional results for relevant parts of the modeling and simulation phase of this work.

B. 1. Additional results for rise in temperature simulations by ATIIM

In this section results for the simulation of temperature rise of all the tires using ATIIM are presented from Table B- 1 to Table B- 6.

Table B- 1: Rise in temperature simulation for all the tires at 2% slip ratio using ATIIM

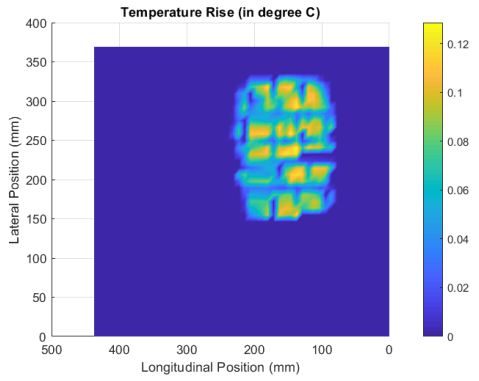	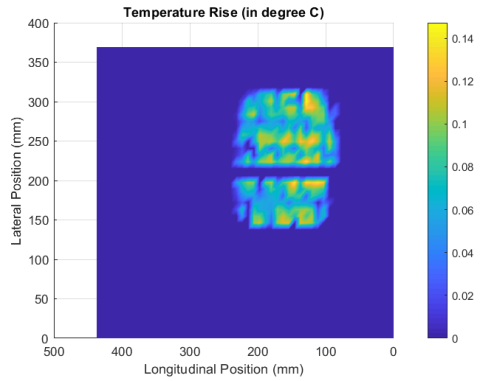
Tire A1	*Tire A3*
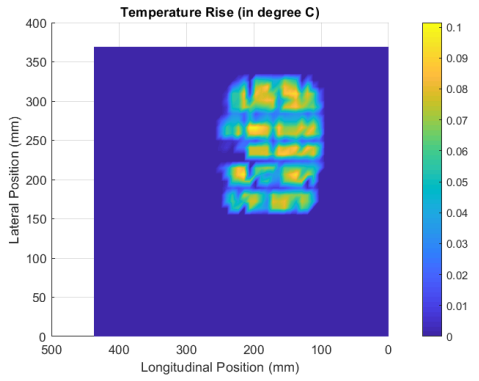	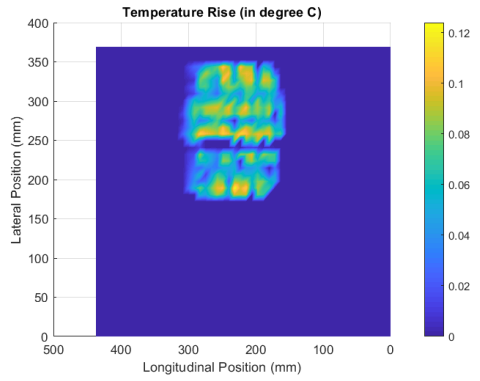
Tire B1	*Tire B3*

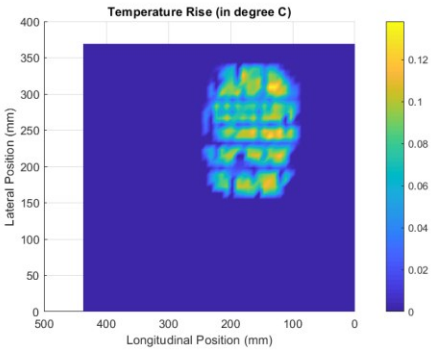

Tire C1

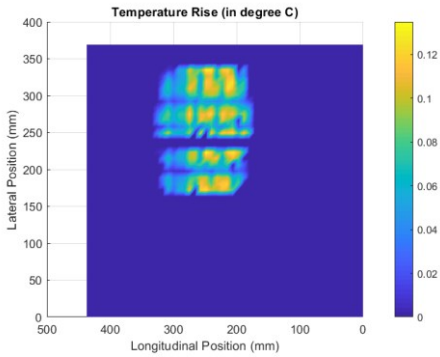

Tire C3

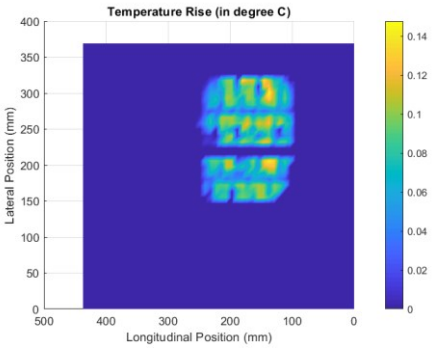

Tire D1

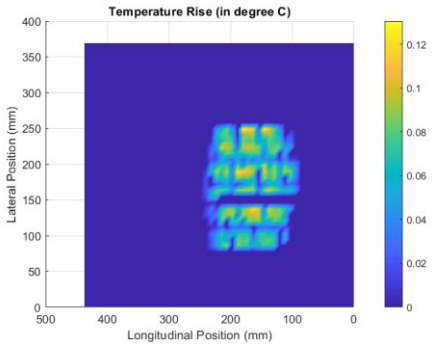

Tire D3

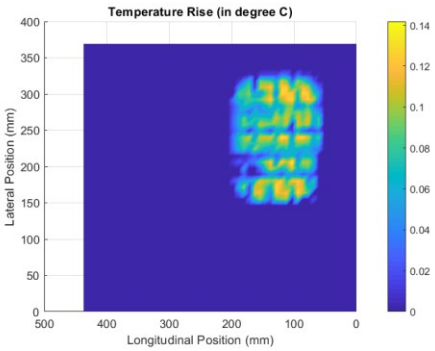

Tire E1

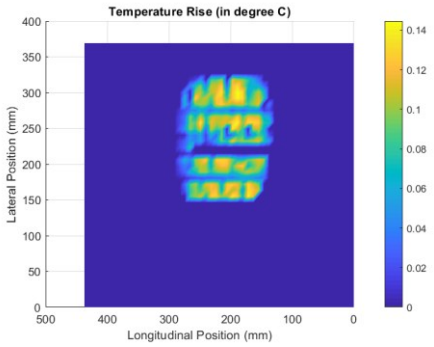

Tire E3

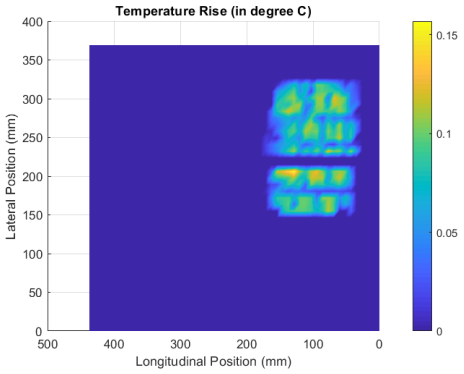

Tire F1

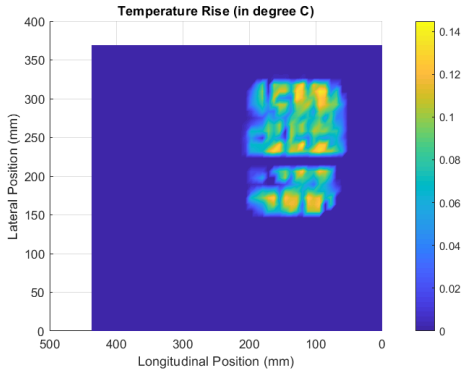

Tire F3

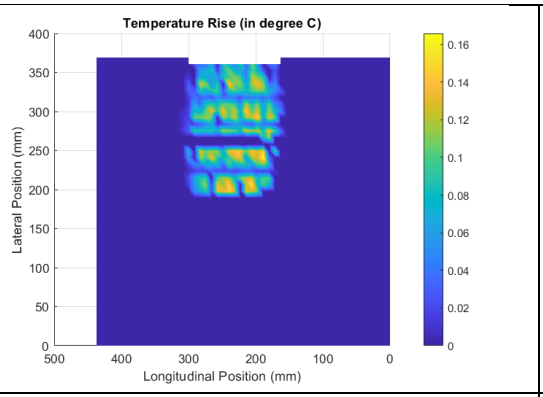	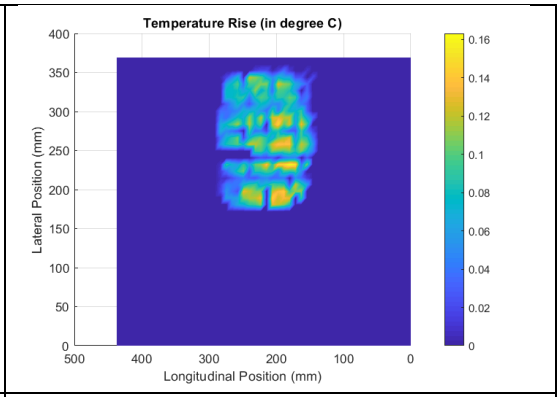
Tire G1	*Tire G3*
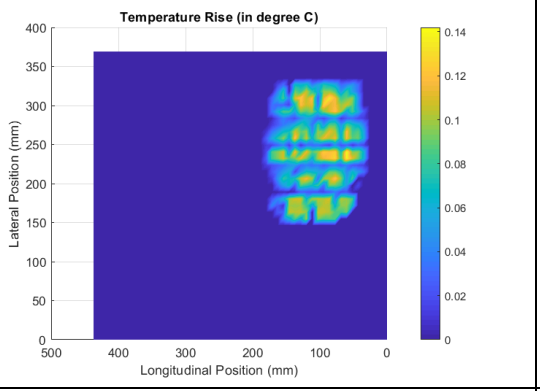	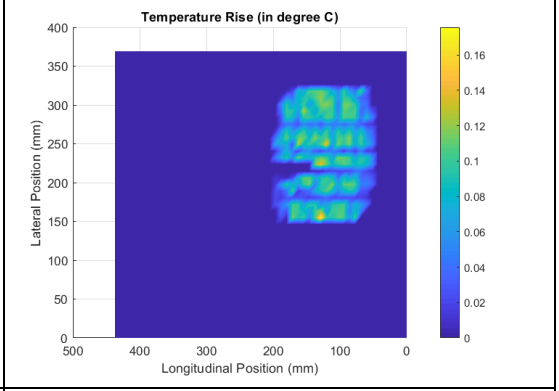
Tire H1	*Tire H3*

Table B- 2: Rise in temperature simulation for all the tires at 6% slip ratio using ATIIM

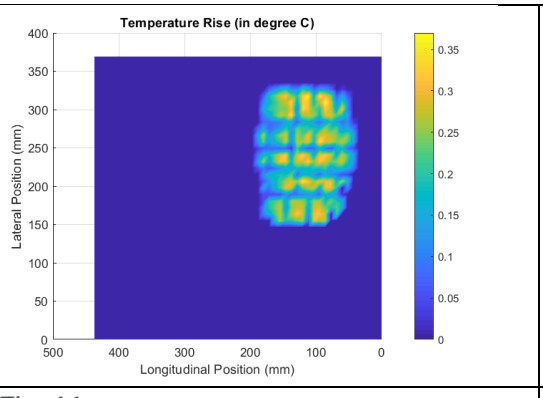	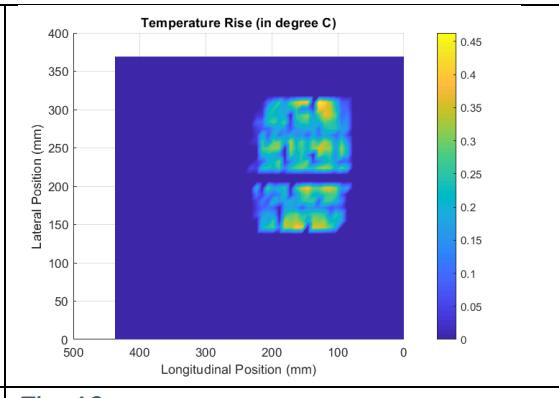
Tire A1	*Tire A3*

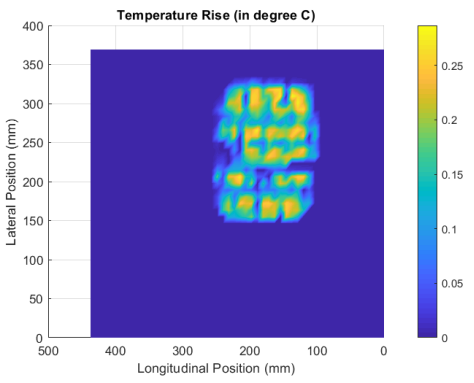

Tire B1

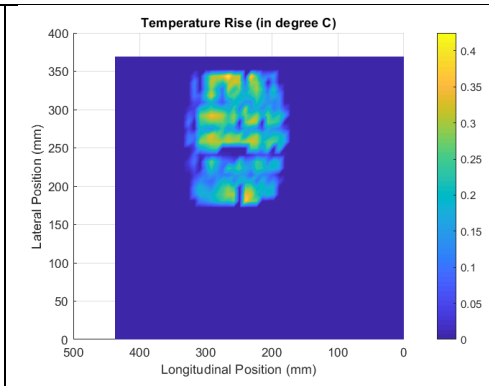

Tire B3

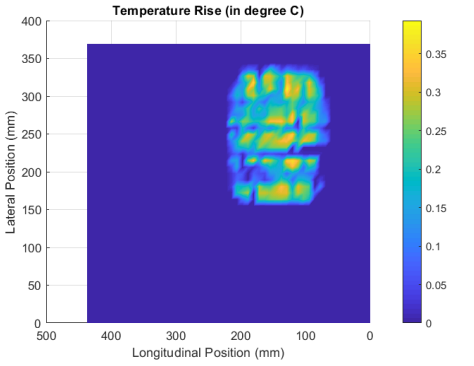

Tire C1

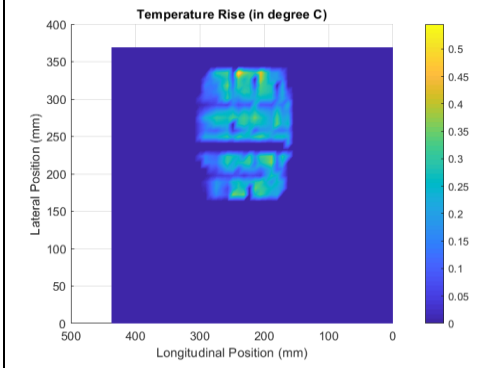

Tire C3

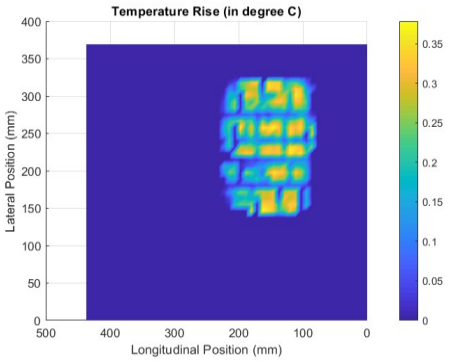

Tire D1

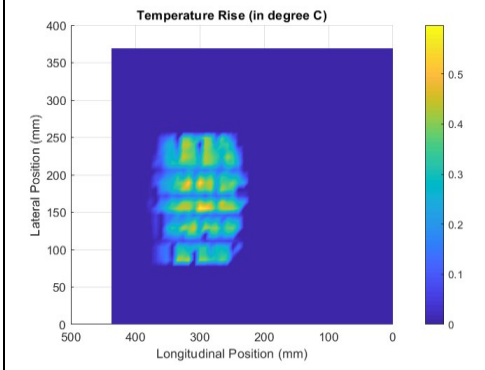

Tire D3

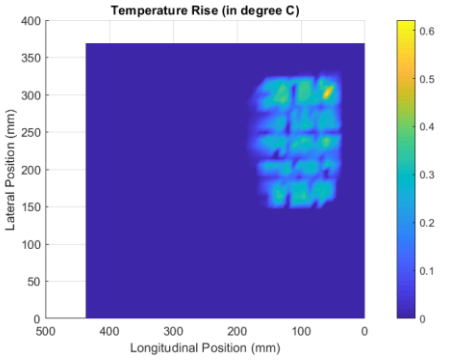

Tire E1

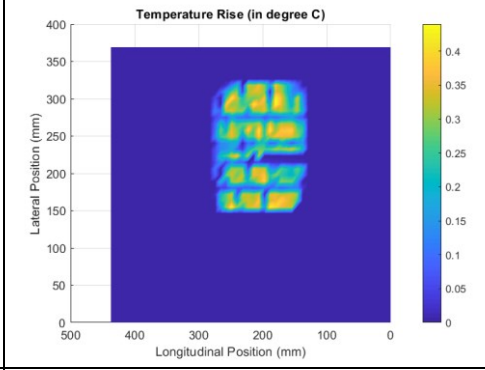

Tire E3

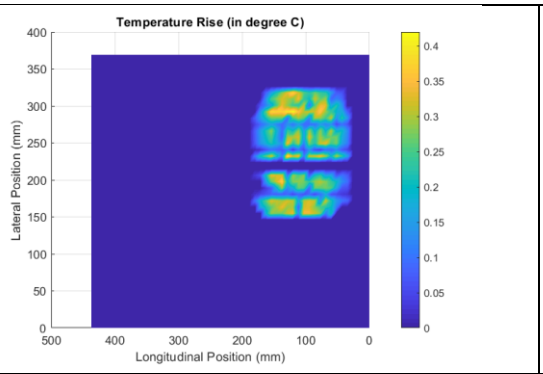	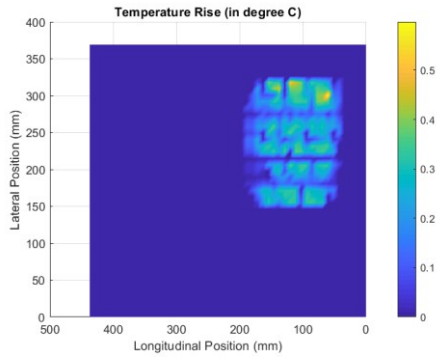
Tire F1	*Tire F3*
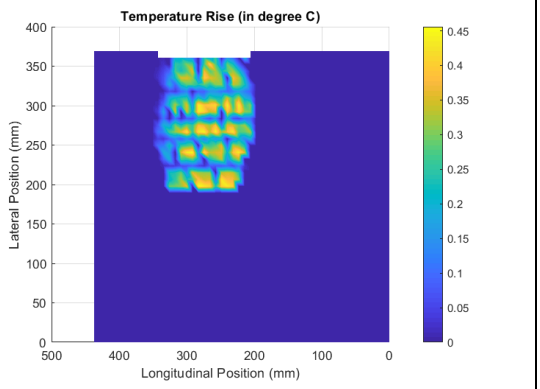	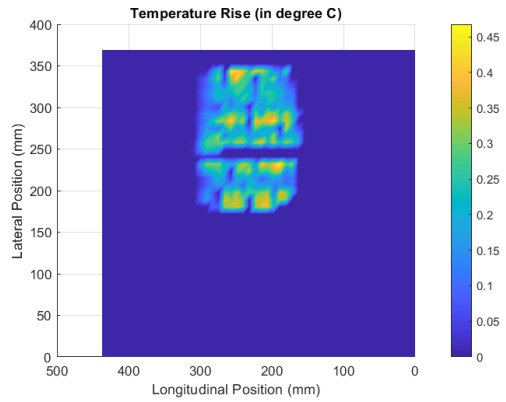
Tire G1	*Tire G3*
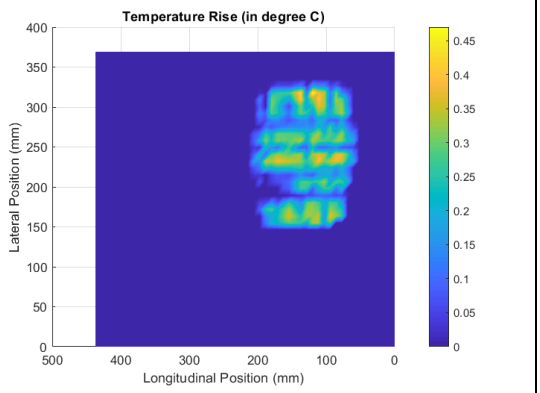	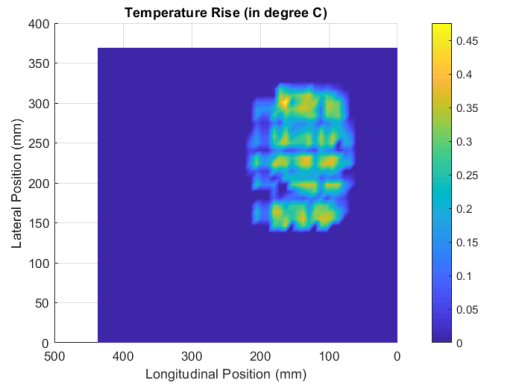
Tire H1	*Tire H3*

Table B- 3: Rise in temperature simulation for all the tires at 8% slip ratio using ATIIM

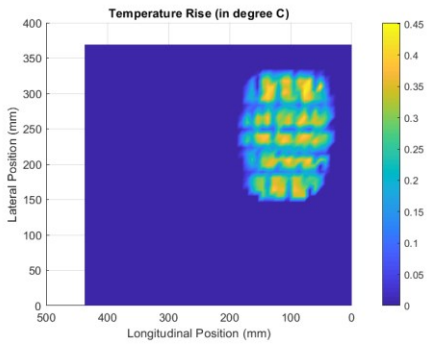

Tire A1

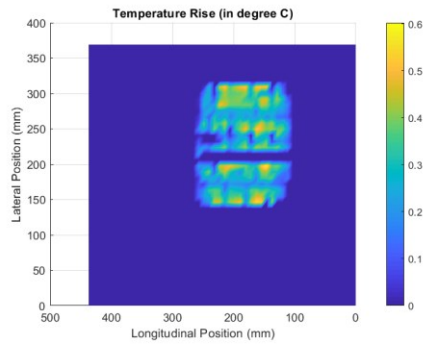

Tire A3

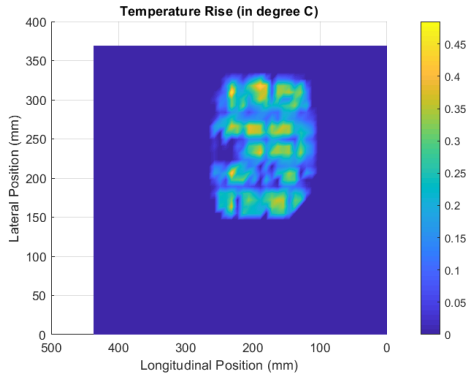

Tire B1

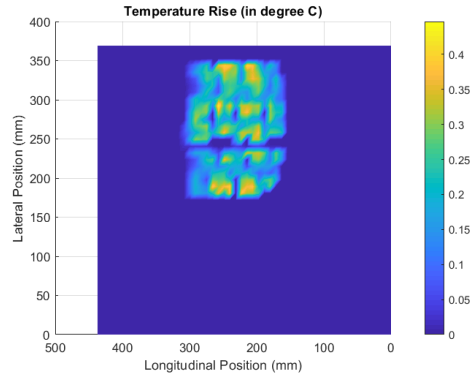

Tire B3

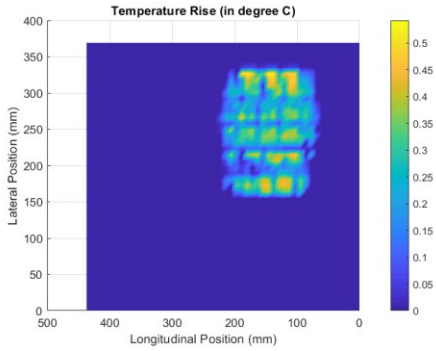

Tire C1

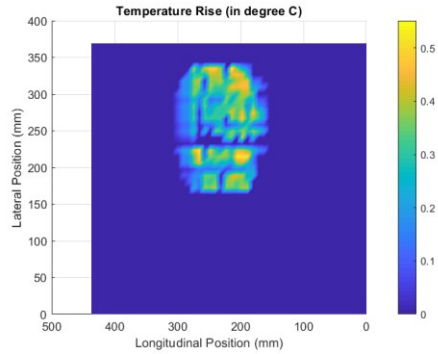

Tire C3

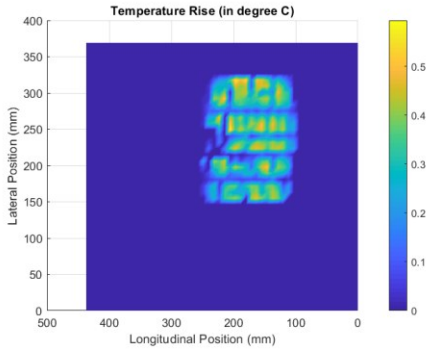

Tire D1

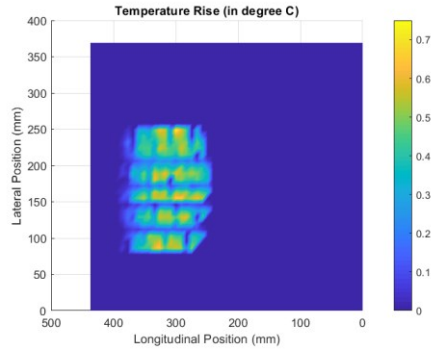

Tire D3

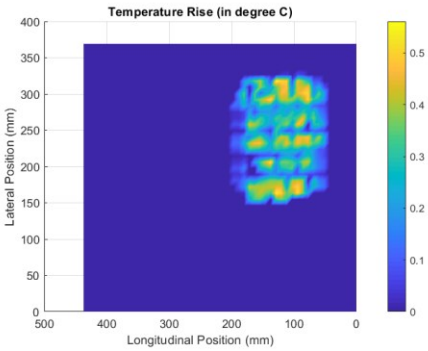

Tire E1

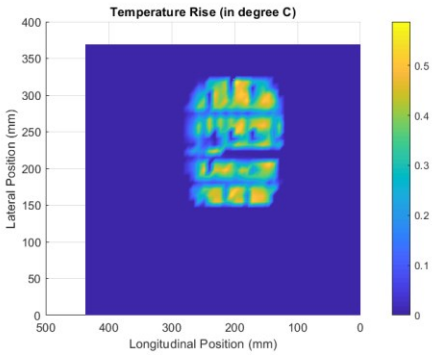

Tire E3

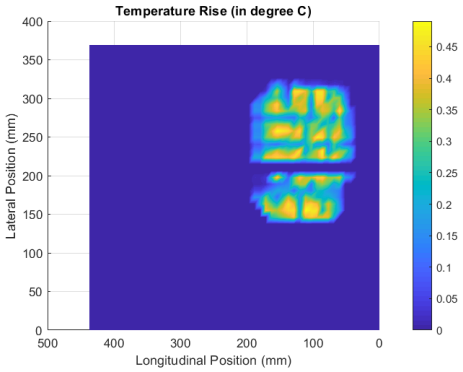

Tire F1

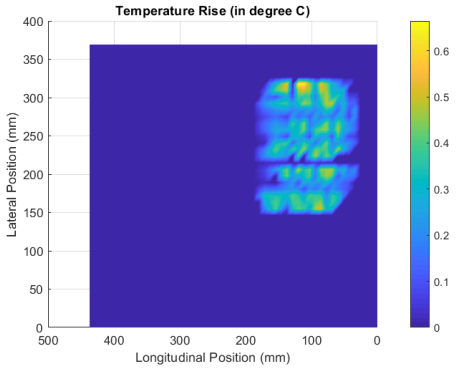

Tire F3

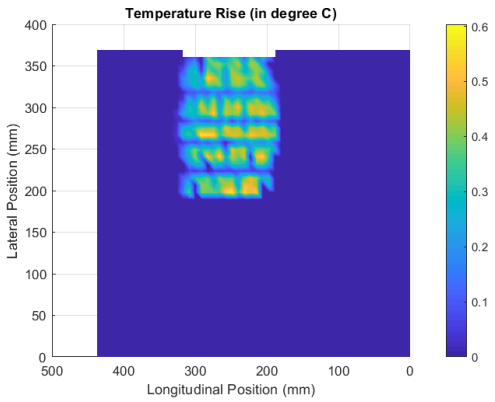

Tire G1

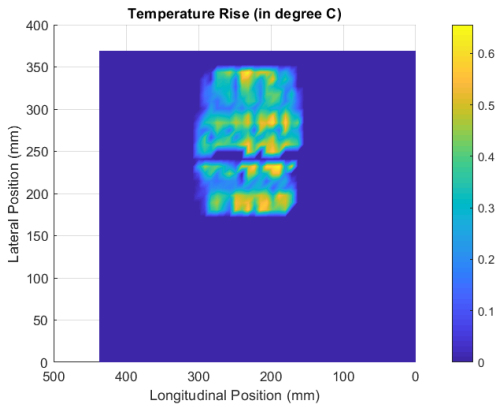

Tire G3

Tire H1	*Tire H3*

Table B- 4: Rise in temperature simulation for all the tires at 10% slip ratio using ATIIM

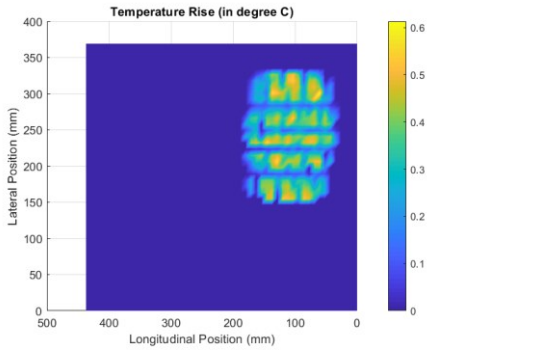	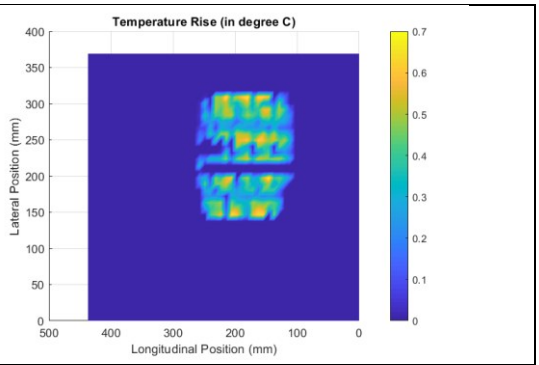
Tire A1	*Tire A3*
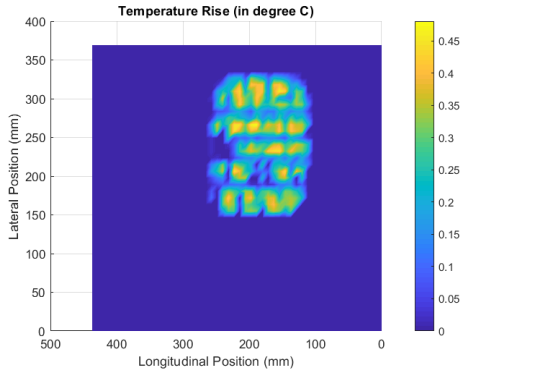	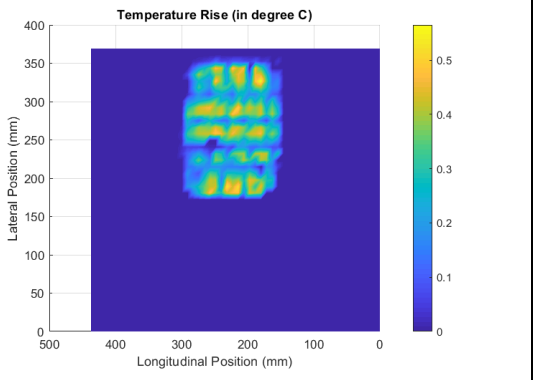
Tire B1	*Tire B3*
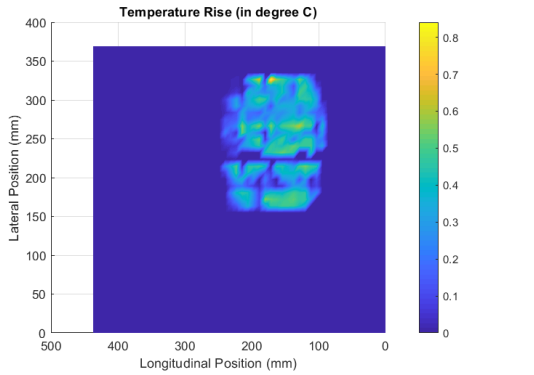	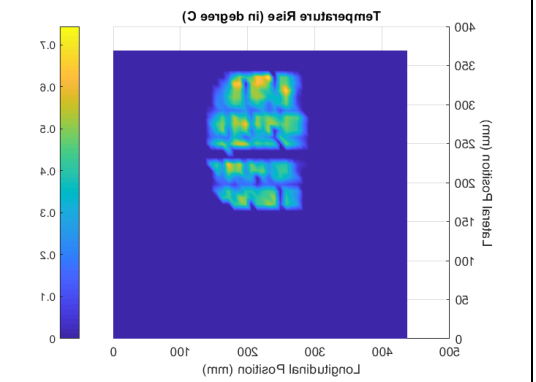
Tire C1	*Tire C3*

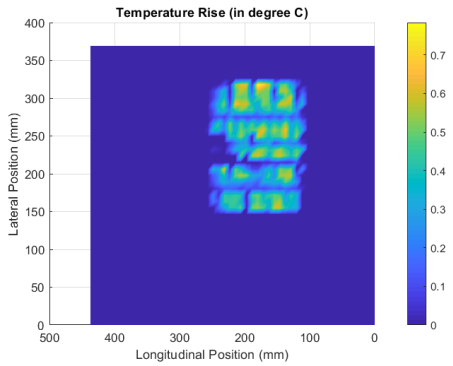

Tire D1

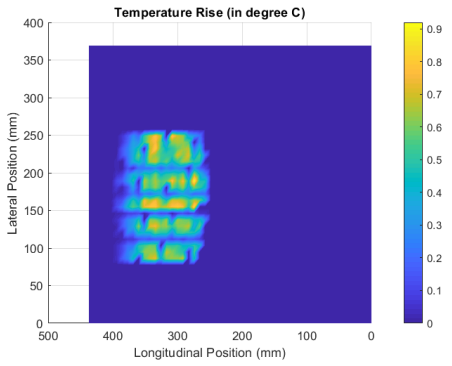

Tire D3

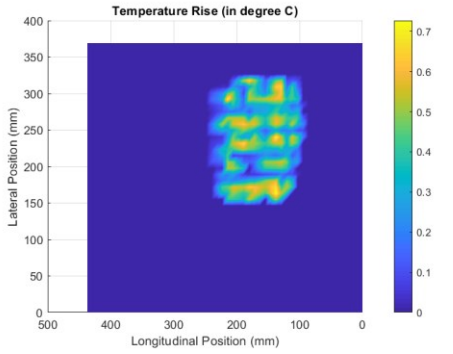

Tire E1

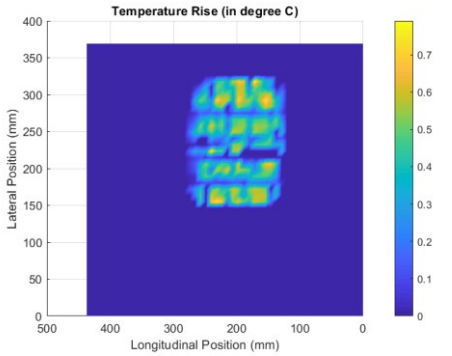

Tire E3

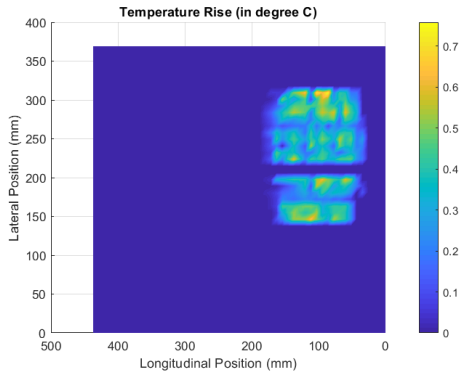

Tire F1

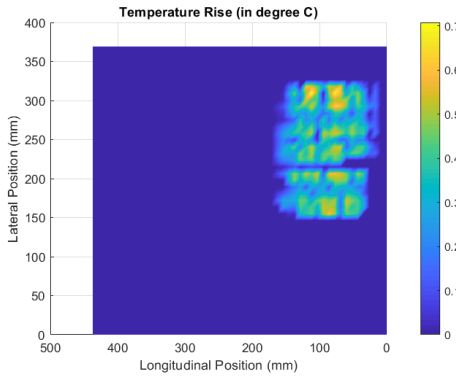

Tire F3

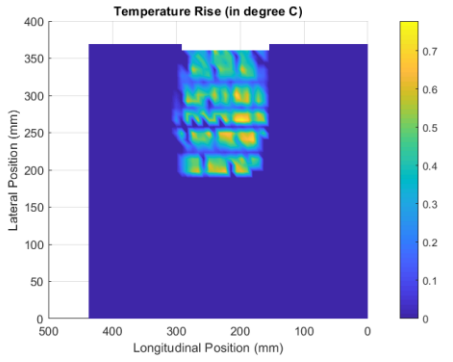

Tire G1

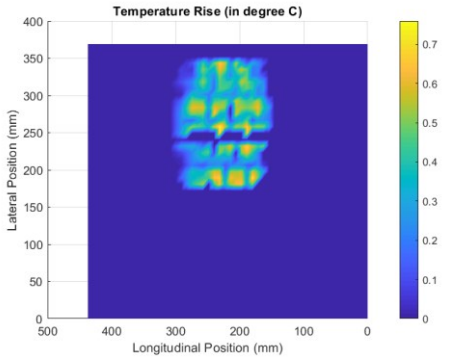

Tire G3

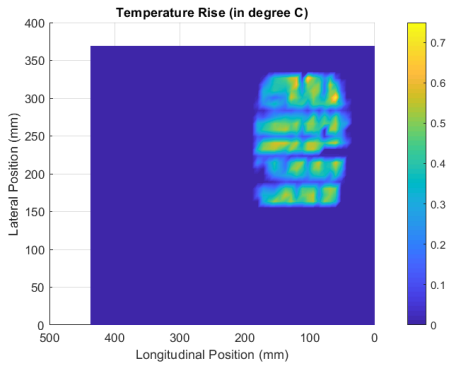	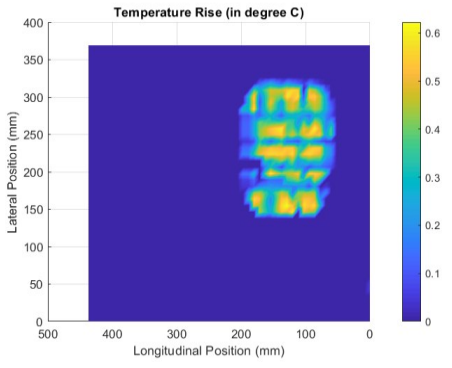
Tire H1	*Tire H3*

Table B- 5: Rise in temperature simulation for all the tires at 12% slip ratio using ATIIM

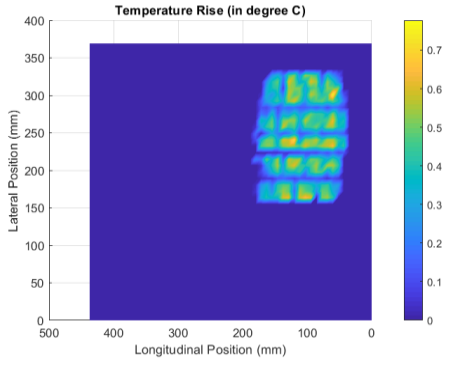	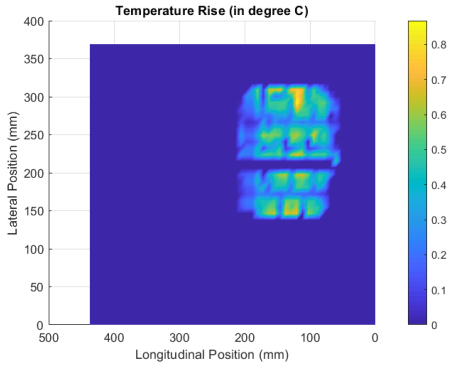
Tire A1	*Tire A3*
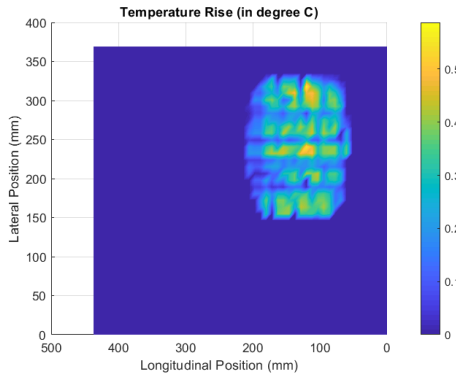	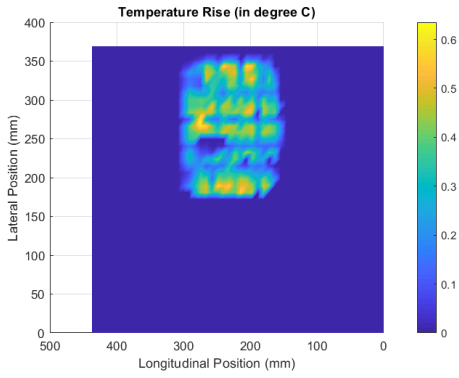
Tire B1	*Tire B3*

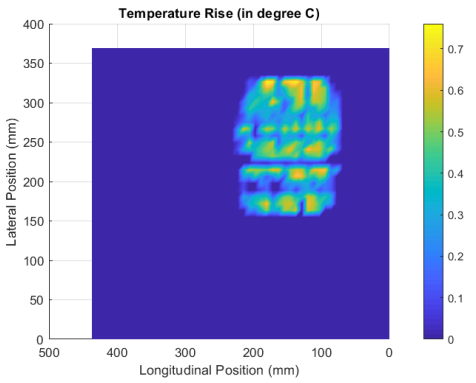

Tire C1

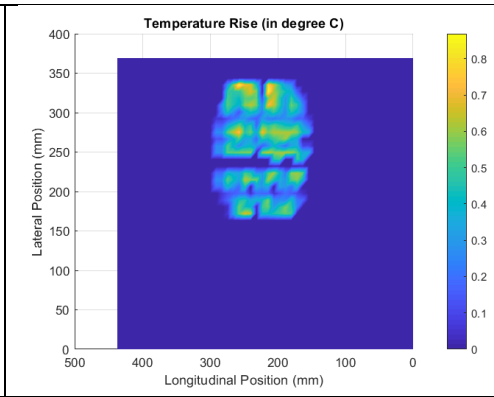

Tire C3

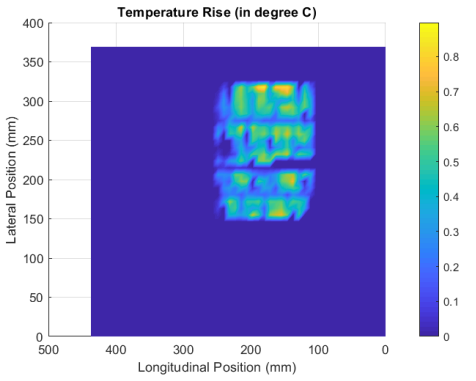

Tire D1

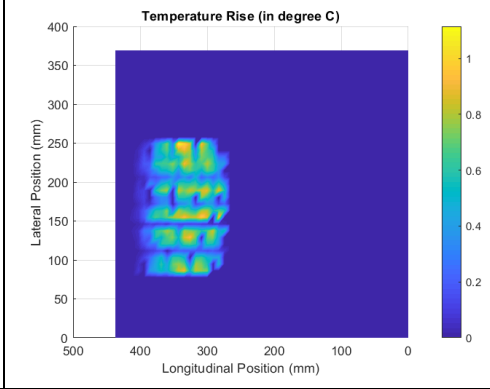

Tire D3

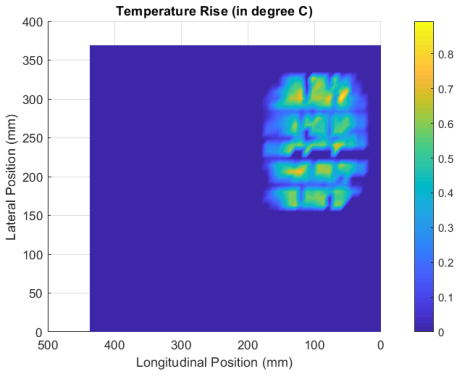

Tire E1

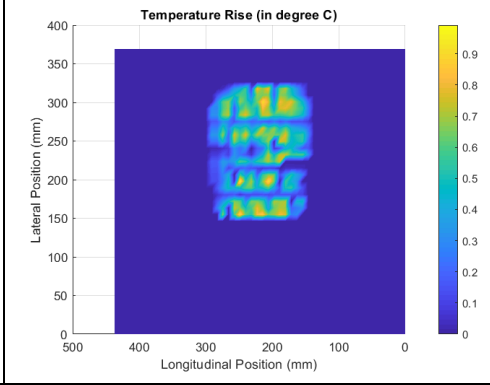

Tire E3

Tire F1	Tire F3
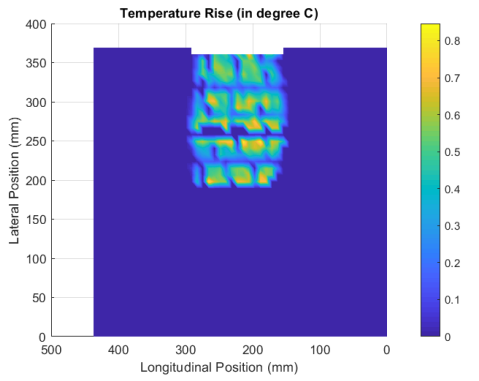	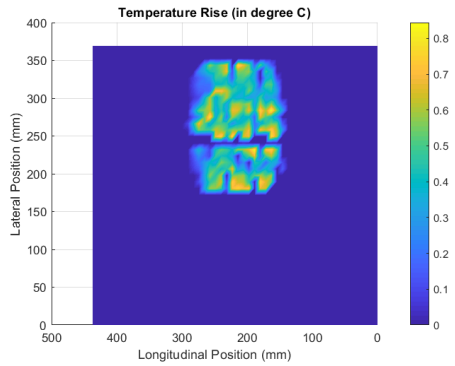
Tire G1	**Tire G3**
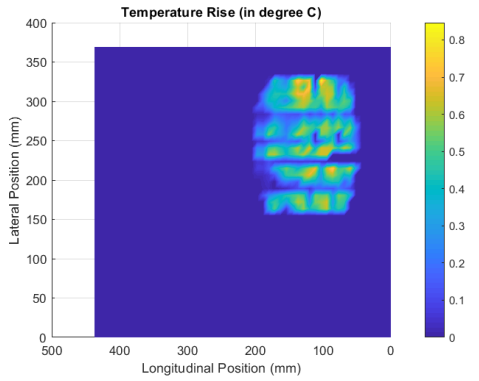	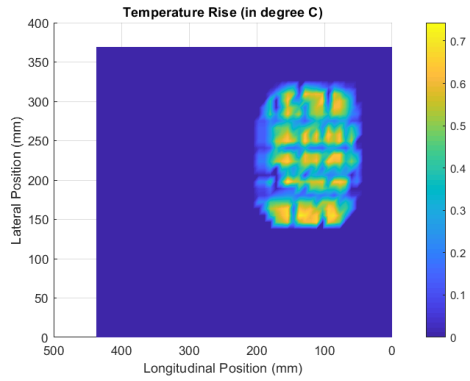
Tire H1	**Tire H3**

Table B- 6: Rise in temperature simulation for all the tires at 15% slip ratio using ATIIM

Tire A1	Tire A3
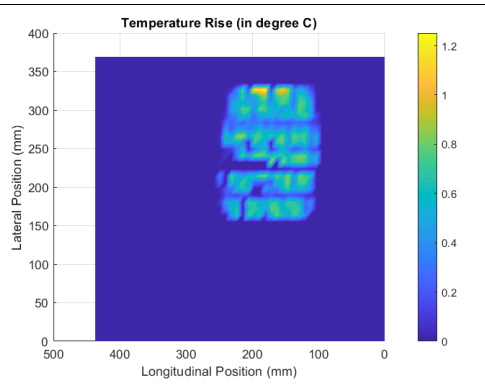	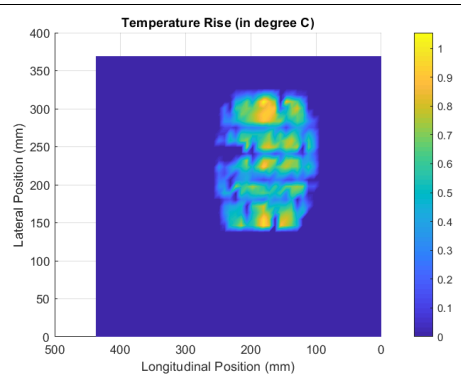

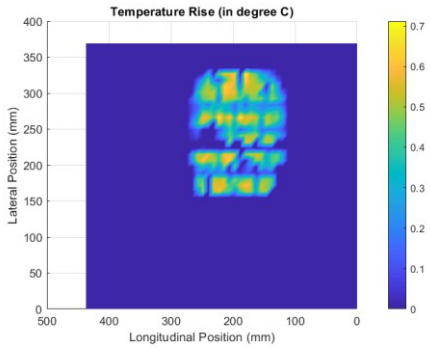

Tire B1

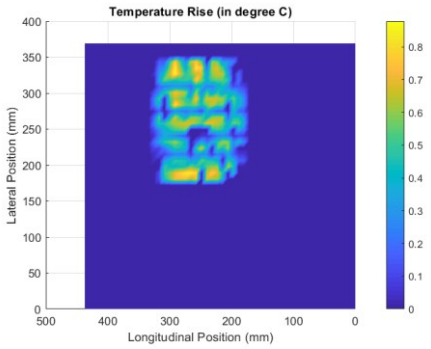

Tire B3

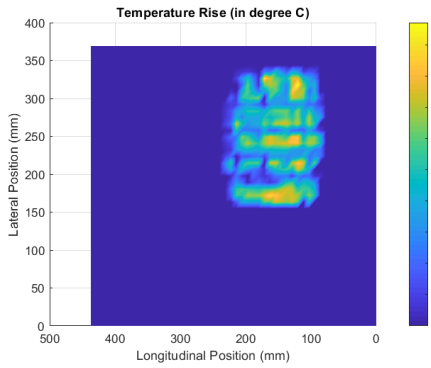

Tire C1

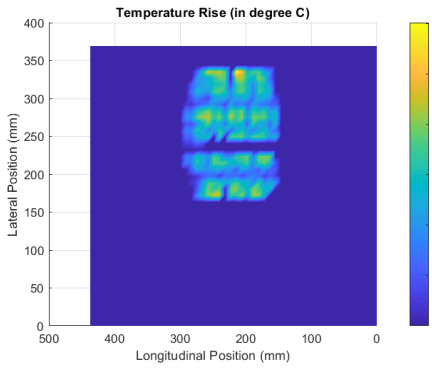

Tire C3

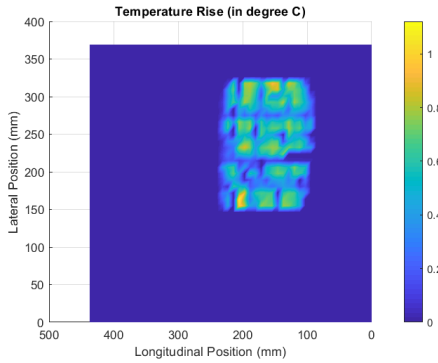

Tire D1

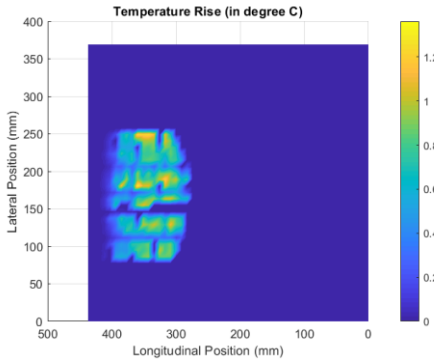

Tire D3

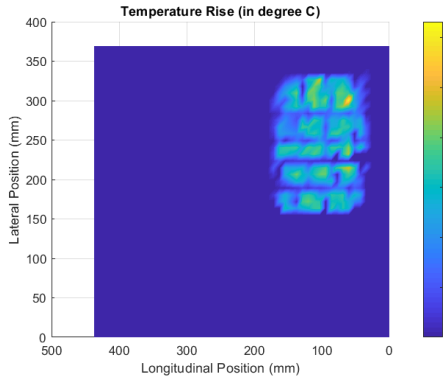

Tire E1

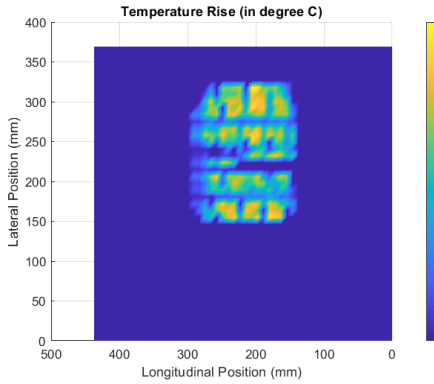

Tire E3

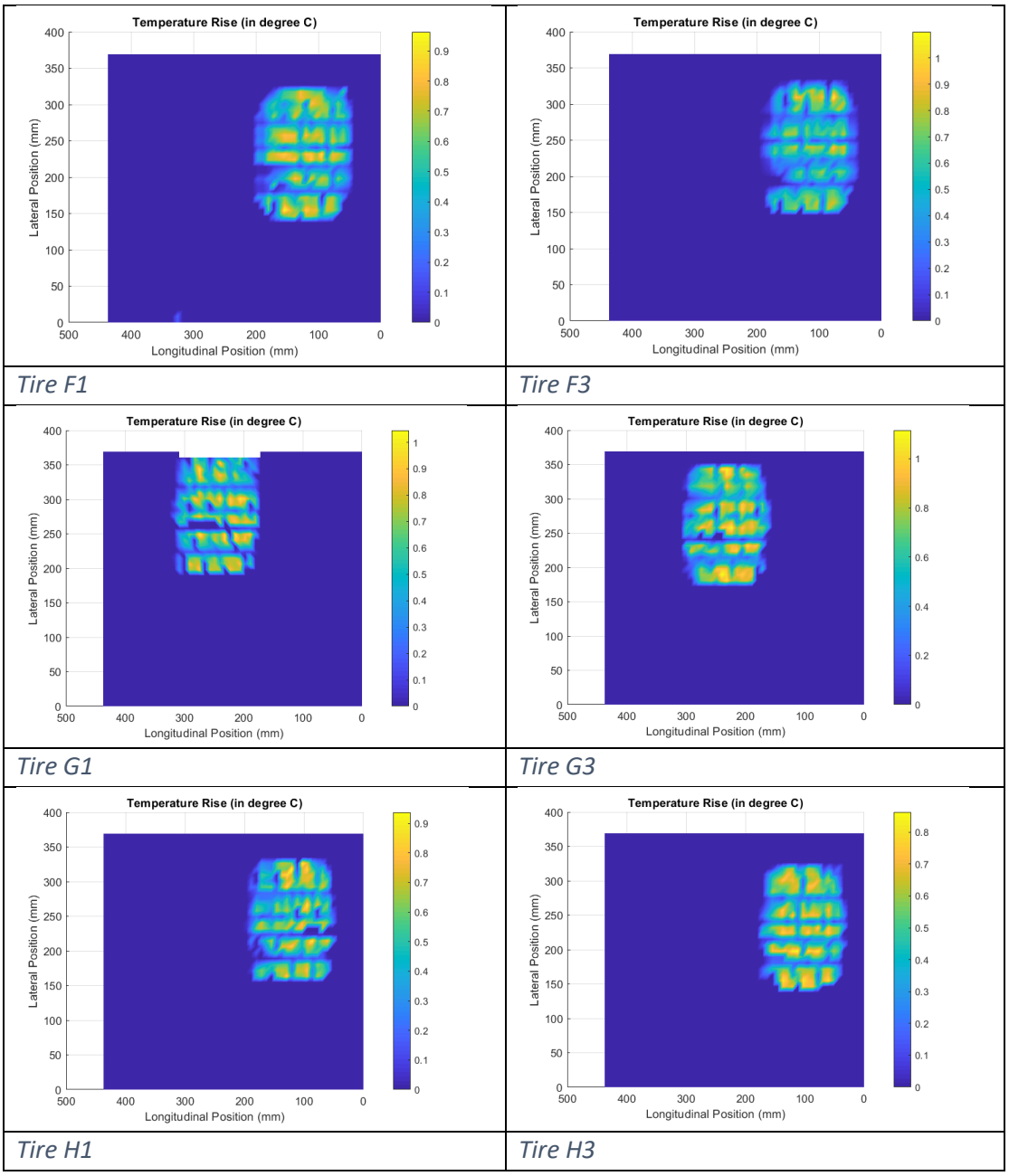

Tire F1 | *Tire F3*

Tire G1 | *Tire G3*

Tire H1 | *Tire H3*

B. 2. Additional results for height of water film simulations by ATIIM 2.0

In this section the predicted height of water film simulated using ATIIM 2.0 is presented for all but tires of rubber compound D from Table B- 7 to Table B- 12.

Table B- 7: Predicted height of water film using ATIIM 2.0 for 2% slip ratio

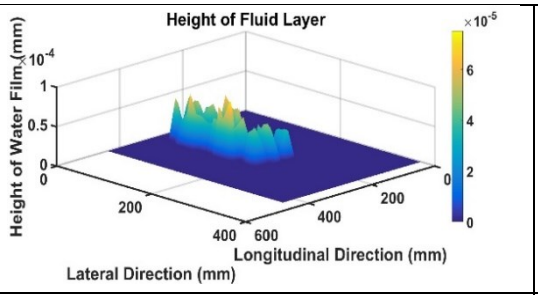	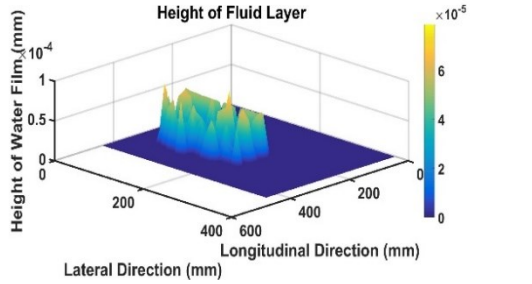
Tire A1	*Tire A3*
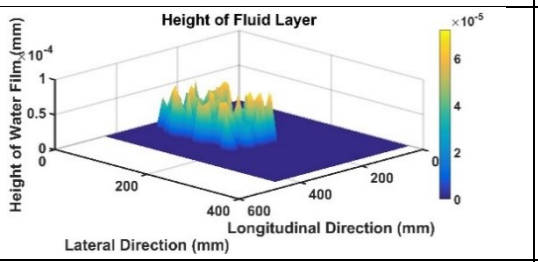	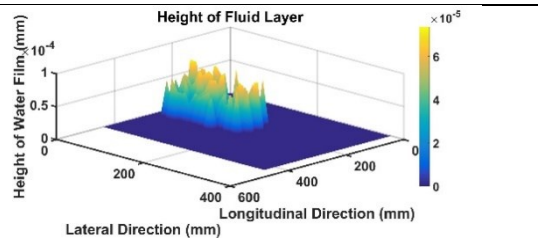
Tire B1	*Tire B3*
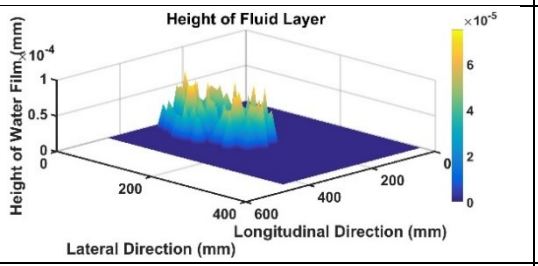	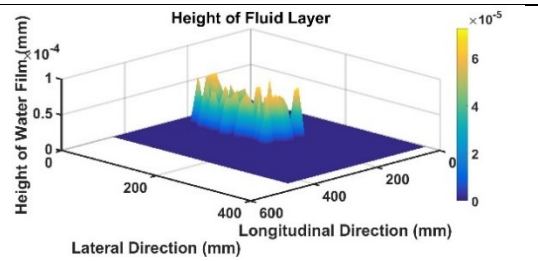
Tire C1	*Tire C3*
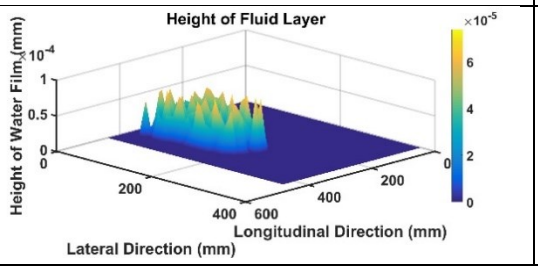	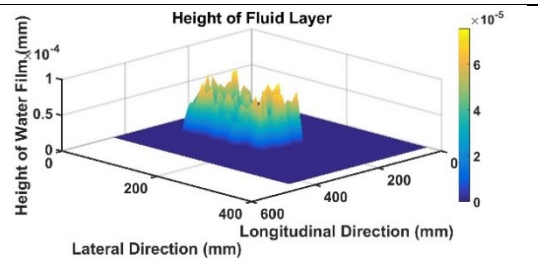
Tire E1	*Tire E3*
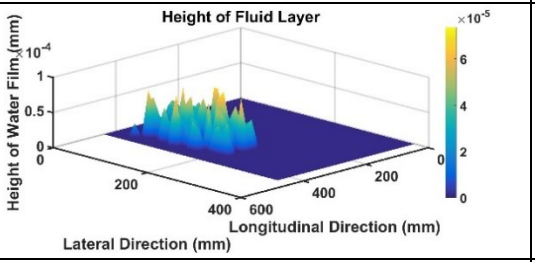	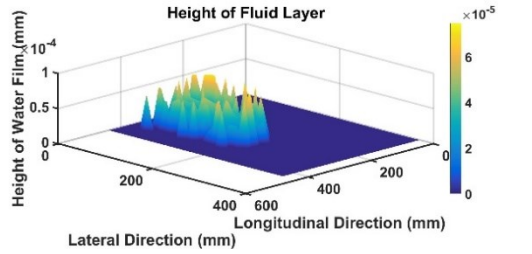
Tire F1	*Tire F3*

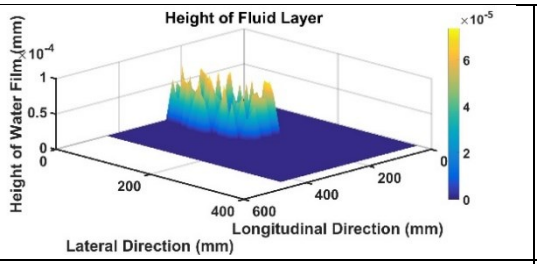	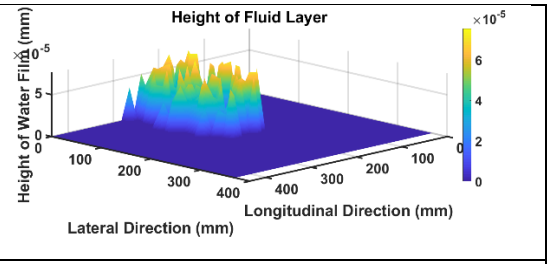
Tire G1	*Tire G3*
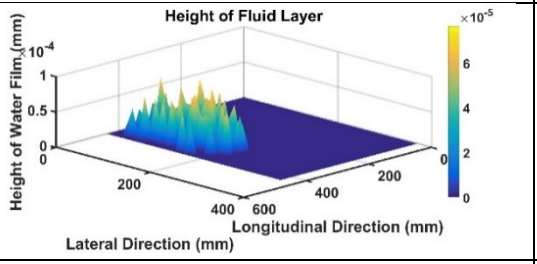	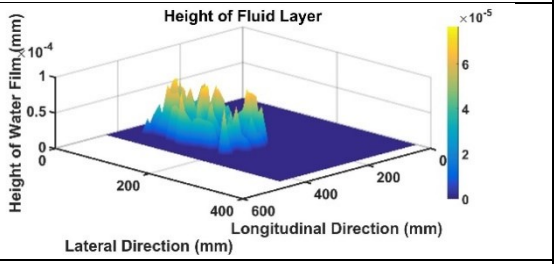
Tire H1	*Tire H3*

Table B- 8: Predicted height of water film using ATIIM 2.0 for 6% slip ratio

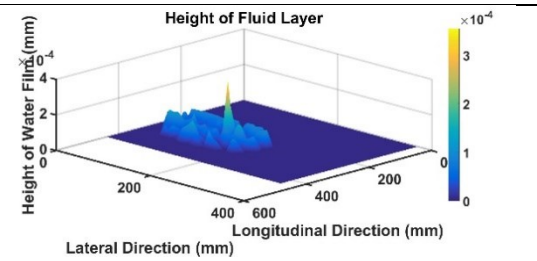	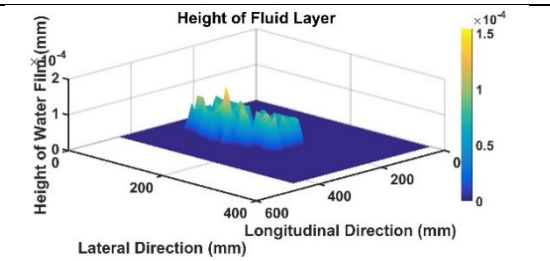
Tire A1	*Tire A3*
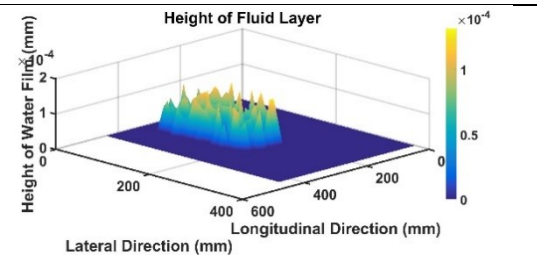	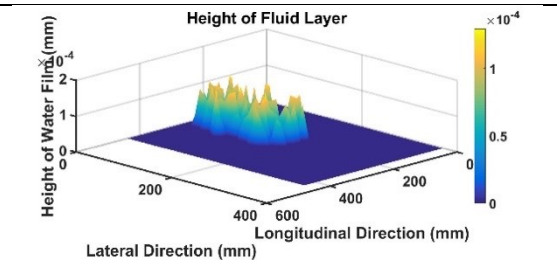
Tire B1	*Tire B3*
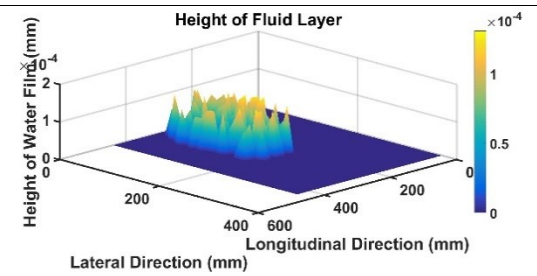	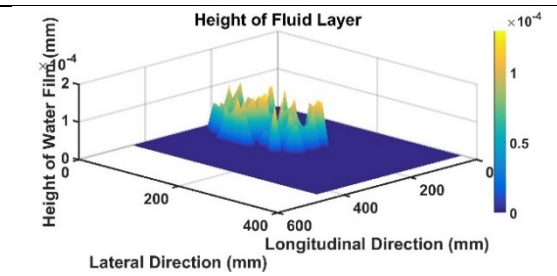
Tire C1	*Tire C3*

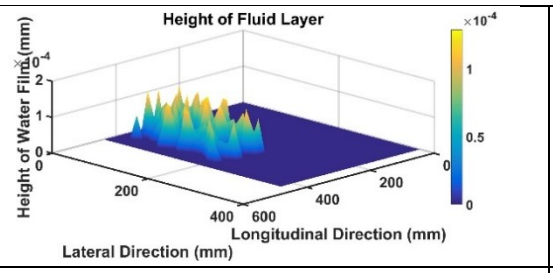	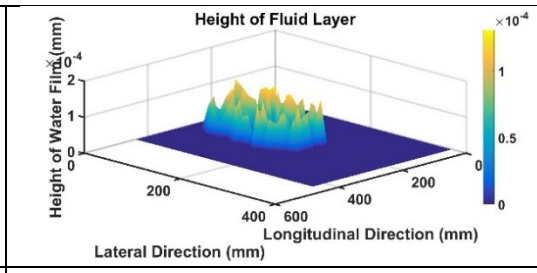
Tire E1	*Tire E3*
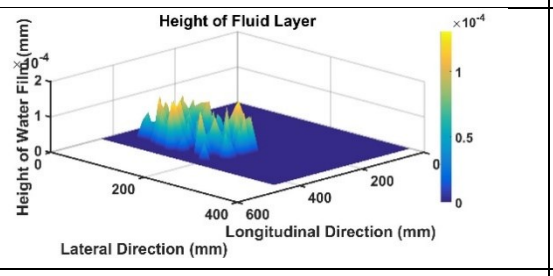	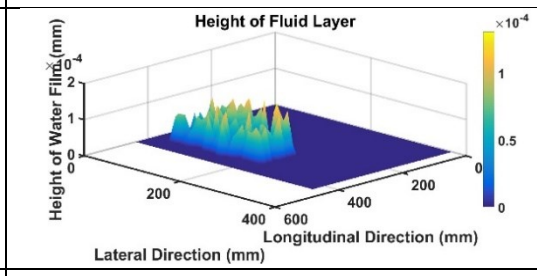
Tire F1	*Tire F3*
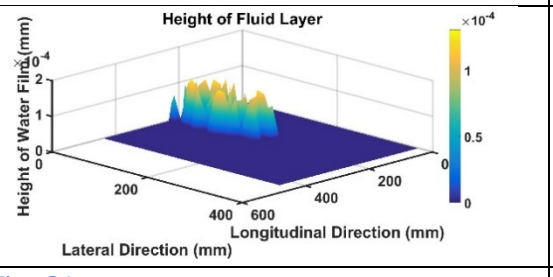	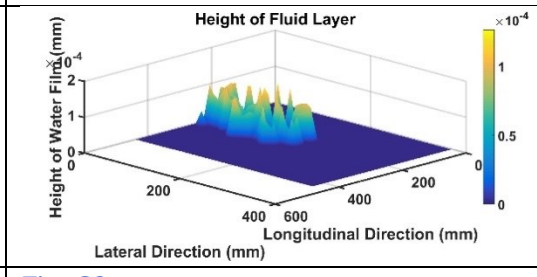
Tire G1	*Tire G3*
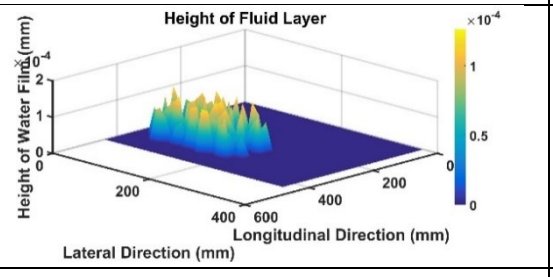	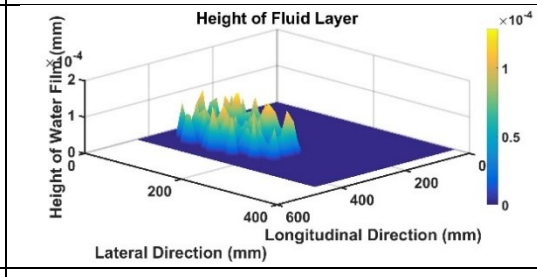
Tire H1	*Tire H3*

Table B- 9: Predicted height of water film using ATIIM 2.0 for 8% slip ratio

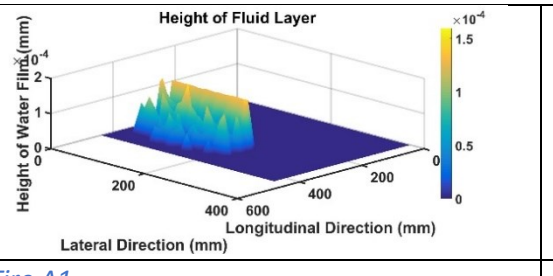	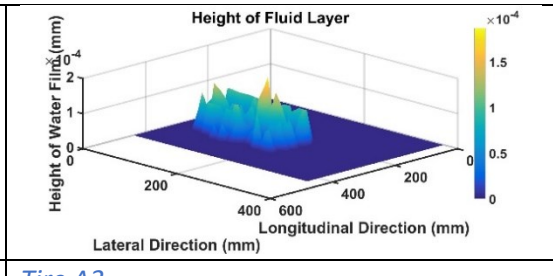
Tire A1	*Tire A3*

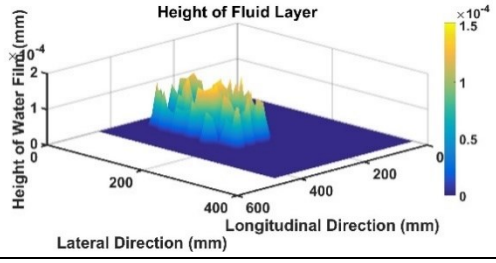

Tire B1

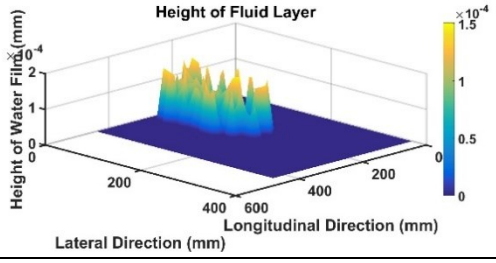

Tire B3

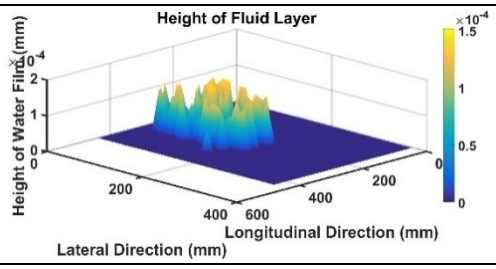

Tire C1

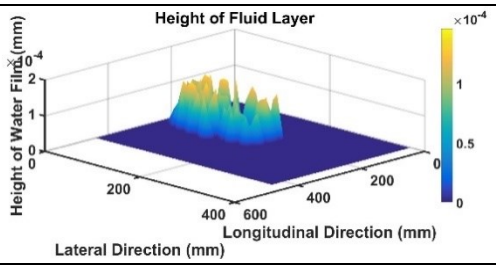

Tire C3

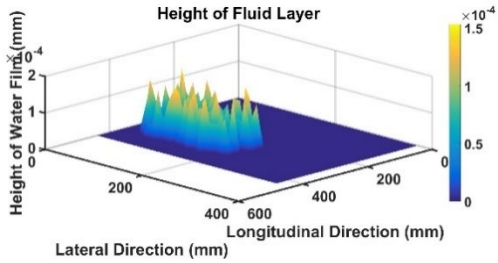

Tire E1

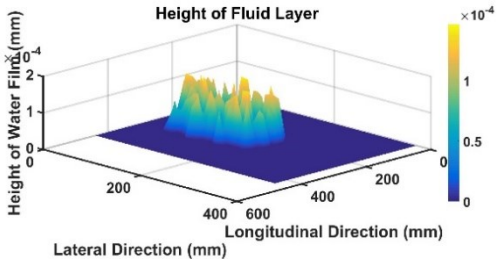

Tire E3

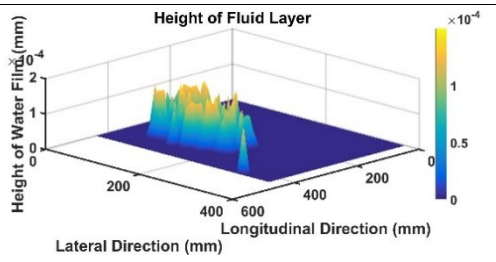

Tire F1

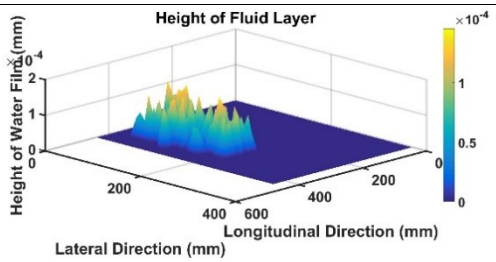

Tire F3

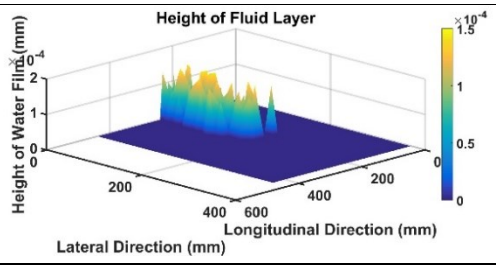

Tire G1

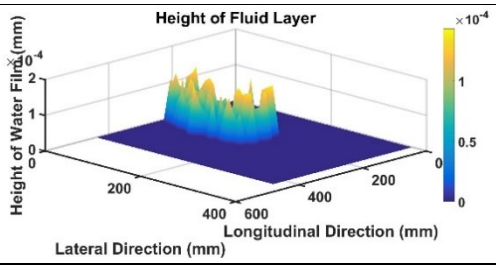

Tire G3

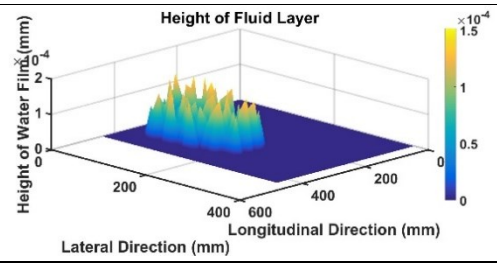	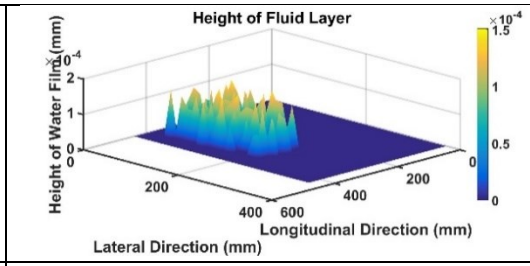
Tire H1	*Tire H3*

Table B- 10: Predicted height of water film using ATIIM 2.0 for 10% slip ratio

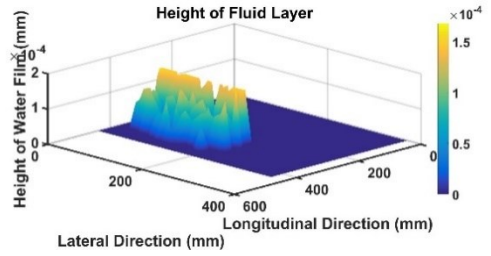	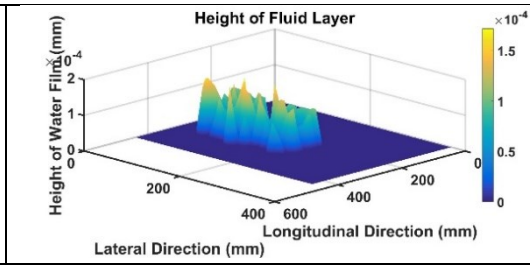
Tire A1	*Tire A3*
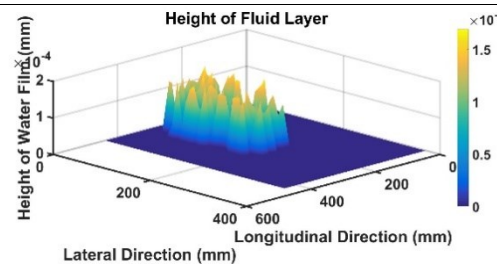	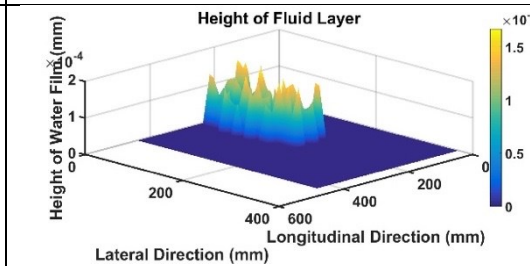
Tire B1	*Tire B3*
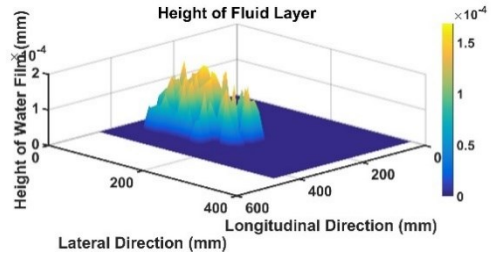	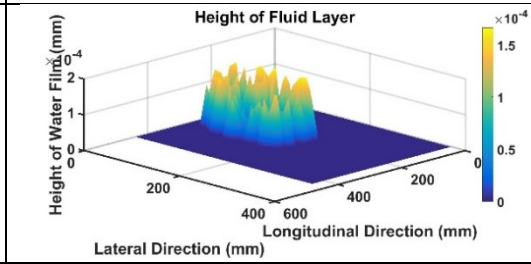
Tire C1	*Tire C3*
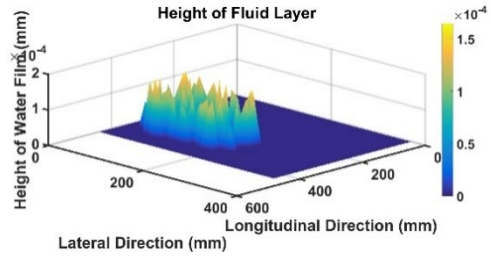	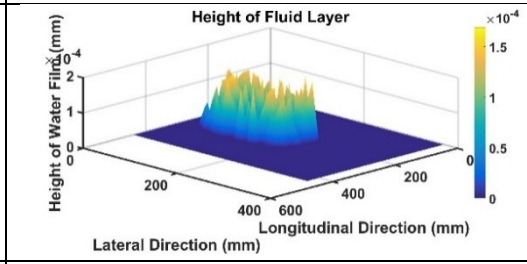
Tire E1	*Tire E3*

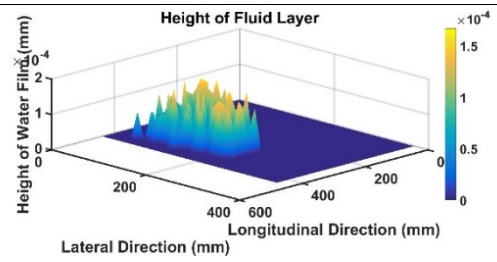	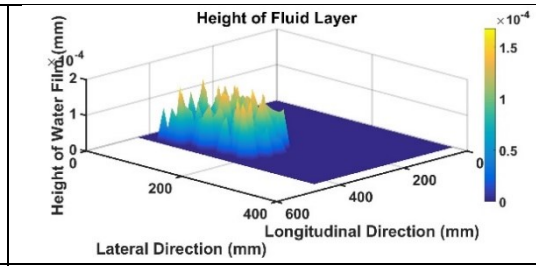
Tire F1	*Tire F3*
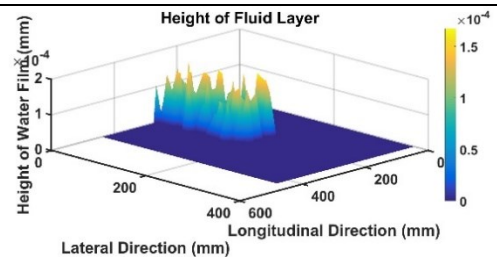	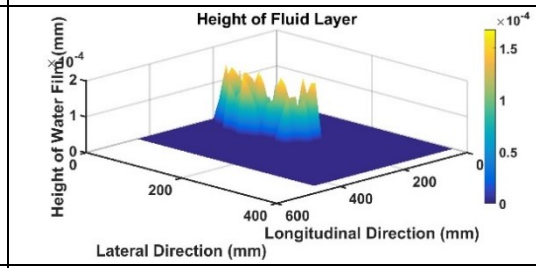
Tire G1	*Tire G3*
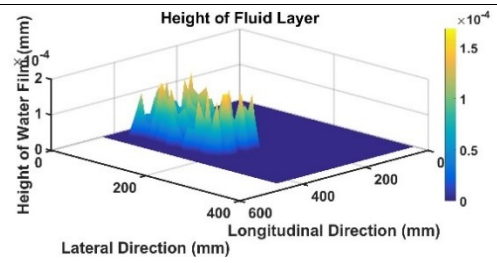	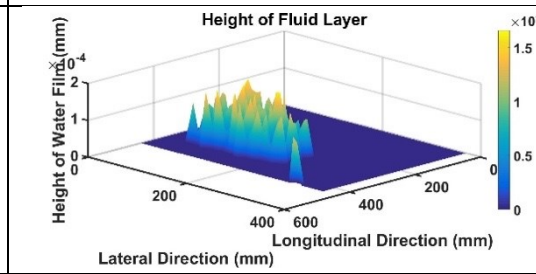
Tire H1	*Tire H3*

Table B- 11: Predicted height of water film using ATIIM 2.0 for 12% slip ratio

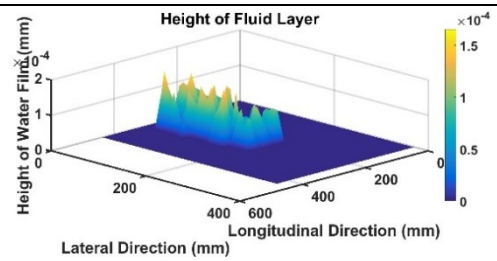	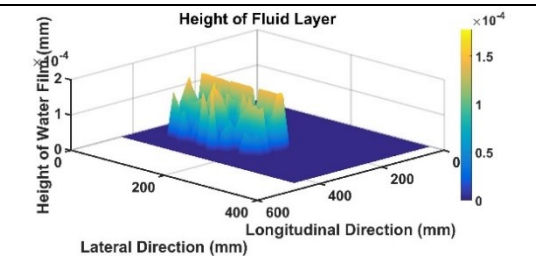
Tire A1	*Tire A3*
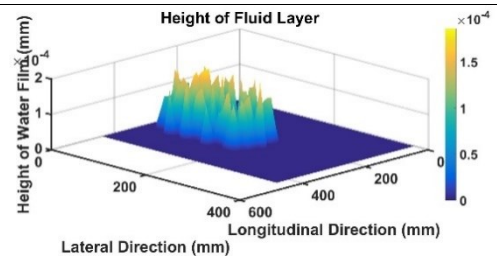	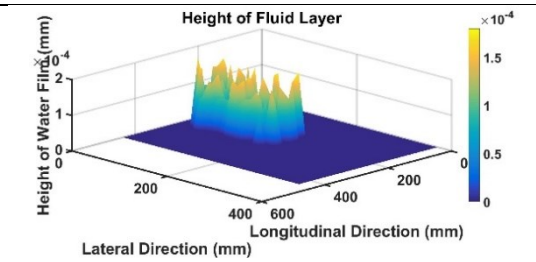
Tire B1	*Tire B3*

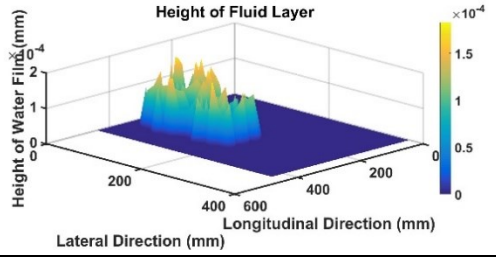

Tire C1

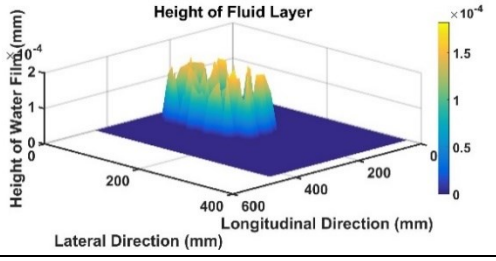

Tire C3

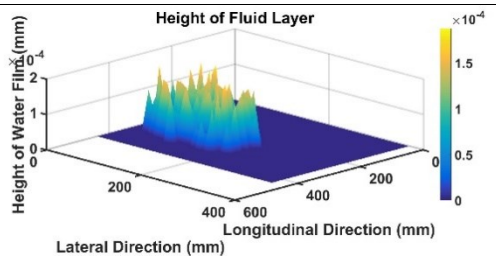

Tire E1

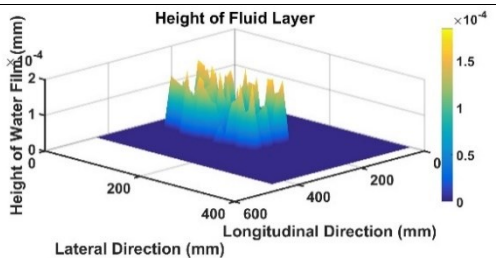

Tire E3

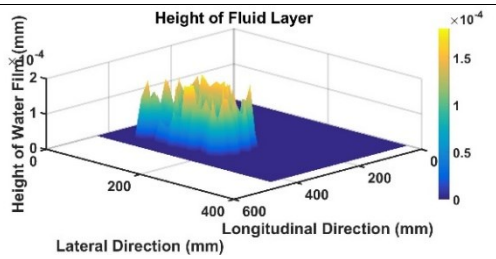

Tire F1

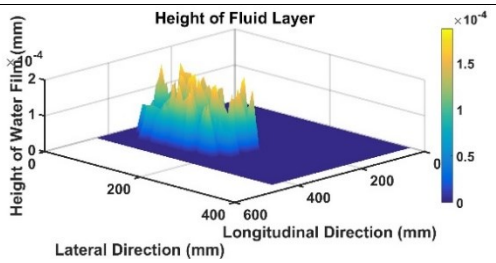

Tire F3

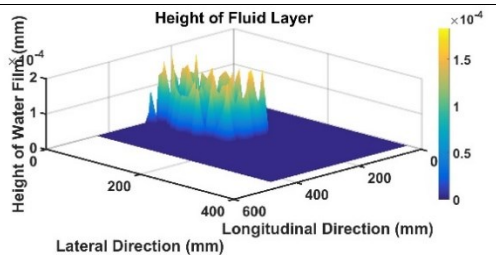

Tire G1

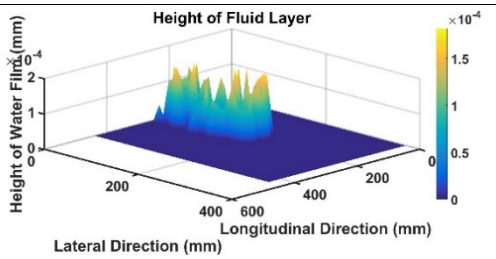

Tire G3

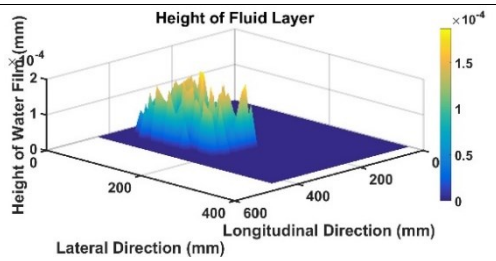

Tire H1

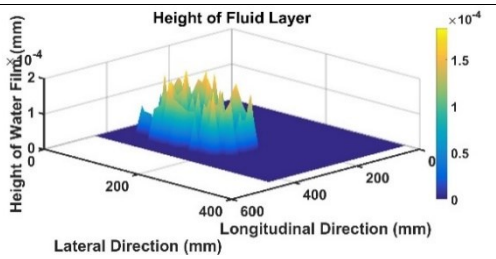

Tire H3

Table B- 12: Predicted height of water film using ATIIM 2.0 for 15% slip ratio

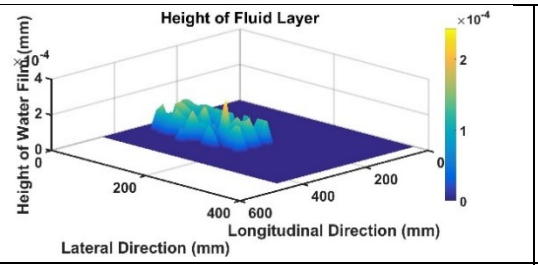	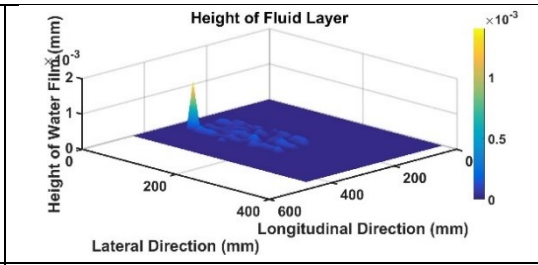
Tire A1	*Tire A3*
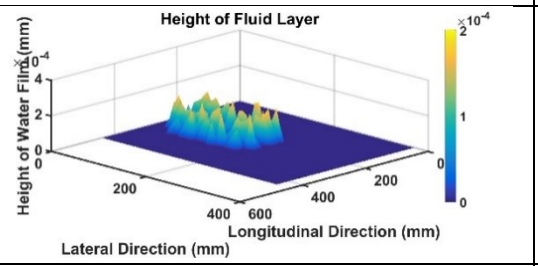	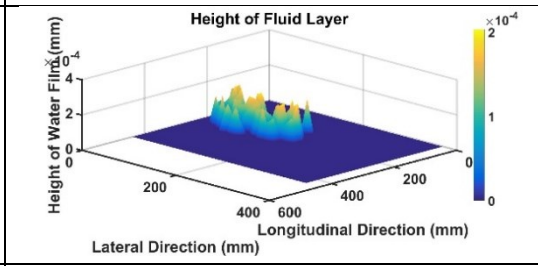
Tire B1	*Tire B3*
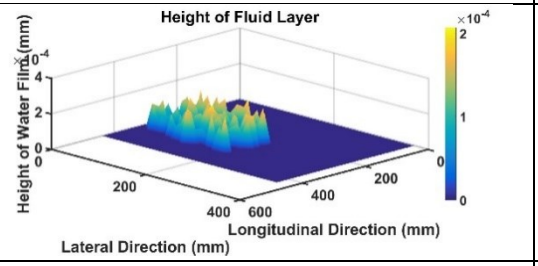	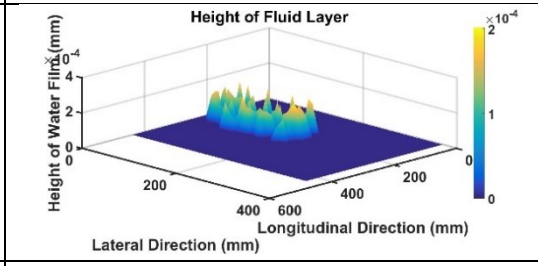
Tire C1	*Tire C3*
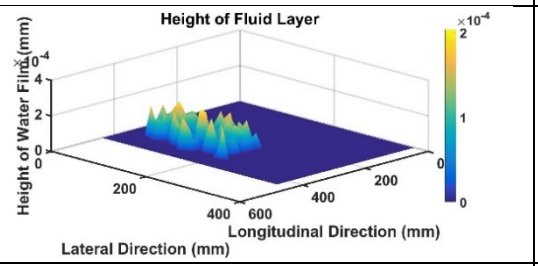	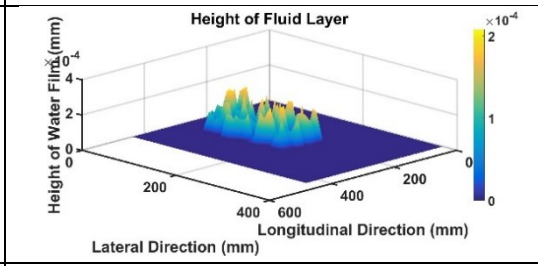
Tire E1	*Tire E3*
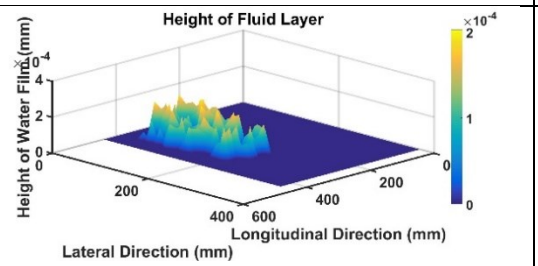	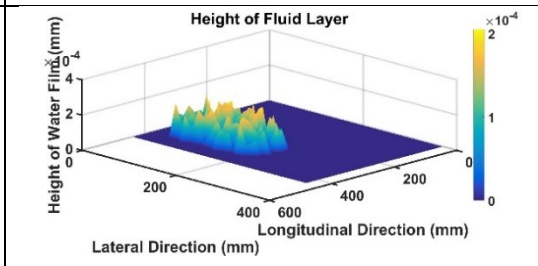
Tire F1	*Tire F3*

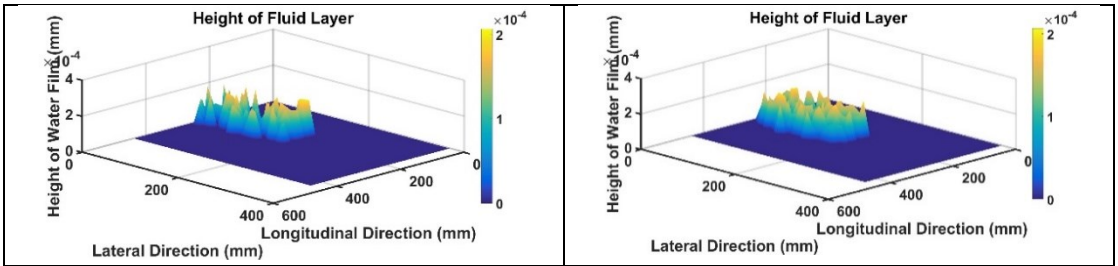

Tire G1

Tire G3

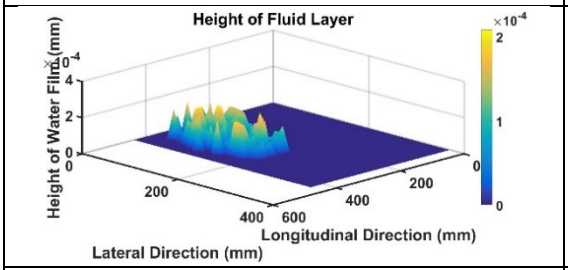

Tire H1

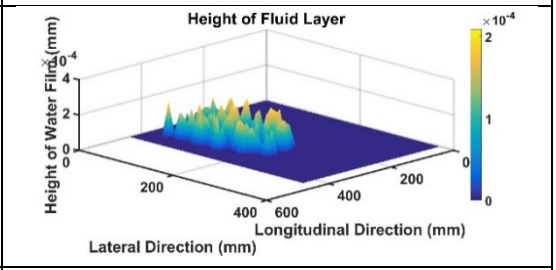

Tire H3

B. 3. Additional results from Hayhoe and Shapley model simulations

In this section the results for temperature rise and water film height simulated using the Hayhoe and Shapley model are presented from Figure B- 1 to Figure B- 15.

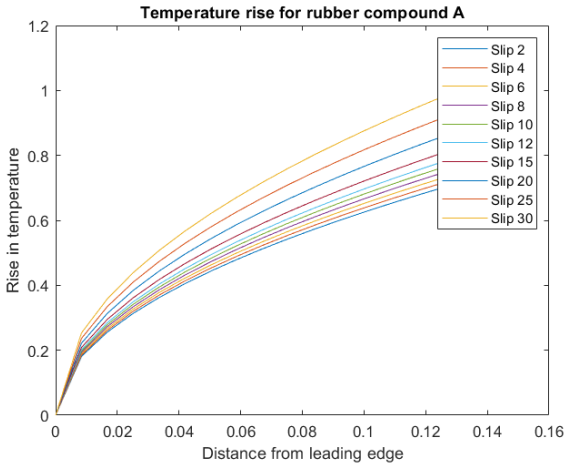

Figure B- 1: Rise in temperature for rubber compound A using Hayhoe model against distance from leading edge

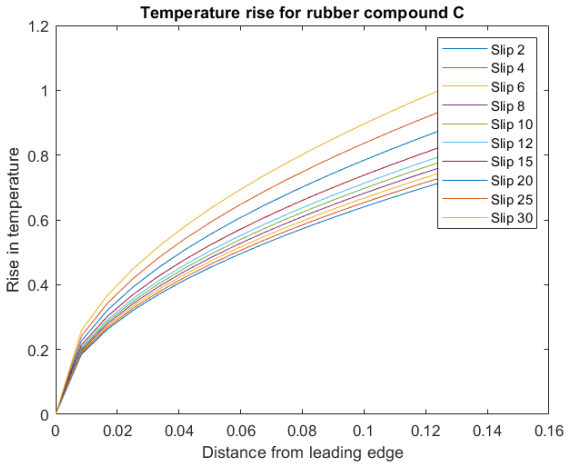

Figure B- 2: Rise in temperature for rubber compound C using Hayhoe model against distance from leading edge

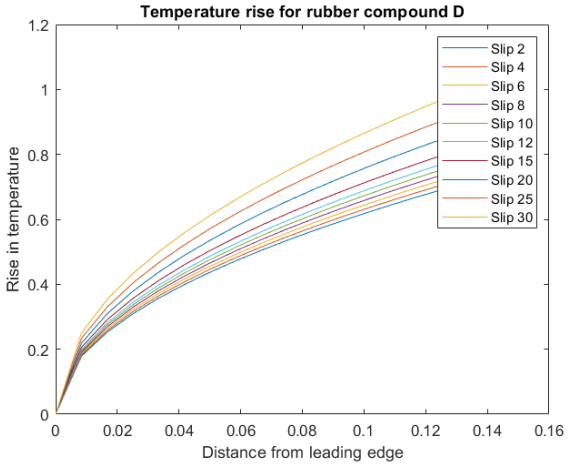

Figure B- 3: Rise in temperature for rubber compound D using Hayhoe model against distance from leading edge

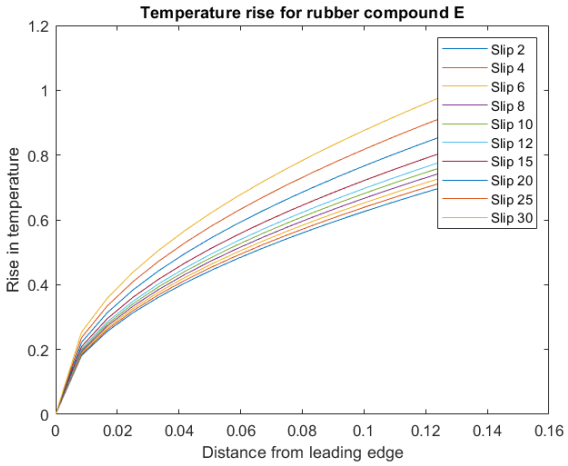

Figure B- 4: Rise in temperature for rubber compound E using Hayhoe model against distance from leading edge

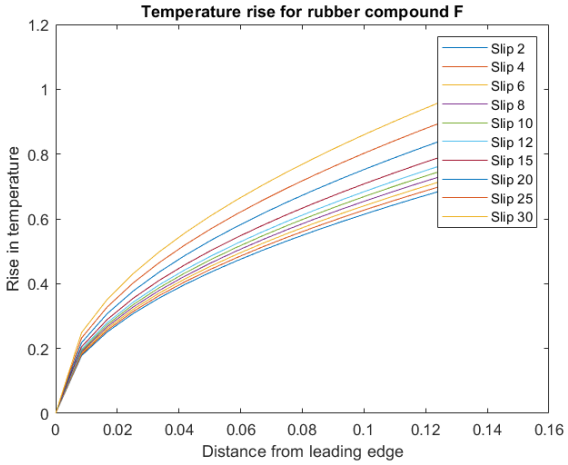

Figure B- 5: Rise in temperature for rubber compound F using Hayhoe model against distance from leading edge

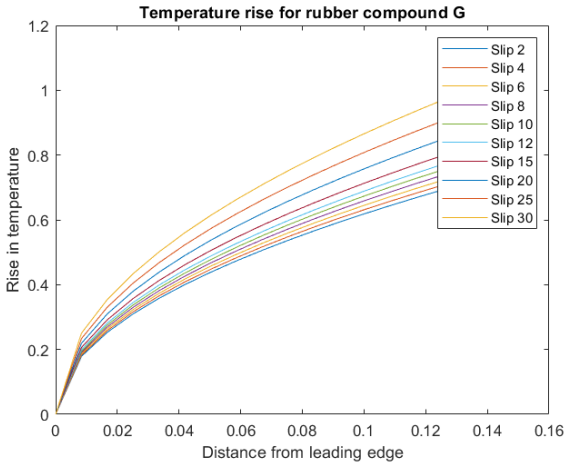

Figure B- 6: Rise in temperature for rubber compound G using Hayhoe model against distance from leading edge

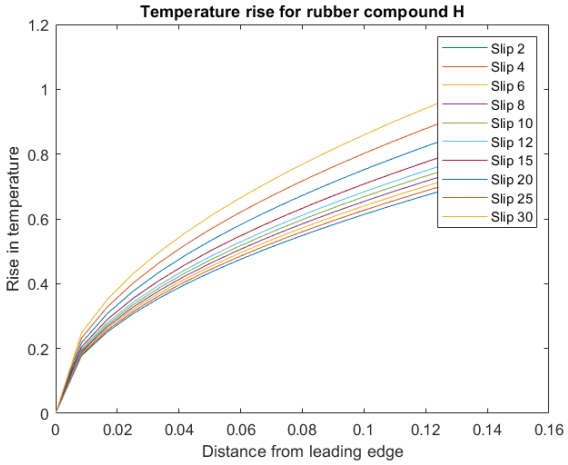

Figure B- 7: Rise in temperature for rubber compound H using Hayhoe model against distance from leading edge

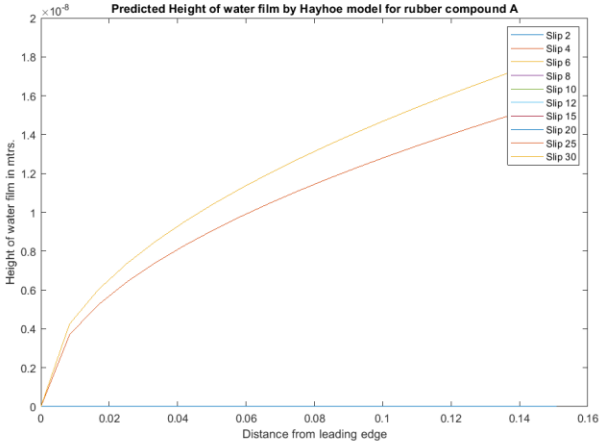

Figure B- 8: Predicted Height of water film by Hayhoe model for rubber compound A

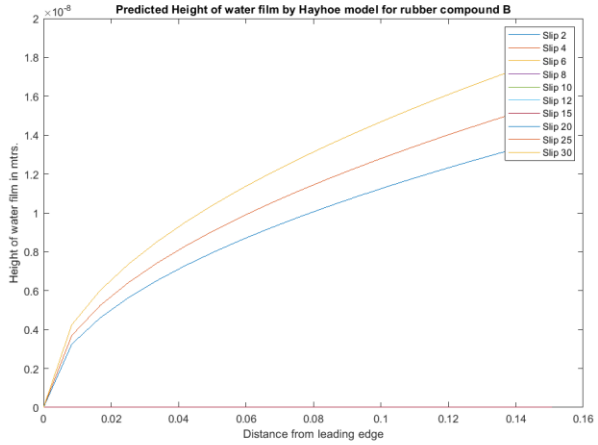

Figure B- 9: Predicted Height of water film by Hayhoe model for rubber compound B

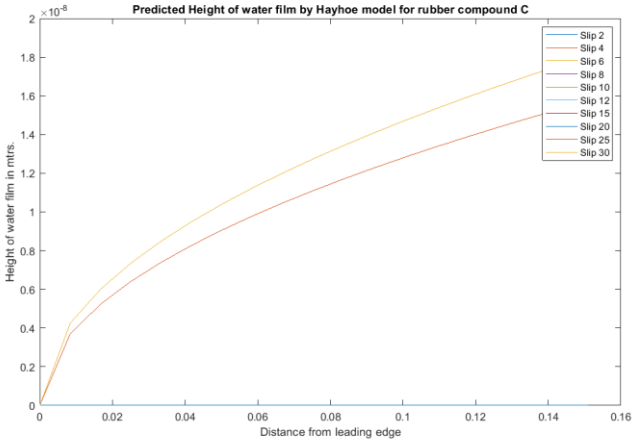

Figure B- 10: Predicted Height of water film by Hayhoe model for rubber compound C

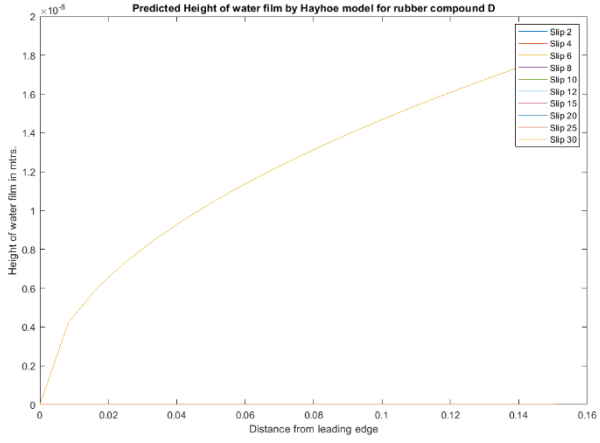

Figure B- 11: Predicted Height of water film by Hayhoe model for rubber compound D

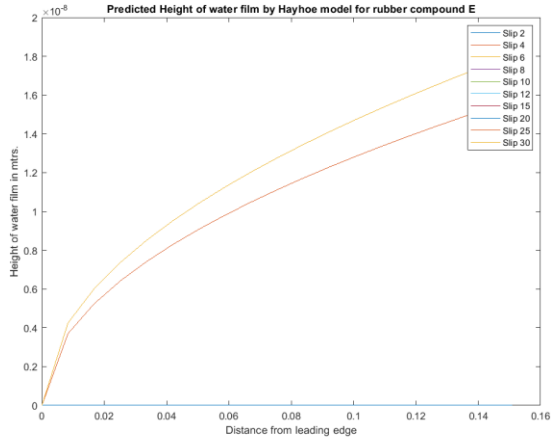

Figure B- 12: Predicted Height of water film by Hayhoe model for rubber compound E

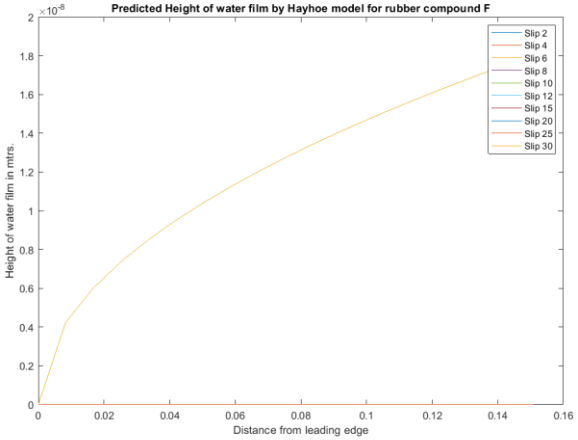

Figure B- 13: Predicted Height of water film by Hayhoe model for rubber compound F

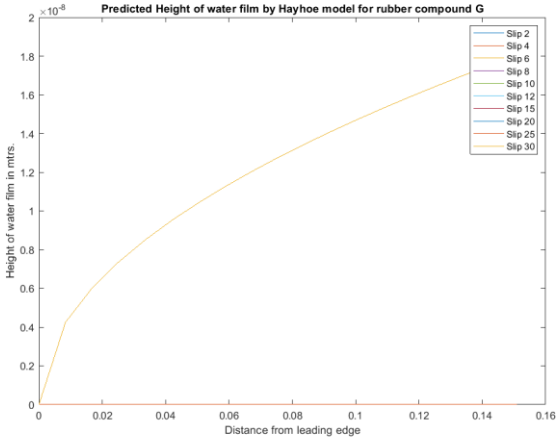

Figure B- 14: Predicted Height of water film by Hayhoe model for rubber compound G

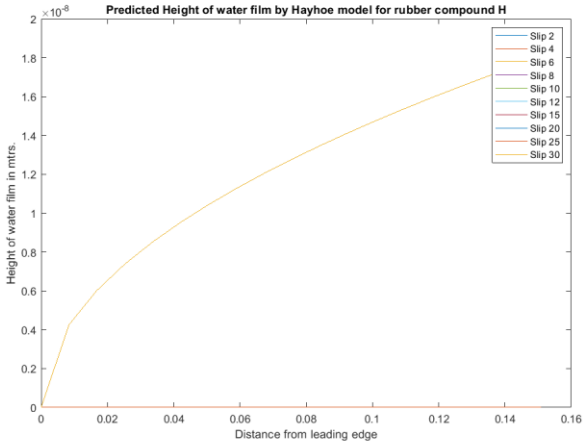

Figure B- 15: Predicted Height of water film by Hayhoe model for rubber compound H

B. 4. Additional results from Genetic Algorithm Optimizations

In this section the results for magic formula parametrized results of all the tires are presented with and without averaging of experimental results are presented in Table B- 13 and Table B- 14 respectively.

Table B- 13: Plot of parametrization of Magic formula by averaging of experimental results

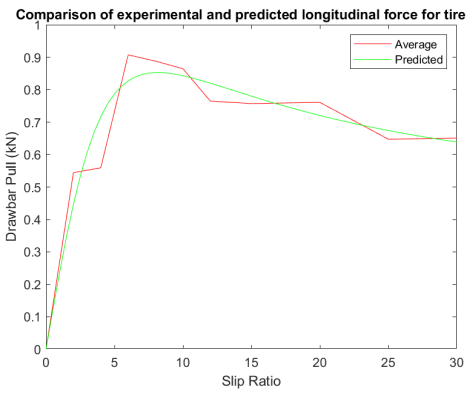	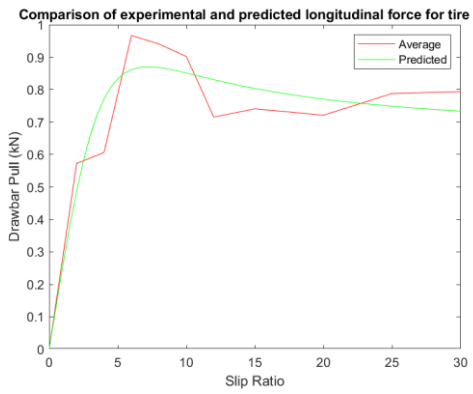
Tire A1	*Tire A3*

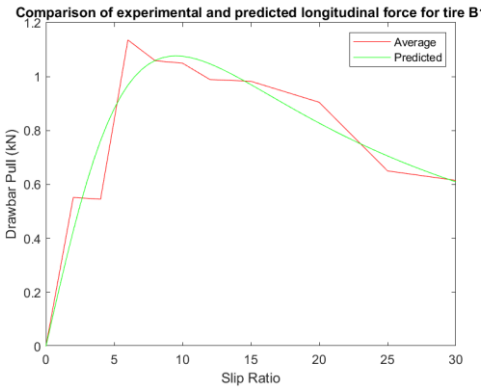

Tire B1

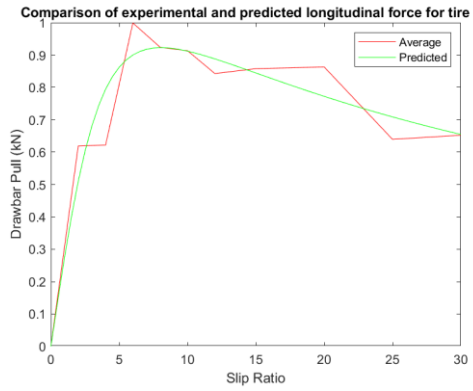

Tire B3

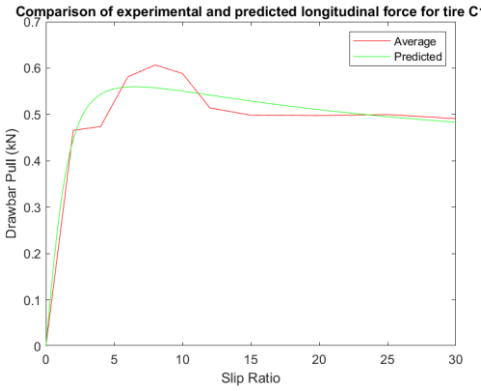

Tire C1

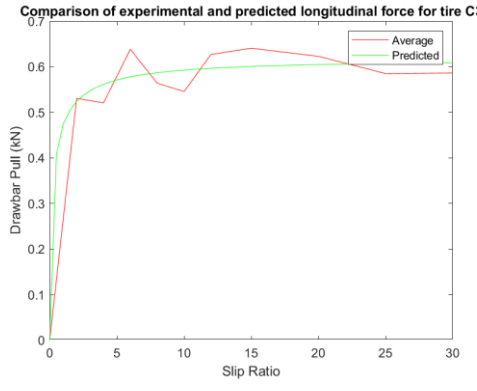

Tire C3

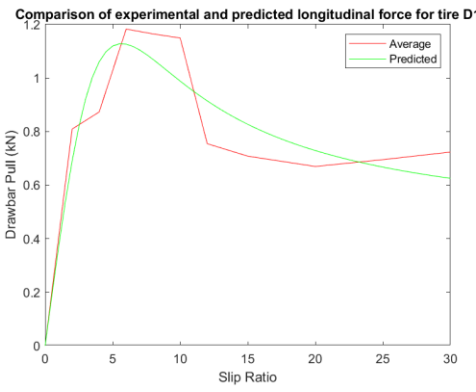

Tire D1

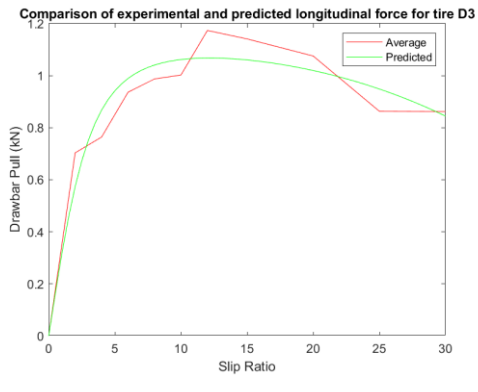

Tire D3

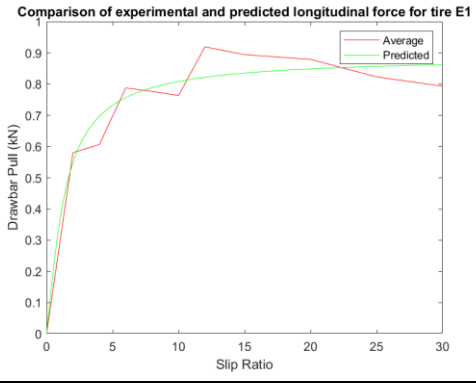

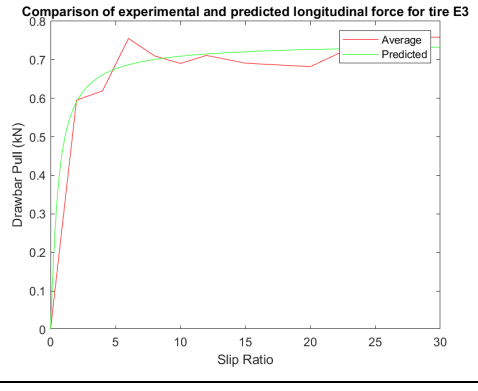

Tire E1	Tire E3
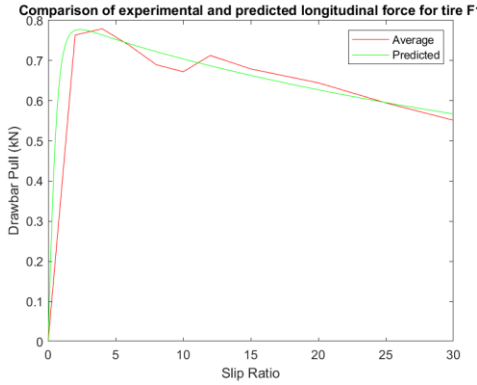	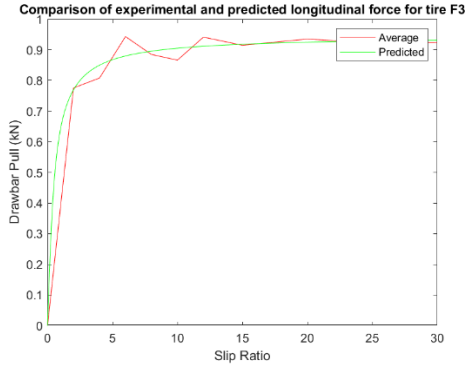
Tire F1	**Tire F3**
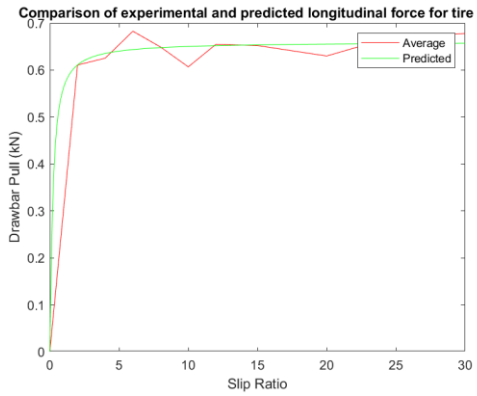	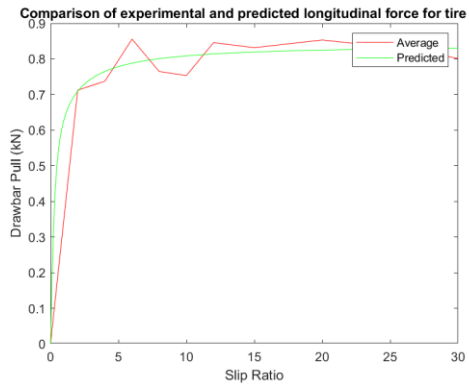
Tire G1	**Tire G3**
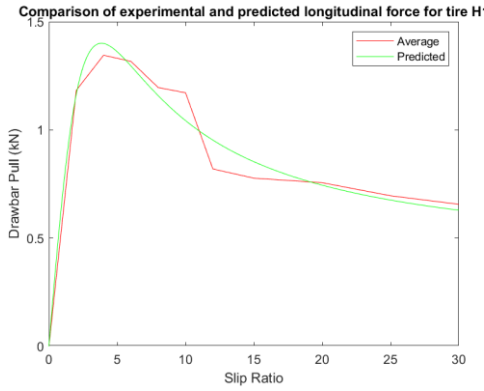	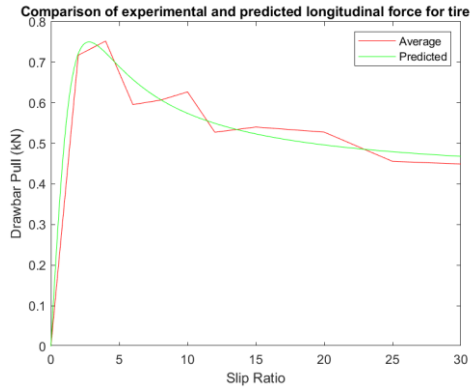
Tire H1	**Tire H3**

Table B- 14: Plot of parametrization of Magic formula without averaging of experimental results

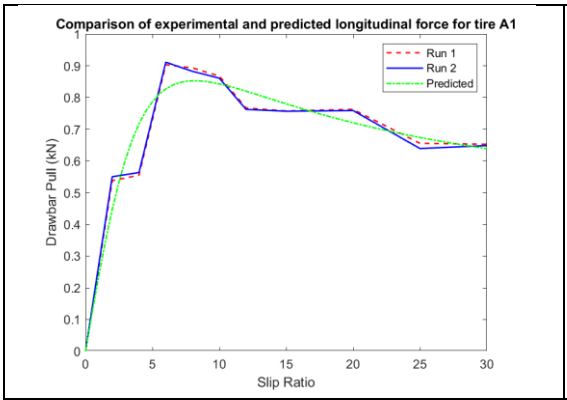

Tire A1

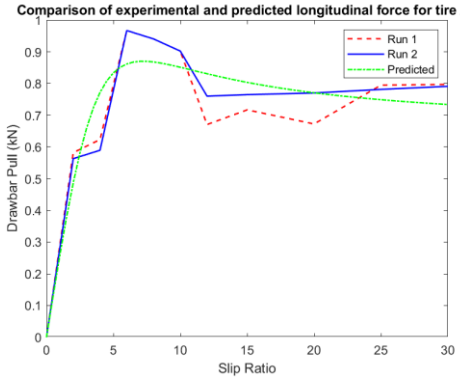

Tire A3

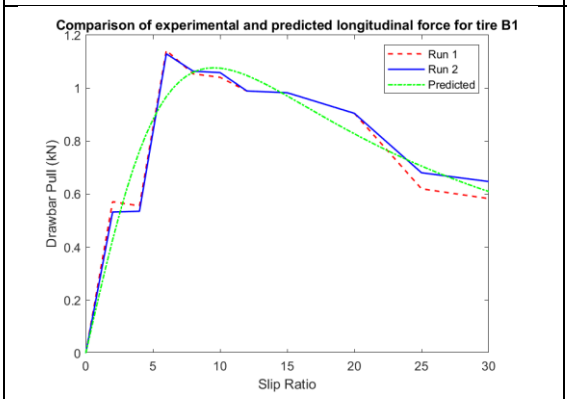

Tire B1

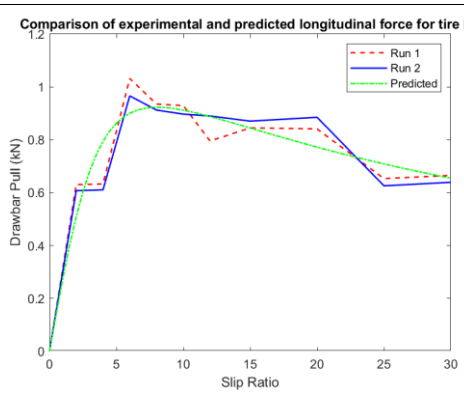

Tire B3

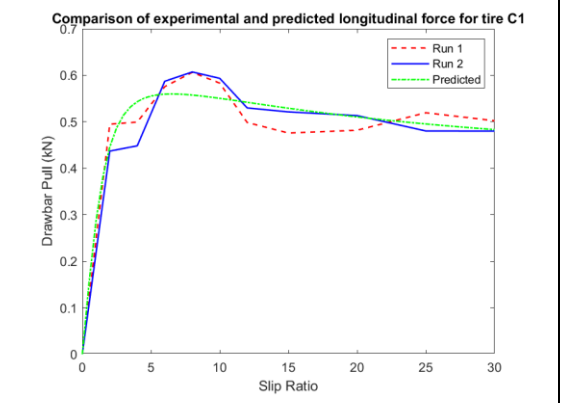

Tire C1

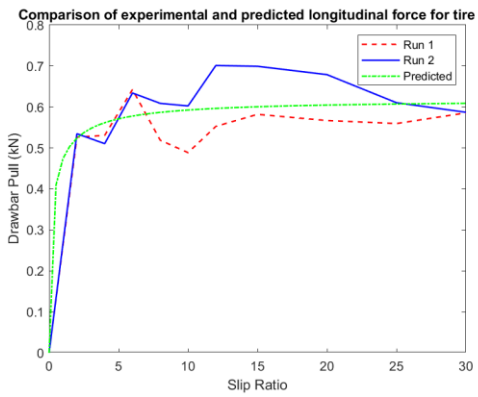

Tire C3

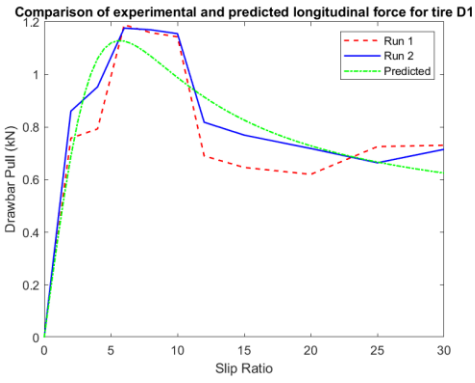

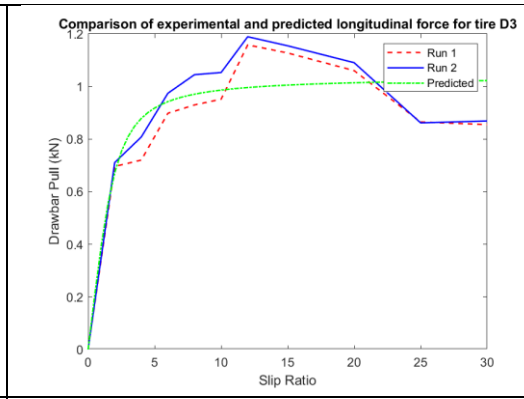

Tire D1

Tire D3

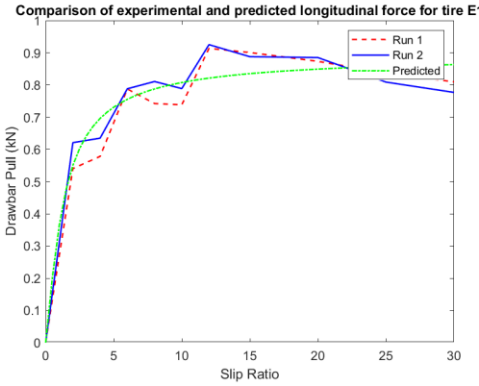

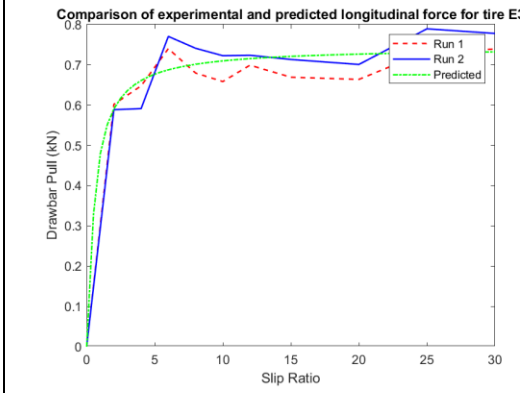

Tire E1

Tire E3

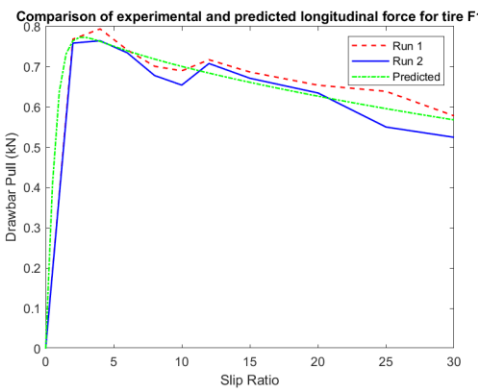

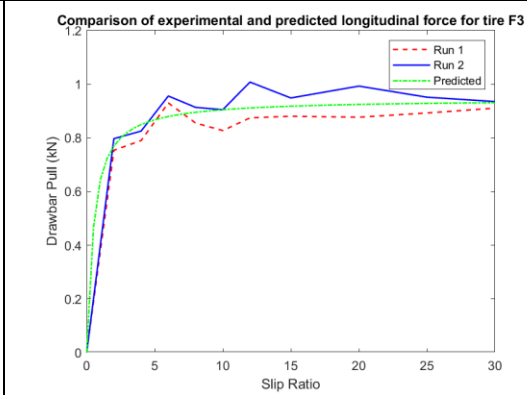

Tire F1

Tire F3

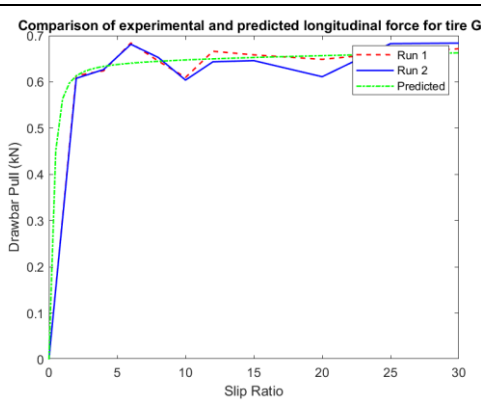

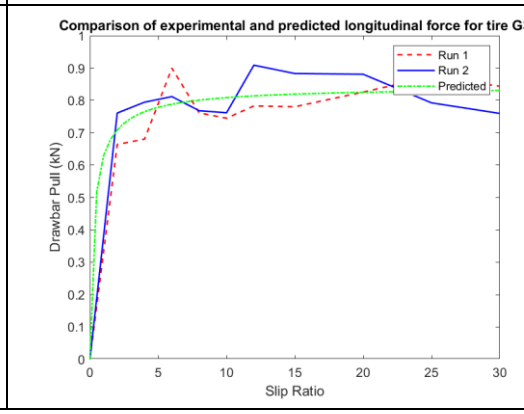

Tire G1	*Tire G3*
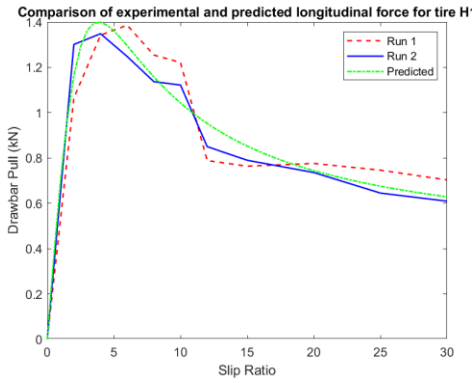	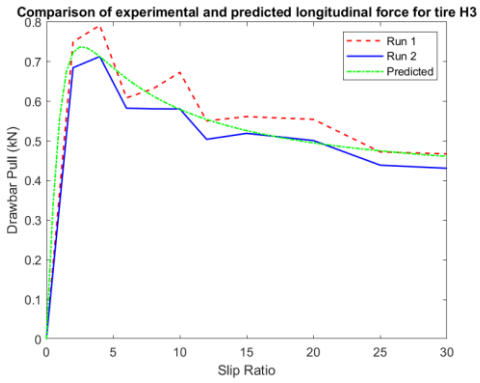
Tire H1	*Tire H3*

Bibliography

Bhoopalam, A.K., 2015. Pneumatic tire performance on ice. Virginia Polytechnic Institute and State University.

Evans, D.C.B.., Nye, J.F., Cheeseman, K.J.., 1976. The Kinetic Friction of Ice, in: Proceedings of the Royal Society of London. Series A, Mathematical and Physical Sciences. Royal Society, pp. 493–512.

Fujikawa, T., Funazaki, A., Yamazaki, S., 1994. Tire Tread Temperatures in Actual Contact Areas. Tire Sci. Technol. 22, 19–41.

Goldberg, D.E., 1989. Genetic Algorithms in Search, Optimization and Machine Learning. Addison-Wesley Publishing Company Inc.

Greenwood, J.A., Williamson, J.B.P., 1966. Contact of nominally flat surfaces. Proc. R. Soc. London. Ser. A. Math. Phys. Sci. 295, 300–319.

Hansen, P.C., Pereyra, V., Scherer, G., 2012. Least squares data fitting with applications, Least Squares Data Fitting with Applications. https://doi.org/10.1353/book.21076

Hayhoe, G.F., Shapley, C.G., 1989. Tire force generation on ice. SAE Tech. Pap. 98, 30–38. https://doi.org/10.4271/890028

He, R., 2019. Systematic Tire Testing and Model Parametrization for Tire Traction on Soft Soil. Virginia Polytechnic Institute and State University.

He, R., Shenvi, M.N., Mousavi, H., Sandu, C., Braun, K., Kruger, R., Schalk, P., 2019. Updates of International Society for Terrain-Vehicle Systems Standards, in: Proceedings of the 15th ISTVS Euorpean-African Regional Conference. International Society for Terrain-Vehicle-Systems, Prague, Czech Republic, pp. 1–91.

Higgins, D.D., Marmo, B.A., Jeffree, C.E., Koutsos, V., Blackford, J.R., 2008. Morphology of ice wear from rubber-ice friction tests and its dependence on temperature and sliding velocity. Wear 265, 634–644. https://doi.org/10.1016/j.wear.2007.12.015

Hiramatsu, K., Kamamizu, K., Komai, M., Okazaki, T., Takino, H., 1991. Rubber and collagen-fiber blends for studless winter tire applications. Rubber World 204, 38–43, 45.

Isitman, N.A., Kriston, A., Fülöp, T., 2017. Role of Rubber Stiffness and Surface Roughness in the Tribological Performance on Ice. Tribol. Trans. 61, 295–303. https://doi.org/10.1080/10402004.2017.1319002

Jimenez, E., 2018. Experimental and Modeling of Pneumatic Tire Performance on Ice. Virginia Polytechnic Institute and State University.

Jung, H.C., Park, W.C., Jeong, K.M., 2018. Finite Element Analysis of Tire Traction Using a Rubber-Ice Friction Model. Open J. Appl. Sci. 08, 495–505. https://doi.org/10.4236/ojapps.2018.811040

Kaltire, 2020. All Weather vs All Season vs Winter Tires [WWW Document]. URL https://info.kaltire.com/all-weather-vs-all-season-vs-winter-tires/ (accessed 6.7.20).

Khan, Aamir K., Sandu, C., 2017. Design and Manufacturing of a Clutch and Brake System for Indoor Tire Testing, in: Proceedings of the ASME 2017 International Design Engineering Technical Conferences and Computers and Information in Engineering Conference IDETC/CIE 2017. pp. 1–10.

Klapproth, C., Kessel, T.M., Wiese, K., Wies, B., 2016. An advanced viscous model for rubber-ice-friction. Tribol. Int. 99, 169–181. https://doi.org/10.1016/j.triboint.2015.09.012

Lahayne, O., Pichler, B., Reihsner, R., Eberhardsteiner, J., Suh, J., Kim, D., Nam, S., Paek, H., Lorenz, B., Persson, B.N.J., 2016. Rubber Friction on Ice: Experiments and Modeling. Tribol. Lett. 62, 1–19. https://doi.org/10.1007/s11249-016-0665-z

Lorenz, B., Persson, B.N.J., Fortunato, G., Giustiniano, M., Baldoni, F., 2013. Rubber friction for tire tread compound on road surfaces. J. Phys. Condens. Matter 25. https://doi.org/10.1088/0953-8984/25/9/095007

Michael Blundell, Damian Harty, 2004. The Multibody Systems Approach to Vehicle Dynamics. Elsevier Butterworth-Heinemann, Burlington, MA.

Misiewicz, P.A., Blackburn, K., Richards, T.E., Brighton, J.L., Godwin, R.J., 2015. The evaluation and calibration of pressure mapping system for the measurement of the pressure distribution of agricultural tyres. Biosyst. Eng. 130, 81–91. https://doi.org/10.1016/j.biosystemseng.2014.12.006

Moore, D.F., 1975. The Friction of Pneumatic Tires.

Mousavi, H., Sandu, C., 2020a. Tire-ice model development for the simulation of rubber compounds effect on tire performance. J. Terramechanics 91, 97–115. https://doi.org/10.1016/j.jterra.2020.06.001

Mousavi, H., Sandu, C., 2020b. Study on the Effects of Rubber Compounds on Tire Performance on Ice. SAE Tech. Pap. 2020-April, 1–9. https://doi.org/10.4271/2020-01-1228

Mousavi, H., Shenvi, M.N., Sandu, C., 2019. Experimental study for free rolling of tire on ice, in: ASME 2019 International Design Engineering Technical Conferences and Computers and Information in Engineering Conference IDETC/CIE 2019. https://doi.org/10.1115/DETC2019-97846

Nakajima, Y., 2019. Advanced Tire Mechanics, Advanced Tire Mechanics. Springer Nature Singapore, Tokyo, Japan. https://doi.org/10.1007/978-981-13-5799-2

Naranjo, S.D., 2013. Experimental investigation of the tractive performance of an instrumented off road tire on a soft soil terrain. Virginia Polytechnic Institute and State University.

Navin, F., Macnabb, M., Nicolletti, C., 1996. Vehicle Traction Experiments on Snow and Ice. SAE Tech. Pap. Ser. 1. https://doi.org/10.4271/960652

Okel, T.A., Rueby, J.A., 2016. Silica morphology and functionality: Addressing winter tire performance. Rubber World 253, 21–33.

Pacejka, H.B., Bakker, E., 1992. The magic formula tyre model. Veh. Syst. Dyn. 21, 1–18. https://doi.org/10.1080/00423119208969994

Peng, X.D., Xie, Y.B., Guo, K.H., 2000. A new method for determining tire traction on ice, in: SAE Technical Papers. https://doi.org/10.4271/2000-01-1640

Peng, X.D., Xie, Y.B., Guo, K.H., 1999. A tire traction modeling for use in ice mobile. SAE Tech. Pap. 108, 873–880. https://doi.org/10.4271/1999-01-0478

Persson, B.N.J., 2014. Role of frictional heating in rubber friction. Tribol. Lett. 56, 77–92. https://doi.org/10.1007/s11249-014-0386-0

Persson, B.N.J., 2011. Rubber friction and tire dynamics. J. Phys. Condens. Matter 23. https://doi.org/10.1088/0953-8984/23/1/015003

Persson, B.N.J., 2006. Rubber friction: Role of the flash temperature. J. Phys. Condens. Matter 18, 7789–7823. https://doi.org/10.1088/0953-8984/18/32/025

Rajamani, R., 2012. Vehicle Dynamics and Control, Integrated Vehicle Dynamics and Control. Springer US. https://doi.org/10.1002/9781118380000.ch5

Ripka, S., Lind, H., Wangenheim, M., Wallaschek, J., Wiese, K., Wies, B., 2012. Investigation of Friction mechanisms of siped tire tread blocks on snowy and icy surfaces. Tire Sci. Technol. 40, 1–24. https://doi.org/10.2346/1.3684409

S. Yamazaki, M. Yamaguchi, E. Hiroki, T. Suzuki, 2000. Effects of the number of siping edges in a tire tread block on Friction Property and Contact with an Icy Road. Tire Sci. Technol.

28, 58–69.

Sandu, C., Taylor, B., Biggans, J., Ahmadian, M., 2008. Building an infrastructure for indoor terramechanics studies: the development of a terramechanics rig at virginia tech, in: Proceedings of 16th ISTVS International Conference, Turin, Italy. pp. 177–185.

Skouvaklis, G., Blackford, J.R., Koutsos, V., 2012. Friction of rubber on ice: A new machine, influence of rubber properties and sliding parameters. Tribol. Int. 49, 44–52. https://doi.org/10.1016/j.triboint.2011.12.015

Sokolovskij, E., 2007. Automobile braking and traction characteristics on the different road surfaces. Transport 22, 275–278. https://doi.org/10.1080/16484142.2007.9638141

Tan, T., Xing, C., Tan, Y., 2020. Rubber friction on icy pavement: Experiments and modeling. Cold Reg. Sci. Technol. 174. https://doi.org/10.1016/j.coldregions.2020.103022

Tekscan Inc., 2018. Pressure Mapping Sensor 3150 Datasheet 20215.

Tuononen, A.J., 2011. Laser triangulation to measure the carcass deflections of a rolling tire. Meas. Sci. Technol. 22. https://doi.org/10.1088/0957-0233/22/12/125304

US. Department of Transportation, 2020. US DOT: How do weather events impact roads? [WWW Document]. URL https://ops.fhwa.dot.gov/weather/q1_roadimpact.htm (accessed 6.5.20).

US. Department of Transportation, Administration, F.H., 2020. US DOT Road Weather Management Program [WWW Document]. URL https://ops.fhwa.dot.gov/weather/weather_events/snow_ice.htm (accessed 6.5.20).

Van der Steen, R., 2007. Tyre/road friction modeling, Eindhoven University of Technology, Department of Mechanical Engineering, Dynamics and Control group,. Eindhoven.

Van Oosten, J., 1999. TIME, tire measurement procedure: steady state force and moment testing, in: European Automotive Congress.

Waluś, K.J., Olszewski, Z., 2011. Analysis of tire-road contact under winter conditions. Proc. World Congr. Eng. 2011, WCE 2011 3, 2381–2384.

Weng, P., Tang, Z., Guo, B., 2020. Solving “magic triangle” of tread rubber composites with phosphonium-modified petroleum resin. Polymer (Guildf). 190, 122244. https://doi.org/10.1016/j.polymer.2020.122244

Wiese, K., Kessel, T.M., Mundl, R., Wies, B., 2012. An analytical thermodynamic approach to friction of rubber on ice. Tire Sci. Technol. 40, 124–150.

Xu, F., Yoshimura, K.I., Mizuta, H., 2013. Experimental study on friction properties of rubber material: Influence of surface roughness on sliding friction. Procedia Eng. 68, 19–23. https://doi.org/10.1016/j.proeng.2013.12.141

Zhang, Y., Gao, J., Li, Q., 2018. Experimental study on friction coefficients between tire tread rubber and ice. AIP Adv. 8. https://doi.org/10.1063/1.5041049